https://orcid.org/0000-0003-4429-6889

VILNIUS UNIVERSITY
PHYSICS INSTITUTE OF CENTRE FOR PHYSICAL SCIENCES AND
TECHNOLOGY

Dovydas Banevičius

Triplet state management in high performance 3rd generation blue OLEDs

DOCTORAL DISSERTATION

Natural Sciences,
Physics (N 002)

VILNIUS 2022

Academic supervisor –
dr. Karolis Kazlauskas (Vilnius University, Natural Sciences, Physics, N 002).

This doctoral dissertation will be defended in a public meeting of the Dissertation Defense Panel:

Chairman – Prof. Habil. Dr. Vidmantas Gulbinas (Center for Physical Sciences and Technology, Natural Sciences, Physics, N 002).
Members:
Prof. Dr. Ramūnas Aleksiejūnas (Vilnius University, Natural Sciences, Physics, N 002),
Dr. Kristijonas Genevičius (Vilnius University, Natural Sciences, Physics, N 002),
Dr. Tadas Malinauskas (Kaunas University of Technology, Natural Sciences, Chemistry, N 003),
Dr. Arvydas Ruseckas (University of St Andrews, Scotland, Natural Sciences, Physics, N 002).

The dissertation shall be defended at a public meeting of the Dissertation Defense Panel at 14 O'clock on 23rd of September 2022 in conference room A101 of the National Center for Physical Sciences and Technology.
Address: Saulėtekio ave. 3, Vilnius, Lithuania
Tel. +370 5 223 4501; e-mail: dovydas.banevicius@ff.vu.lt.

The text of this dissertation can be accessed at the libraries of Vilnius University as well as on the website of Vilnius University:
www.vu.lt/lt/naujienos/ivykiu-kalendorius

https://orcid.org/0000-0003-4429-6889

VILNIAUS UNIVERSITETAS
FIZINIŲ IR TECHNOLOGIJOS MOKSLŲ CENTRAS

Dovydas Banevičius

Mėlynų trečios kartos aukšto našumo organinių šviestukų kūrimas valdant tripletines būsenas

DAKTARO DISERTACIJA

Gamtos mokslai,
Fizika (N 002)

VILNIUS 2022

Disertacija rengta 2018–2022 metais Vilniaus universiteto Fizikos fakulteto Fotonikos ir nanotechnologijų institute.

Mokslinis vadovas –

dr. Karolis Kazlauskas (Vilniaus universitetas, gamtos mokslai, fizika, N 002).

Gynimo taryba:

Pirmininkas – Prof. habil. dr. Vidmantas Gulbinas (Fizinių ir technologijos mokslų centras, gamtos mokslai, fizika, N 002).

Nariai:

Prof. dr. Ramūnas Aleksiejūnas (Vilniaus universitetas, gamtos mokslai, fizika, N 002),

Dr. Kristijonas Genevičius (Vilniaus universitetas, gamtos mokslai, fizika, N 002),

Dr. Tadas Malinauskas (Kauno technologijos universitetas, gamtos mokslai, chemija, N 003),

Dr. Arvydas Ruseckas (University of St Andrews, Škotija, gamtos mokslai, fizika, N 002).

Disertacija ginama viešame Gynimo tarybos posėdyje 2022 m. rugsėjo mėn. 23 d. 14 val. Nacionaliniame fizinių ir technologijos mokslų centre (NFTMC), A101 auditorijoje.

Adresas: Saulėtekio al. 3, Vilnius, Lietuva

Tel. +370 5 223 4501; el. paštas: dovydas.banevicius@ff.vu.lt.

Disertaciją galima peržiūrėti Vilniaus universiteto bibliotekoje ir VU interneto svetainėje adresu:

https://www.vu.lt/naujienos/ivykiu-kalendorius

ACKNOWLEDGEMENTS

I would like to say a sincere thank you to my supervisor, colleagues, friends and family for all the support and advices during the time of this Thesis.

First of all, I thank my supervisor dr. Karolis Kazlauskas. Karolis showed me the way of research and taught me to think about different scenarios before spending money and time on experiments that first came to mind. Also, I thank Karolis for our chats on all possible topic from sports to electricity prices and for beach tennis matches. Karolis, you are awesome leader.

Secondly, I want to express my gratitude to co-workers at the Institute of Photonics and Nanotechnology. Especially I thank the skillful dr. Gediminas Kreiza. Discussions with and advices from Gediminas are some of the most invaluable thing in the time of this Thesis. As he is an expert in experimental technology and physics, he is a master of speech and humor.

It is very important to keep good work – rest balance. I thank my colleagues at Institute's Coffee-room for the chats with coffee cups, for history, literature, sports, biology and, sometimes, human biology lectures and for debates on physics.

I want to thank my friends from all different portions of my after-research time. I thank my lovely friends from *basketball spectating* group and *karaoke* group. I thank my friends from the badminton court. I thank my brothers and sisters with whom I oath to serve. With you, the time of this Thesis flew by.

I am grateful to Jūratė, who managed to grow my emotional intelligence, supported me through ups and downs and with whom I am having fantastic time together. I am also grateful to my dad Arūnas, who encouraged me to keep pursuing my goals.

Finally, I want to express gratefulness to my mother Rima, who is not able to witness the end of this road. Despite the sorrow that you left – I am grateful for the time we spent.

LIST OF ABBREVIATIONS

A	Acceptor
CT	Charge transfer
Cz	Carbazole
D	Donor
DF	Delayed fluorescence
EQE	External quantum efficiency
EL	Electroluminescence
EML	Emissive layer
FL	Fluorescence
FWHM	Full width at half maximum
HOMO	Highest occupied molecular orbital
ICT	Intramolecular charge transfer
IPN	Isophthalonitrile
ISC	Intersystem crossing
LE	Locally excited
LUMO	Lowest unoccupied molecular orbital
ND	Naphthyridine
OLED	Organic light emitting diode
PF	Prompt fluorescence
PL	Photoluminescence
QY	Quantum yield
rISC	Reverse intersystem crossing
STA	Singlet – triplet annihilation
TADF	Thermally activated delayed fluorescence
tCz	*tert*-butyl-carbazole
TTA	Triplet – triplet annihilation

TABLE OF CONTENTS

INTRODUCTION

In our modern society, commonness and communication cannot be imagined without screens and information displays. Many people spend their evenings in front of TVs, read the news using tablets and talk to each other being thousands kilometers apart using video call services. None of those would be possible without displays.
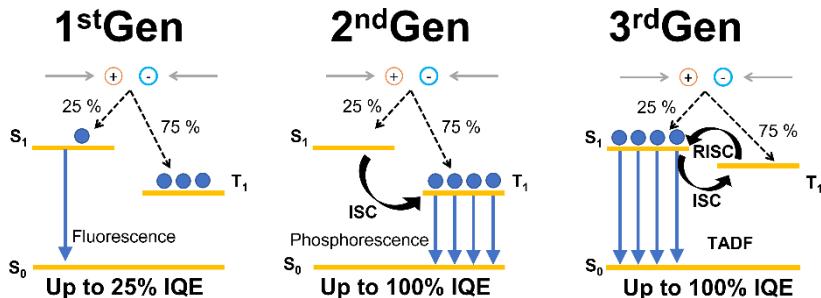
One of preferred display technology type is organic light emitting diodes (OLEDs). Here are some of the OLED displays advantages over LCD displays: 1. improved image quality due to better contrast ratio, higher brightness, wider color range and much faster refresh rates; 2. Lower power consumption; 3. Simpler design that enables very thin, flexible and even transparent displays [1]–[4]. Therefore, manufacturers have been trying to implement OLED displays in their devices for more than 20 years. In 1997, the first ever consumer product with commercialized OLED device was introduced by Pioneer. This was car radio console, which had a passive matrix OLED display [4]. Later, in 2003, famous photo camera company Kodak released a digital camera, which was first ever product with AMOLED display [5]. A few years later, in 2008, Nokia announced the first mass market mobile phone with AMOLED display (N85), and in 2010, Samsung started the longest running (thirteen years and counting) Galaxy series with smartphone model S; this series was made exclusively with OLED displays from the beginning [6]. Thus far, Samsung dominates the smartphone OLED display market with approximately half of all small area OLED displays made by Samsung, meanwhile LG displays is the world's largest manufacturer of OLED TVs with a market share of over 60% [7], [8].

Consumer electronics business is huge because there are so many buyers desiring new gadgets every or every second year. For this reason the market of OLED displays is growing rapidly, i.e., roughly doubling every four years [9]. Display Supply Chain Consultants estimates that in the year of 2022, more than 1 billion units of OLED displays will be manufactured, and the total OLED market revenue will add up to nearly 50 billion USD [10]. Another 50 billion USD are currently locked in TV market. Only 7 percent of the overall TV market is based on OLEDs. It is estimated that in ten years OLED TVs will contribute to at least 15% of the TV market and another 10 billion USD to the OLED market revenue. To sum up, every person from developed countries uses at least 4 different gadgets and most of the gadgets utilize OLED display technology. Big market requires not only huge industrial capabilities, but also great input from the scientific community to suggest novel materials, advanced technologies, and future guidelines.

Despite dominating smartphone market aiming to take over others, OLED community is still coping with a lot of challenges. Some of them are caused by purely engineering problems, e.g., related to production of the larger size or higher resolution displays. Yet, most of the problems faced such as emitted color purity, efficiency or stability of the device involves fundamental knowledge in physics [11].

The most important component of an OLED is emitting material, the so-called emitter. Since the emergence of OLEDs, there are three main emitter generation [12]. Generation one is called fluorescent emitters and can successfully utilize up to 25% electrical excitations. Second generation emitters are called phosphorescent. These emitters are able to utilize 100% excitations, but due to the complicated synthesis and the need for the precious metals, such as platinum, palladium or iridium, they are very expensive [13], [14]. Furthermore, these emitters do not meet the stability requirements in the blue spectral range. A decade ago, a new generation of emitters was introduced [15]. The process behind the 3rd generation emitters was named Thermally Activated Delayed Fluorescence (TADF). Due to the smart molecular design, TADF emitters can utilize up to 100% excitations without employing precious element. Thus, TADF emitters are potentially cheap and energy-efficient.

Fig. 1 displays the principle schemes of different OLED generations. During electrical excitation, only 25% of all excitons are formed as „bright" singlet species, while another 75% are formed as „dark" triplets [16]. 1st generation emitters are only able to utilize singlets, but the triplets are lost for good in an unequal struggle against quantum mechanics. In case of particularly aligned singlet and triplet energy levels of the 1st generation emitter such that two triplets add up close to one singlet, we can achieve favorable conditions for triplet-triplet annihilation (TTA) enabling to convert two triplets into one singlet exciton [17]. This process can add another 37.5%, giving rise to up to 62.5% internal emitter efficiency [18], [19].


Fig. 1 Principle scheme of different generations of OLED devices.

The 2nd generation emitters are able to utilize 100% of excitons due to the enhanced intersystem crossing facilitated by the heavy metal atom effect. In this way singlets are converted to triplets and from here efficiently recombine in radiative manner [20]. Alignment of the singlet and triplet energy levels achieved via smart molecular engineering permitted to efficiently convert triplet excitations to singlet manifold by thermally assisted process, where they can be effectively utilized to produce light. This type of emitters is indispensable for the future OLED technologies, however further research is required to find the ways of producing efficient, low efficiency roll-off and stable 3rd generation blue OLEDs.

Aim of this dissertation

The realization of high-performance blue OLEDs necessarily involves triplet state management as the ways of efficient harvesting of "dark" triplet species must be found out. Since green and red TADF OLEDs are ready to hit the market, scientific community must find efficient and stable blue TADF emitters and exploit them in optimized OLED configurations.

The prime goal of this work was to develop novel blue emitters expressing thermally activated delayed fluorescence behavior and to tailor them for the fabrication of high-performance OLEDs by vacuum and solution processing technologies. Several tasks were set to reach the goal:

1. Design blue TADF emitters and evaluate the influence of triplet species to an overall emission.

2. Assess the key TADF parameters of the synthesized emitters and determine suitable host materials for each of the emitters.

3. Design OLED stack configuration with appropriate functional layers, fabricate TADF OLEDs, and characterize working devices.

4. Analyze obtained results and, if needed, optimize OLED architecture to improve device performance.

Novelty and relevance

To boost the performance of blue TADF OLEDs based on benzophenone acceptor, novel method for the suppression of triplet quenching was suggested. The substitution on loose phenyl moiety with methoxy group enabled to diminish the triplet quenching and achieve almost unity quantum yield.

The obtained excellent isophthalonitrile-based device performance, in terms of EQE and efficiency roll-off, was found to be among the best for solution-processed TADF-OLEDs emitting in the blue/sky-blue spectral range and was comparable to the best green emitting devices. This is particularly relevant in the field as it demonstrates the achieved progress and potential of the cost-efficient solution processing technique.

Industry demands deep-blue (λ_{max} < 460 nm) and narrow-band TADF emitters for the fabrication of TADF-only displays, yet the development of efficient blue emitters with low efficiency roll-off is very challenging. Naphthyridine-based TADF emitters with carbazole-based donors delivered high performance, narrow-band deep-blue OLEDs and were among the best-performing conventional D-A-type blue/deep-blue TADF emitters in terms of EQE and efficiency roll-off properties of their devices.

Thesis statements

1. Non-radiative triplet quenching promoted by loose phenyl moiety in benzophenone-based blue TADF emitters is effectively suppressed by substituting the loose moiety with methoxy group, which results in near unity PL QY.

2. Carbazole donor methylation at the first position induces intramolecular twisting subsequently lowering the singlet-triplet gap of carbazole-naphthyridine- and carbazole-isophthalonitrile-derived TADF compounds resulting in enhanced TADF contribution and improved emission quantum yield (up to 86%).

3. Asymmetric carbazole-donor motif compared to the symmetric one facilitates CT and LE triplet state mixing in naphthyridine acceptor-based TADF emitter; this doubles rISC rate (up to 1.3×10^6 s^{-1}) and shortens delayed fluorescence lifetime (down to 4.4 μs) resulting in high efficiency OLEDs (external quantum efficiency of 21%) with a reduced efficiency roll-off.

4. Novel acridine(D)-pyrimidine(A) derived host in a bridgeless D-A configuration featuring high triplet energy (>3eV) is applicable for the fabrication of low efficiency roll-off blue TADF OLEDs.

Layout of the dissertation

This dissertation is based on a collection of research papers with chapters 1 to 3 summarizing the main findings. The papers are denoted as **A1** – **A5** in chronological order of their publication.

In chapter one, based on the paper **A1**, the role of widely used benzophenone acceptor responsible for the triplet quenching of this acceptor based TADF emitter is discussed; a solution to suppress this quenching is suggested and deep insight into emitter excitonic processes is presented. Chapter two covers the research papers **A2** and **A5**. Here we demonstrate the potential of differently substituted naphthyridine acceptor and carbazole-donor-based blue TADF emitters in OLEDs. Discussion on TADF parameters and OLED performances dependence on emitter architecture is presented. Lastly, the 3rd chapter based on the research papers **A3** and **A4** discusses possible ways to achieve OLEDs with low efficiency roll-off. In the case of high exciton density, exciton annihilation processes such as triplet-triplet and singlet-triplet annihilation begin dominating. The processes reduce triplet exciton concentration lowering OLED efficiency as well as produce higher-energy "hot" states causing emitter degradation at higher current density. The possible solution to maintain high efficiency at higher current densities is to ensure fast reverse intersystem crossing or to suppress the conditions for exciton annihilation by dispersing emitter molecules in a host.

Author contribution

The author has fabricated each and every OLED presented in this dissertation. He performed material deposition calibration experiments, designed stack configurations for OLEDs, investigated device parameters using state-of-the-art measuring technique, analyzed results and suggested configuration changes for improved OLED performance. Typically, for one research paper with optimized OLED devices, around 20 batches of OLEDs were fabricated with slight modifications in the stack configuration. Each batch consisted of at least 6 substrates with 6 pixels each, adding up to more than 3600 OLED pixels in total fabricated and majority of them tested.

Author also prepared most of the samples for photophysical characterization and was involved in some of the measurements.

The synthesis of the molecules presented in this dissertation was performed in three different organic chemistry groups lead by prof. Edvinas Orentas (Vilnius University), prof. Juozas V. Gražulevičius (Kaunas University of

LIST OF PUBLICATIONS

Basis of the dissertation

A1   Gediminas Kreiza, **Dovydas Banevičius**, Justina Jovaišaitė, Karolina Maleckaitė, Dalius Gudeika, Dmytro Volyniuk, Juozas V. Gražulevičius, Saulius Juršėnas, Karolis Kazlauskas, Suppression of benzophenone-induced triplet quenching for enhanced TADF performance, J. Mater. Chem. C **7**(37), 11522-11531 (2019).

A2   Gediminas Kreiza, **Dovydas Banevičius**, Justina Jovaišaitė, Saulius Juršėnas, Tomas Javorskis, Vytenis Vaitkevičius, Edvinas Orentas, Karolis Kazlauskas, Realization of deep-blue TADF in sterically controlled naphthyridines for vacuum- and solution-processed OLEDs, J. Mater. Chem. C **8**(25), 8560-8566 (2020).

A3   Gediminas Kreiza, Domantas Berenis, **Dovydas Banevičius**, Saulius Juršėnas, Tomas Javorskis, Edvinas Orentas, Karolis Kazlauskas, High efficiency and extremely low roll-off solution- and vacuum-processed OLEDs based on isophthalonitrile blue TADF emitter, Chem. Eng. J. **412**, 128574 (2021).

A4   Francesco Rodella, Rishabh Saxena, Sergey Bagnich, **Dovydas Banevičius**, Gediminas Kreiza, Stravos Athanasopoulos, Saulius Juršėnas, Karolis Kazlauskas, Anna Kohler, Peter Strohriegl, Low efficiency roll-off blue TADF OLEDs employing a novel acridine–pyrimidine based high triplet energy host, J. Mater. Chem. C **9**(48), 17471-17482 (2021).

A5   **Dovydas Banevičius**, Gediminas Kreiza, Rokas Klioštoraitis, Saulius Juršėnas, Tomas Javorskis, Vytenis Vaitkevičius, Edvinas Orentas, Karolis Kazlauskas, Enhanced blue TADF in D-A-D type naphthyridine derivative with asymmetric carbazole-donor motif, J. Mater. Chem. C **10**(12), 4813-4820 (2022).

Other publications

B1 Tomas Serevičius, Rokas Skaisgiris, Jelena Dodonova, Laimis Jagintavičius, **Dovydas Banevičius**, Karolis Kazlauskas, Sigitas Tumkevičius, Saulius Juršėnas, Achieving Submicrosecond Thermally Activated Delayed Fluorescence Lifetime and Highly Efficient Electroluminescence by Fine-Tuning of the Phenoxazine–Pyrimidine Structure, ACS Appl. Mater. Interfaces **12**(9), 10727–10736 (2020).

B2 Tomas Serevičius, Rokas Skaisgiris, Irina Fiodorova, Vytautas Steckis, Jelena Dodonova, **Dovydas Banevičius**, Karolis Kazlauskas, Saulius Juršėnas, Sigitas Tumkevičius, Achieving efficient deep-blue TADF in carbazole-pyrimidine compounds, Org. Electron. **82**, 105723 (2020).

B3 Tomas Serevičius, Jelena Dodonova, Rokas Skaisgiris, **Dovydas Banevičius**, Karolis Kazlauskas, Saulius Juršėnas, Sigitas Tumkevičius, Optimization of the carbazole–pyrimidine linking pattern for achieving efficient TADF, J. Mater. Chem. C **8**(32), 11192-11200 (2020).

B4 Tomas Serevičius, Rokas Skaisgiris, Irina Fiodorova, Gediminas Kreiza, **Dovydas Banevičius**, Karolis Kazlauskas, Sigitas Tumkevičius, Saulius Juršėnas, Single-exponential solid-state delayed fluorescence decay in TADF compounds with minimized conformational disorder, J. Mater. Chem. C **9**(3), 836-841 (2021).

B5 Rokas Skaisgiris, Tomas Serevičius, Jelena Dodonova, **Dovydas Banevičius**, Karolis Kazlauskas, Sigitas Tumkevičius, Saulius Juršėnas, Tuning of HOMO-LUMO localization for achieving thermally activated delayed fluorescence, J. Lumin. **241**, 118473 (2022).

Conference presentations

C1 **Dovydas Banevičius**, Gediminas Kreiza, Dalius Gudeika, Juozas V. Gražulevičius, Dmytro Volyniuk, Saulius Juršėnas, Karolis Kazlauskas, High efficiency sky-blue TADF OLEDs based on pentacarbazolyl-substituted benzene derivatives, Open Readings 2019, Vilnius, 2019.

C2 **Dovydas Banevičius**, Gediminas Kreiza, Dalius Gudeika, Juozas V. Gražulevičius, Dmytro Volyniuk, Saulius Juršėnas, Karolis Kazlauskas, High efficiency blue thermally activated delayed fluorescence OLEDs based on pentacarbazolyl-substituted benzene derivatives, Fpi-14, Berlin, 2019.

C3 **Dovydas Banevičius**, Domantas Berenis, Edvinas Radiunas, Saulius Grigalevičius, Saulius Juršėnas, Karolis Kazlauskas, Phenantro[9,10- d]imidazole based new host materials for efficient red TADF OLEDs, Optical probes 2019, Vilnius, 2019.

C4 **Dovydas Banevičius**, Gediminas Kreiza, Dalius Gudeika, Juozas V. Gražulevičius, Dmytro Volyniuk, Saulius Juršėnas, Karolis Kazlauskas, Effective suppression of benzophenone-induced triplet quenching for enhanced TADF performance, IKSS 24, Krutyn, 2019.

C5 **Dovydas Banevičius**, Gediminas Kreiza, Dalius Gudeika, Juozas V. Gražulevičius, Dmytro Volyniuk, Saulius Juršėnas, Karolis Kazlauskas, Effective suppression of benzophenone-induced triplet quenching for enhanced TADF performance, LNFK 43, Kaunas, 2019.

C6 **Dovydas Banevičius**, Gediminas Kreiza, Justina Jovaišaitė, Tomas Javorskis, Vytenis Vaitkevičius, Edvinas Orentas, Saulius Juršėnas, Karolis Kazlauskas, Deep blue to blue TADF-OLEDs with low efficiency roll-off based on new naphthyridine emitters, Open Readings 2020, Vilnius, 2020.

C7 **Dovydas Banevičius**, Gediminas Kreiza, Justina Jovaišaitė, Tomas Javorskis, Vytenis Vaitkevičius, Edvinas Orentas, Saulius Juršėnas, Karolis Kazlauskas, Naphthyridine-based deep-blue TADF OLEDs with low efficiency roll-off, APROPOS 17, Vilnius, 2020

C8 **Dovydas Banevičius**, Gediminas Kreiza, Domantas Berenis, Tomas Javorskis, Edvinas Orentas, Saulius Juršėnas, Karolis Kazlauskas, Substantial TADF OLED performance improvement by simple emitter structure modification, Open Readings 2021, Vilnius, 2021.

C9 **Dovydas Banevičius**, Gediminas Kreiza, Domantas Berenis, Tomas Javorskis, Edvinas Orentas, Saulius Juršėnas, Karolis Kazlauskas, Substantial TADF OLED performance improvement by simple emitter structure modification, LNFK 44, Vilnius, 2021.

C10 **Dovydas Banevičius**, Gediminas Kreiza, Domantas Berenis, Tomas Javorskis, Edvinas Orentas, Saulius Juršėnas, Karolis Kazlauskas, Substantial TADF OLED performance improvement by simple emitter structure modification, TADF Workshop 2021, Kuyshiu, 2021.

C11 **Dovydas Banevičius**, Gediminas Kreiza, Domantas Berenis, Tomas Javorskis, Edvinas Orentas, Saulius Juršėnas, Karolis Kazlauskas, Substantial TADF OLED performance improvement by simple emitter structure modification, SPIE Photonics Europe, Strasbourg, 2022.

BRIEF INTRODUCTION TO TADF OLEDS

This chapter will introduce the reader to the basics of the processes governing the 3rd generation OLEDs and the challenges of the blue TADF devices.

Management of the "dark" triplet states
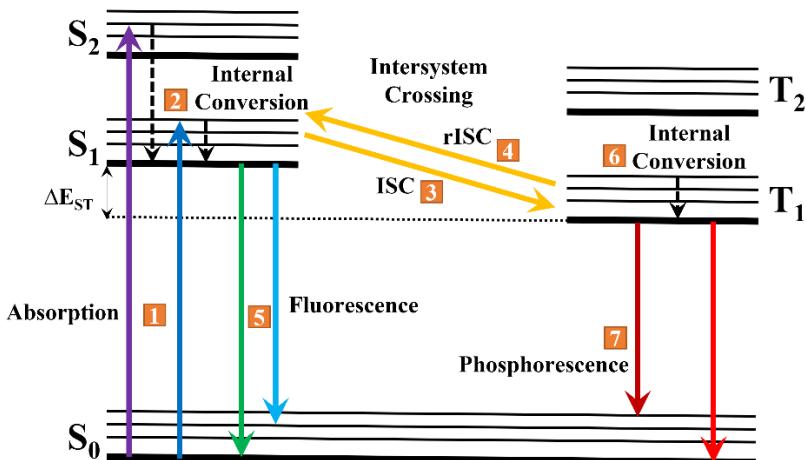
For efficient OLEDs, we need luminescent material that could harvest all excitons generated in the emissive layer and convert them into photons. Quantum statistics determined the ratio of electrically excited excitons to be 1 singlet to 3 triplets [21]. Due to completely different relaxation properties of the two species, special mechanisms to utilize all of the excitons are required [22]. More than 25 years ago, third-row transition metal complexes, especially those containing Ir (III) or Pt (II) metal centers, were found to be applicable for such exciton harvesting processes due to enhanced spin – orbit coupling (SOC) [13], [23]–[26] between the lowest lying triplet state T_1 and energetically higher singlet states S_n [20], [22], [27]–[29]. As a result of SOC, fast intersystem crossing (ISC) from singlets to triplet states can occur within the time range of a few tens of femtoseconds [30]. SOC also, enables quite high radiative rates from T_1 to the electronic ground state S_0. These phosphorescent rates can be as fast as 10^6 per second [13], [31], [32]. When used in OLEDs, these phosphorescent materials can harvest all singlet and triplet excitons and achieve up to 100% internal quantum efficiency. For example, phosphorescent OLEDs with (ppy)2Ir(acac) emitter and various host systems can be nearly 100% efficient [20], [33].

The downsides of the phosphorescent emitters is that they require expensive rare metals for the synthesis, but most important is that blue phosphorescent materials are not stable enough to be used in mass production [13], [14], [34], [35]. Novel triplet harvesting mechanism was proposed about ten years ago. This mechanism, called thermally activated delayed fluorescence, rely on the upconversion of triplet excitons into singlet manifold and then radiative recombination down to S_0 [15], [36]. TADF luminescent materials do not require heavy metal atom centers, because high SOC is not necessary to allow transition from T_1 to ground state S_0. Usually, the energy difference between lowest singlet state and the lowest triplet state is around 700 meV [37], but in case of TADF emitters, this energy difference can be very close to zero [37]–[39]. Small ΔE_{ST} facilitates relatively fast triplet conversion to singlet via reverse intersystem crossing (rISC) process [40]. Typically, for good TADF emitters, the rate of rISC is in the order of 10^6 s^{-1}

[41]. After conversion to singlet manifold triplet excitons are effectively utilized with delayed fluorescence process on a time scale of several to tens of microseconds [42]. The most important advantages of TADF emitters versus second generation phosphorescence emitters are that expensive and rare heavy metal atoms are not needed for the design of TADF emitters; TADF emitters can be a lot faster, and above all is the potential of blue TADF emitters to be more stable than phosphorescent emitter, so they are more favorable for OLED displays.

Exciton transition processes

Jablonski diagram (see **Fig. 2**) describes the variety of organic luminescence mechanisms and different paths for excitons from excited state to be deactivated into the ground state. As mentioned before, the radiative deactivation can occur with different spin multiplicity, such as singlet or triplet excited states, resulting in fluorescence or phosphorescence, and with a few additional processes – in delayed fluorescence.

Fig. 2 The transition processes of excitons created by photogeneration, fluorescence happens through transitions 1-2-5, phosphorescence through 1-2-3-6-7, TADF through 1-2-3-4-5. Here 1 – absorption, 2 and 6 – internal conversion, 3 – intersystem crossing, 4 – reverse intersystem crossing, 5 – fluorescence, 7 – phosphorescence. (Adapted from [42])

The selection rule of quantum mechanics theory allows the transition between two electronic states having the same spin multiplicity (without spin changes), and electrons are prohibited from jumping between two states of

different spin multiplicity (crossing systems with spin changes) [43]. The ground state of organic molecules is singlet (S_0 state); hence, the radiative transition of singlet excitons from the lowest singlet excited state S_1 to the ground state is theoretically allowed. This process, called fluorescence, is fast and has a short lifetime of approximately nanoseconds. On the contrary to the emission from singlet level, is the phosphorescence – emission from triplets, which is theoretically forbidden. Triplet excitons radiative transition from the lowest triplet state T_1 to the ground state exhibits way longer decay times from microseconds up to milliseconds. Phosphorescence can be easily hindered by external conditions such as oxygen in the environment or temperature. Many pure organic luminescent materials whose energy gap between S_1 and T_1 is large would only exhibit fluorescence and no phosphorescence. Heavy metal atom effect increases spin-orbit coupling in organic metal complexes, consequently, increasing the rate of ISC and the intensity of phosphorescence.

If emitters are designed such that the lowest triplet state T_1 is close to the lowest singlet state S_1, additional intersystem transition can take place converting triplet excitons into singlet manifold. As this transition process requires energy from the ambient and its direction in Jablonski diagram (**Fig. 2**) is opposite to the ISC, this process is called reverse ISC. Thermally activated excitons from the triplet manifold are upconverted into the singlet manifold and from here can be effectively utilized with the same spectral position as fluorescence but in the timescale of a few microseconds. TADF can be achieved in purely organic molecules, it can efficiently harvest up to 100 % excitons generated in the OLED, and it can be more stable than 2nd generation counterparts (especially blue emitters), so it is believed that this technology can conquer the industry.
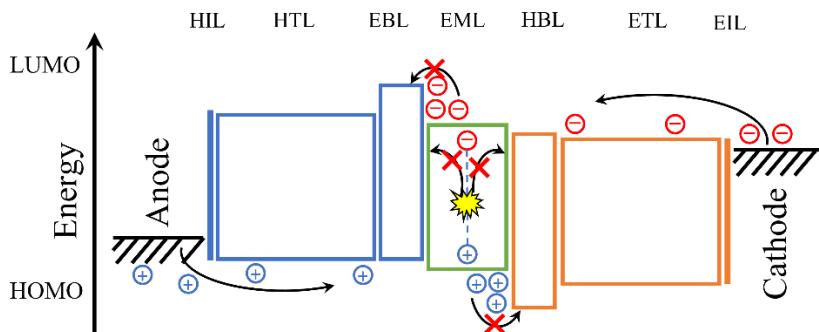
Organic Light Emitting Diodes

Electroluminescence in organic crystals was first observed almost sixty years ago [44]. This discovery has generated a great deal of scientific interest in organic material-based light emitting devices. At the beginning of the research, only one organic layer was sandwiched between two electrodes. The first organic LED with a heterojunction consisting of hole- and electron-transferring layers was demonstrated in the late 1980s [45]. To ensure the highest possible performance of OLEDs, their structures have been made increasingly complex using organic materials with dedicated functions. OLEDs can be formed with various "wet" methods by casting layers of a

solution, but the highest efficiency OLEDs are manufactured by vacuum evaporation technology [46].

Modern OLEDs are made up of 4-9 different layers of organic material, each of which can be from 5 to 50 nm thick [46]. Typically, a transparent layer of indium tin oxide (ITO), which acts as an anode for hole injection, is formed on the glass or plastic substrate. Hole injection (HIL) and transfer layers (HTL), emission layer (EML), and electron transfer (ETL) and injection layers (EIL) are later formed. Additionally, electron blocking (EBL) and hole blocking layers (HBL) can be also formed in designated positions. After forming all the required organic layers, a cathode is deposited, which is made of a very thin layer of lithium fluoride (LiF) and a thick layer of aluminum. Lithium fluoride is used to improve electron injection from aluminum. The emission layer of modern OLEDs is usually composed of a mixture of two organic materials. A material that exhibits good charge carrying properties and has a wide band gap is used as a matrix into which the emitter molecules are embedded. Such emission layer has optimal charge transfer and emission properties.

A generalized structure of an OLED is shown in **Fig. 3**. Electrons and holes are injected from the electrodes, move through the transport layers, bind into exciton in the emission layer, and recombine to generate a photon. Charge carriers cannot escape from the emission layer due to the energy barriers of the blocking layers.

Fig. 3 Generalized structure of an OLED device. (Adapted from [45])

Layers that compose OLEDs are all with different optical refractive indices. Layers formed from organic molecules have a refractive index of 1.7 to 2.2, which also depends on the wavelength of light. The refractive index of ITO is similar – it ranges from 1.8 to 2, the refractive index of the glass substrate is lower – 1.5, ambient air features the lowest refractive index n = 1 [47], [48]. Due to the different refractive indices, light falling at a certain angle

experiences full reflections in the contact planes of different materials. Due to the formation of internal reflection in the LED, according to the equation

$$\eta_{OUT} \approx \frac{1}{2n^2}, \tag{1}$$

the maximum light out-coupling is just over 20%, when emission dipole is oriented isotropically and light out-coupling structures are not used [48]. As some emitters tend to orient themselves –better light out-coupling and higher external quantum efficiencies (EQE) of the device can be achieved. When fabricating the devices, we are looking for maximum efficiency of a specific device to be not less than IQE times 0.2. If the EQE_{max} is lower than that – optimization of OLED architecture is needed.

As efficiency roll-off is one of the most important characteristic of the OLED we should also discuss the parameters to distinguish between high and low efficiency roll-off. To surpass other blue TADF OLEDs our devices must not only demonstrate maximum achievable EQE, but also low efficiency roll-off. Efficiency roll-off is considered low when the efficiency at the luminance of 1000 cd/m^2 has decreased no more than 15% from EQE_{max}. Comparison between our device performance and the performance of OLEDs form the literature can be found in ESI of paper **A3**.

Importance of rISC

Efficient TADF emitters rely on the several things. The most important, is the small energy difference between lowest triplet and lowest singlet states. But the small ΔE_{ST} must be accompanied with minimized non-radiative and radiative transitions from the triplet state. Parameter, showing how rapidly the triplets are converted to the singlet state – rISC rate (k_{rISC}) can be expressed using Boltzmann distribution:

$$k_{rISC} = A\exp(-[\Delta E_{ST}/kT]). \tag{2}$$

Efficient rISC can occur only when ΔE_{ST} energy gap is close to room temperature energy ($kT \approx 25$ meV) or is not too big (up to 200 meV).

One way of making organic emitter to exhibit small ΔE_{ST}, and consequently good TADF properties, is to synthesize the molecule with twisted separate donor (D) and acceptor (A) molecular groups [49] to ensure that highest occupied (HOMO) and lowest unoccupied (LUMO) molecular orbitals are spatially decoupled [50]. D-A molecule architecture gives rise to intramolecular charge-transfer (ICT) states. Generally, emitters with high k_{rISC} are desired for efficient TADF and high PL quantum yield (Φ_{PL}) [51], [52]. It

was also shown that high PLQY can also be achieved in low rISC compounds with $k_{\text{rISC}} \sim 10^3 \text{s}^{-1}$ when the competing exciton relaxation pathways, such as triplet non-radiative decay, are suppressed [53]. Thus, to have efficient TADF, the ratio between k_{rISC} and k_{nr}^{T} has to be as large as possible.

Blue TADF OLEDs

As already noted, the development of high-performance blue OLEDs is vital for full-color flat-panel displays and white lighting sources. Over the last five years, many TADF materials emitting in various spectral regions have been developed, and TADF-OLEDs with EQE of up to 38% were demonstrated [54]. Nevertheless, deep-blue TADF emitters exhibiting high EQE in OLEDs going along with suitable color purity (Commission Internationale de l'Eclairage (CIE) chromaticity coordinates of x ≤ 0.15 and x+y ≤ 0.30) are still scarce [55]–[57].

To achieve blue TADF, a combination of deep HOMO level donor(s) and shallow LUMO level acceptor is required [54]. Many suitable acceptor unis, such as pyrimidine [58]–[61], triazine [57], [62], [63], benzophenone [64], diphenylsulfone [55], triarylborane [65], [66], isophthalonitrile [15], and more, have been used to design blue TADF molecules, but when it comes to the selection of donor groups, there is only a few suitable candidates like acridan [59], phenoxazine [67] and carbazole [60], [61], which restricts the diversity in blue TADF material design [54], [68].

By the time the work for this thesis started, there were around 90 peer-reviewed papers per year fulfilling search phrase "blue TADF OLED*". At the end of this dissertation more than 170 peer-reviewed paper are being published per year on the topic of blue TADF OLEDs. This shows how important is the research in the field of blue TADF OLEDs and how neatly timed was the topic of the dissertation you are reading.

EXPERIMENTAL METHODS

This chapter describes the research methods, sample and device preparation techniques, and equipment used in the preparation of this dissertation.

Quantum chemical simulations

Before the expensive and time-consuming synthesis of new TADF materials, the structural and electronic properties of them is being assessed by quantum chemical simulations. Density functional theory (DFT) is used with the Gaussian 09 software packages at the B3LYP/6-31G(d) level [69]. Quantum chemistry calculations allows to see the probable distribution of HOMO and LUMO orbitals as well as the energy values of them and singlet and triplet distribution. Dr. Gediminas Kreiza (Vilnius University) produced the calculations for papers **A1**, **A2**, **A3**, **A5** and dr. Stavros Athanasopoulos (Carlos III University of Madrid) produced the calculations for paper **A4**.

Synthesis of material

After quantum chemical calculations were performed and data was analyzed, the synthesis of new compounds took place. The synthetic and molecular characterization details are presented in respective research papers and their supplementary information. Compounds were synthesized and their structural properties were tested by prof. Juozas V. Gražulevičius group (Kaunas University of Technology) for paper **A1**, by prof. Edvinas Orentas group (Vilnius University) for papers **A2**, **A3** and **A5**, and by prof Peter Strohriegl group (University of Bayreuth) for paper **A4**.

Sample preparation for photophysical characterization

To measure single molecule photophysical properties, materials were dissolved in spectroscopic toluene solvent at a concentration of 10^{-5} M. Required volume of solution was filled in quartz cuvette. In order the check how materials would perform in solid state, thin film samples were fabricated using drop-casting, spin-coating or vacuum evaporation techniques. To prepare drop-casted samples, materials were dissolved in various organic solvents at the concentrations of several g/L and then few hundreds of microliters of solution was poured on the precleaned glass or quartz substrate.

After the solvent have evaporated, only the pure material is left on the substrate. Spin-coated samples were prepared as follows: required amount of material was dissolved in chloroform solvent at the concentration of a few g/L. Then 200μL of solution were poured on precleaned glass or quartz substrate and the substrate was spun at the spinning speed of 1000-4000 rotations per minute. After 1 minute, the chloroform evaporated, and the substrate stopped spinning. To remove residual solvent from the thin film, the sample was placed on hot plate of 65 °C. To examine how the materials perform in the same configuration as would perform in OLEDs, solid-state thin film samples were fabricated using identical thermal vacuum evaporation procedure as for OLED fabrication. Quartz substrates with thin films were then capsulated to cancel any plausible oxygen or ambient atmosphere effects.

To produce host-guest samples consisting of two materials the same procedure as for spin-coating of vacuum evaporation is executed with two different materials with the ratio of desired concentrations.

Photophysical measurements

Steady-state absorption spectra of prepared samples were scanned using Perkin Elmer Lambda 950 spectrophotometer.

Luminescence spectra of materials under CW xenon lamp photoexcitation controlling the excitation wavelength with monochromator, CCD spectrometer PMA-12 (Hamamatsu) was used to record the signal of photoluminescence.

Quantum efficiency Φ_F is the ratio between the amount of absorbed and emitted photons and is an intrinsic material property. The quantum yield of compounds was determined using integrating sphere (Sphere Optics) with PMA-12 spectrometer and three configurations measurement technique [70]. Configuration A, empty sphere response to excitation is recorded. Configuration B, sample is placed in the sphere but is only excited indirectly with light scattered from the surface of the sphere. Configuration C, direct excitation response is recorded. Recorded spectra are divided into two parts: L is incident light region and P is the region of emission. Quantum yield is determined by the following equation [71]–[73]:

$$\Phi_{\mathrm{PL}} = \frac{P_C L_B - P_B L_C}{L_A (L_B - L_C)}.$$ (3)

For oxygen sensitive samples, degassed quantum efficiency was recalculated using fluorescence signal growth method where the Φ_F of the samples is

measured in ambient and then samples are inserted into cryostat, the signal of PL is recorded and then recorded once again, when vacuum is created in the sample camera and all the oxygen particles are out of the sample. Quantum yield value is multiplied by the ration between PL spectral area in vacuum and in ambient.

To better analyze how the excited states act in the molecules, time-resolved spectroscopy was performed using time-gated intensified CCD camera iStar DH340T (Andor) with spectrograph SR-303i (Shamrock). The camera is synchronized with YAG:Nd^{3+} nanosecond lased NT 242 (Ekspla) with an optical parametrical generator. Time-resolved fluorescence, fluorescence decay transients and phosphorescence spectra were recorded. From decay transient fittings with bi-exponential decay profiles fluorescence and delayed fluorescence lifetimes τ_F and τ_{DF} were obtained and from decay characteristic area calculation, the prompt and delayed fluorescence yields Φ_{PF} and Φ_{DF} were estimated.

Calculation of TADF parameters

Most important TADF parameters were calculated using the method explained in detail in the paper by Dias et al. [50]. k_{rISC} was determined by employing delayed fluorescence lifetime, prompt and delayed fluorescence quantum efficiencies and rISC efficiency (Φ_{rISC}).

$$k_{rISC} = \frac{\Phi_{rISC}}{\tau_{DF}}\left(\frac{\Phi_{PF} + \Phi_{DF}}{\Phi_{PF}}\right). \tag{4}$$

Here

$$\Phi_{rISC} = \frac{\Phi_{DF}}{\Phi_{PL}\Phi_{ISC}}. \tag{5}$$

The most important assumption is that non-radiative deactivation of the singlet excitons to the ground state is neglected and, therefore, all non-radiative losses were associated to the decay of long-lived triplet species. As the only non-radiative path for singlets is the ISC process:

$$\Phi_{ISC} = 1 - \Phi_{PF}. \tag{6}$$

And non-radiative triplet rate can be expressed as:

$$k_{nr}^{T} = k_{rISC}/\Phi_{rISC} - k_{rISC}. \tag{7}$$

OLED device fabrication

Pre-patterned indium tin oxide (ITO)-coated glass plates (Kintec company) were used as the substrates for OLEDs. The substrates were cleaned by sonicating consecutively in detergent (Hellmanex II), distilled water, acetone and isopropyl alcohol, and thereafter treated with O2-plasma for 10 min. For fabrication of vacuum-processed devices, the substrates were transferred to a vacuum chamber (Vacuum Systems and Technologies Ltd, base pressure of <10−6 Torr) inside the glove box where stack of organic layers was deposited at ~1 Å/s deposition rate. Afterwards, samples were transported by the robotic arm to metal deposition chamber without breaking the vacuum which was followed by deposition of LiF and Al layers at a rate of 0.2 and 1 Å /s, respectively.

For solution-processed OLEDs, poly(3,4-ethylenedioxythiophene)-poly(styrenesulfonate) (PEDOT:PSS, Al 4083) filtered through 0.45 μm syringe filter was first deposited on the ITO substrates by spin-coating at 5000 rpm for 1 min. The resulting 50-nm-thick layer was annealed at 200 °C for 20 minutes. Poly(9-vinylcarbazole) (PVK) layer was spin-coated on top from chlorobenzene solution at 2000 rpm for 1 min and annealed at around 155 °C for 30 min. Thereafter, emissive layers were formed by spin-coating host/emitter mixture (at 2000 rpm for 1 min) dissolved in cyclohexane or cyclohexane/chloroform (4:1) solutions (concentrations varied, see research papers). Afterwards, samples were transferred to vacuum deposition chamber and further organic and metal layers were formed by the same procedure as described above for fully vacuum-processed OLEDs. The active area of the devices was 1×1, 2×2 or 4×4 mm2, which was defined by ITO pattern and the shadow mask used for cathode deposition.

Eventually, the fabricated devices were removed from vacuum chamber to N2-filled glove box without exposing to air and encapsulated by using a glass cover and UV-curable epoxy resin KATIOBOND LP655 (DELO).

Laboratory equipment for the fabrication of OLED devices is installed in ISO 7 class cleanroom. System consist of 6 nitrogen-filled gloveboxes each equipped with different set-up for: wet cleaning, dry cleaning, vacuum evaporation, encapsulation. **Fig. 4** shows the author of this dissertation near glovebox no. 5 with organic deposition system and vacuum evaporation device form the back-end. Vacuum evaporation system consists of two vacuum chambers connected via vacuum transfer chamber. Organic deposition chamber comprises 8 material deposition channels with PC controllable temperature. Material deposition is registered using quart crystal monitors (QCM). One QCM is dedicated for two neighboring channels, so co-

evaporation of two, three of four different materials is possible. Metal deposition chamber has four material deposition channels. As higher temperature is required for the evaporation of metals – evaporation sources in the metal chamber are more powerful. To relocate samples from one evaporation chamber to another – vacuum transfer chamber with robot manipulator is used.

Fig. 4 The author of this dissertation in cleanroom facility and vacuum evaporation system back-end side.

OLED device characterization

A system consisting of calibrated integrating sphere (ORB Optronix), spectrometer PMA-11 (Hamamatsu) and source-meter unit 2601A (Keithley) was utilized for evaluation of electrical-optical properties of OLEDs such as current–voltage-luminance (I-V-L) characteristics, EQE and efficiency roll-off. As emitted light intensity increases with increasing source voltage, the exposition time of spectrometer is reduced in order to avoid over-exposure and saturation of CCD detector. At every voltage step-point the turn-on time of the OLED and the exposure time of spectrometer is kept at low, such that signal level is just enough to precisely calculate EQE. Short as possible OLED working time at every measurement step ensure that the measurement result is not affected by the device degradation during measurement.

1. SUPPRESSION OF TRIPLET QUENCHING

This chapter summarizes the research published in paper **A1** and suggests a possible solution to non-radiative triplet quenching issue in widely researched benzophenone based blue TADF OLEDs.
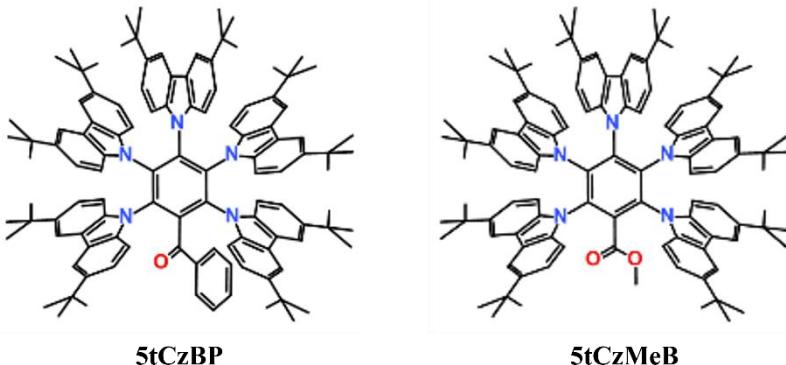
Motivation

Efficient TADF relies on effective reverse intersystem crossing from triplet to singlet manifold, and therefore the transition rate associated with this process must outcompete non-radiative decay rate of the triplets. Some TADF systems have been demonstrated to have slow k_{rISC}, yet efficient TADF. These properties can be achieved only if triplet exciton non-radiative deactivation is negligible. When the ratio between k_{rISC}/k_{nr}^T is large, most of the triplets can be utilized for efficient TADF.

Benzophenone group is widely used in blue TADF emitters as acceptor unit [74]–[77]. It was shown that benzophenone unit is responsible for non-radiative decay of triplet excitons [75], [77], [78] when benzophenone is linked to the other units of the TADF molecule and one phenyl moiety is left loose. In such case, non-radiative triplet decay is facilitated by intramolecular rotations [79] and vibrations and could not be suppressed even in solid state, preventing TADF emitters form reaching unity PL QY [75], [80]. Resolving the issue of the non-radiative triplet quenching is anticipated to improve TADF performance and consequently EQE of benzophenone derived OLEDs.

1.1. Suppression of benzophenone-induced triplet quenching

To analyze how benzophenone-induced triplet exciton quenching could be suppressed and to evaluate the performance of our suggested method, we have synthesized a pair of TADF behavior demonstrating molecules. As a donor groups we chose carbazole fragment decorated with tert-butyl groups at 3rd and 6th positions of carbazole moiety. Such donor was selected because of many reports stressing that carbazole-derived donor groups induce great stability, excellent hole transport and enhanced twisting to lower ΔE_{ST} [81], [82]. One compound, namely **5tCzBP**, was designed with benzophenone acceptor and was considered triplet quenching example in this study, while the second compound, named **5tCzMeB**, had modified phenone derived methyl benzoate acceptor unit. While molecular structures of these compounds are shown in **Fig. 5**, the details of synthetic procedure are provided in the publication **A1**.

5tCzBP   **5tCzMeB**
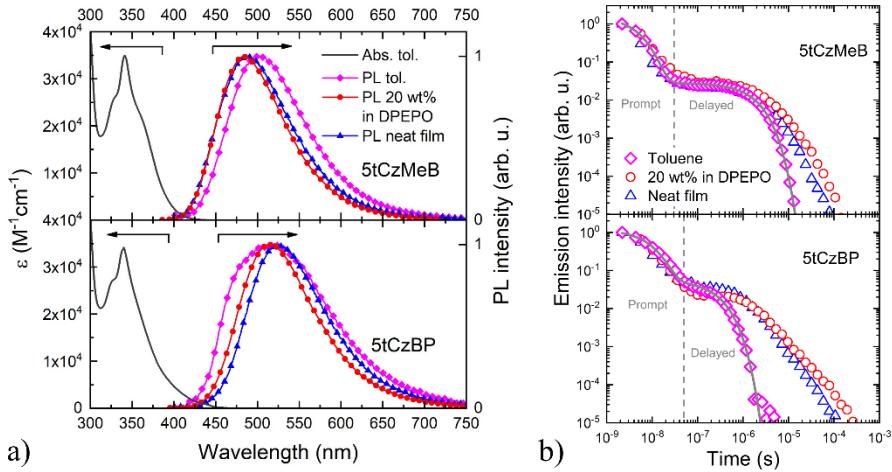
Fig. 5 Molecular structures of the investigated compounds.

The optimized geometries from DFT calculations revealed that twisting angles between carbazole groups and central phenyl fragment varied from 64° to 76° for **5tCzBP** and from 63° to 73° for **5tCzMeB** due to strong steric crowding. Time-depended DFT method calculations showed that LUMO is very well localized on acceptor unit and HOMO is spread throughout several carbazole fragments for both molecules (see Fig. 1 of paper **A1**). Strong spatial separation of molecular orbitals ensured small singlet-triplet gap of 0.05 eV and 0.25 eV for **5tCzBP** and **5tCzMeB**, respectively, while the remaining small overlap of HOMO and LUMO maintained reasonable oscillator strengths (f) for the $S_0 \rightarrow S_1$ transition and high k_r.

Extended photophysical characterization (see **Fig. 6**) was carried out for both compounds. Despite similarly strong steady state absorption at around 340 nm, differences were observed at longer wavelength where weak and

broad absorption tail was governed by ICT between donor and acceptor groups. **5tCzBP** demonstrated red shifted absorption as compared to **5tCzMeB**. PL measurements of toluene solutions also showed by 26 nm red shifted emission of **5tCzBP** in respect to **5tCzMeB** (peaking at 498 nm). PL quantum yield of diluted toluene solutions in an oxygen-free environment were estimated to be 0.43 and 0.084 for **5tCzMeB** and **5tCzBP** respectively. In a rigid DPEPO material matrix, 20 wt% doping concentration samples exhibited impressive PL QY increase up to 0.99 for **5tCzMeB** and 0.53 for **5tCzBP**. While **5tCzMeB** exhibited unity PL QY, almost half of excitations in **5tCzBP** decayed non-radiatively, showing that it is impossible to entirely restrict intramolecular torsions provoked by the benzophenone moiety even in rigid DPEPO matrix, similar to previously reported results [75], [80].

Fig. 6 Absorption and fluorescence spectra of **5tCzMeB** and **5tCzBP** in toluene solution (10^{-5} mol L^{-1}), their fluorescence spectra in neat and DPEPO films at 20 wt% doping (a) and spectrally integrated PL transients of compounds in degassed toluene solutions, 20 wt% DPEPO and neat films (b). Lines indicate double-exponential decay fits of PL transients in solutions.
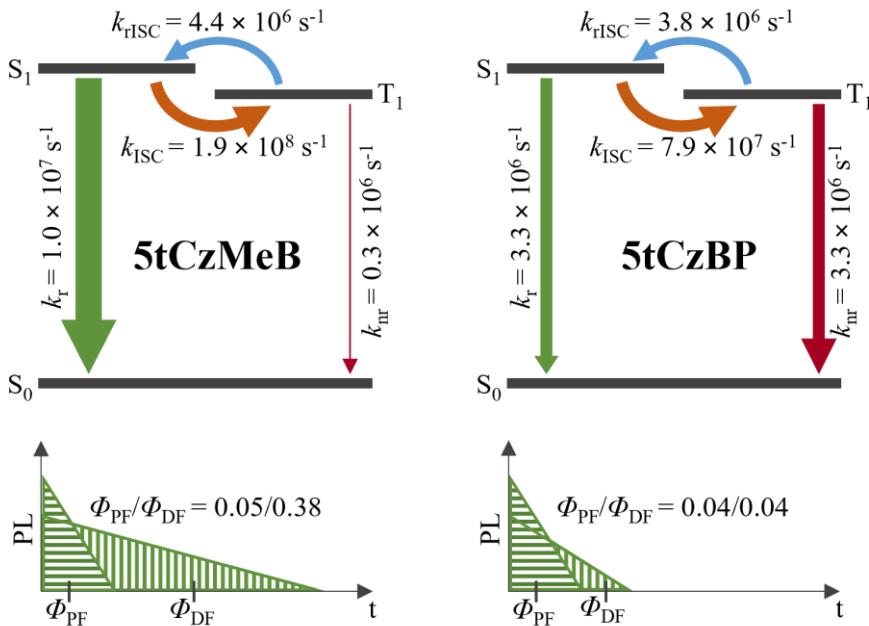
Furthermore, measurement of PL transients (see **Fig. 6(b)**) revealed double-exponential decay profiles, with PF lifetimes (τ_{PF}) of 11.2 ns and 4.9 ns for **5tCzBP** and **5tCzMeB**, respectively. These lifetimes were used to determine radiative rates of singlet states (k_r). **5tCzBP** exhibited k_r of 3.3×10^6 s^{-1}, and **5tCzMeB** utilized singlets 3-fold faster with k_r of 1.02×10^7 s^{-1}. Slower components of PL decay transiens were significantly reduced with introduction of oxygen so they were associated with triplet species and as no phosphorescence could be observed at room temperature,

and as PL intensity was directly proportional to excitation power, the triplet related PL was confirmed to be TADF.

Following the formalism presented in [50] and shortly summarized in § "Calculation of TADF parameters" most important excitonic rates were determined. As Φ_{PF} and τ_{PF} were found to be similar for solutions and rigid samples, non-radiative decay of singlet excitons to the ground state was neglected and all non-radiative losses were associated with triplets. Most important fluorescence and TADF properties are presented in **Table 1**, meanwhile summary of exitonic processes is visualized in **Fig 7**.

Table 1 Photophysical properties of investigated TADF compounds in [a] toluene, [b] DPEPO matrix and [c] neat films. Rates $\times 10^6$ s^{-1}.

| Compound	Φ_{PL} [a, b, c]	$\Phi_{DF}/ \Phi_{PF}/ \Phi_{ISC}/ \Phi_{rISC}$ [a]	$k_r/ k_{rISC}/ k_{ISC}/ k_{nr}^T$ [a]
5tCzBP	0.084/ 0.53/ 0.28	0.043/ 0.041/ 0.96/ 0.53	3.3/ 3.81/ 79/ 3.32
5tCzMeB	0.43/ 0.99/ 0.58	0.38/ 0.05/ 0.95/ 0.93	10.2/ 4.44/ 194/ 0.33

Fig. 7 Energy diagrams representing viable energy transfer routes along with their rates for compounds **5tCzMeB** and **5tCzBP** in solutions (top) and schematic representations of PF and DF contributions in PL transients for each compound in solutions (bottom).

The fulfillment of conditions $k_{ISC} > k_r$ and $k_{rISC} > k_{nr}^T$ ensures that spin cycling is repeated multiple times. From data in **Table 1** we can stress that for both compounds over 95% of generated singlets are converted into triplet manifold vis ISC, whereas the triplet conversion into singlets is nearly as efficient (~93%) for **5tCzMeB** and only half as efficient (~53%) for **5tCzBP**. Such poor performance of the latter is caused by similar k_{rISC} and k_{nr}^T forcing almost half of the triplets to decay non-radiatively. Large k_{nr}^T determines small DF contribution for **5tCzBP** ($\Phi_{DF} = \Phi_{PF} = 0.04$). Conversely, significantly suppressed non-radiative triplet quenching in **5tCzMeB** achieved upon substituting the loose phenyl moiety in the benzophenone by a methoxy group enabled to enlarge the ratio k_{rISC}/k_{nr}^T and retrieve the majority of the triplets. This resulted in longer τ_{DF} and reinforced thermally activated DF contribution ($\Phi_{DF} = 8 \times \Phi_{PF} = 0.38$) in solution. Considering near unity PL QY of **5tCzMeB** dispersed in a rigid DPEPO host, the substitution of loose phenyl to methoxy group completely suppressed k_{nr}^T in the solid state and boosted Φ_{rISC} up to unity. Such efficient rISC and large k_r obtained for **5tCzMeB** is a perfect combination for TADF OLEDs [83].
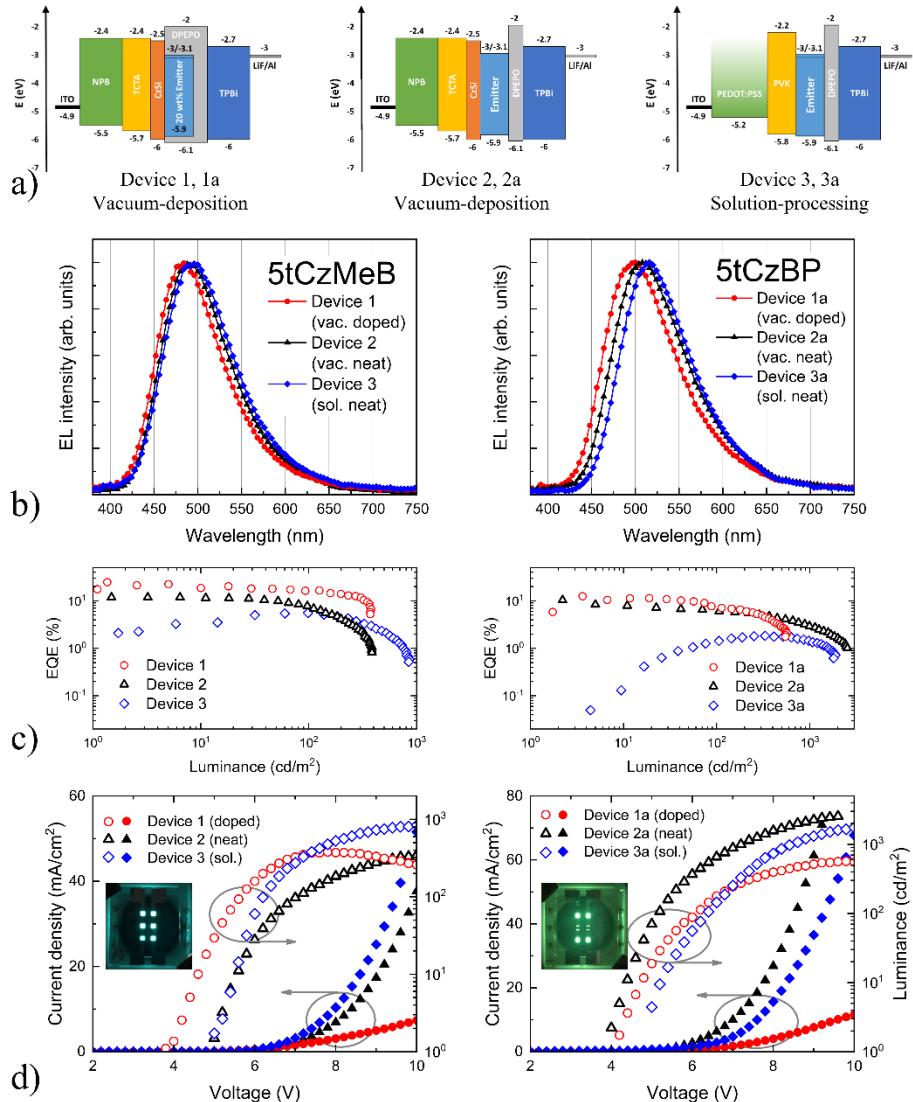
Electroluminescence (EL) properties of TADF compounds were investigated (see **Fig. 8**) by employing them in doped and non-doped emitting layers of OLEDs.

Doped emissive layer devices were made by vacuum deposition, whereas neat emissive layer OLEDs were produced using vacuum deposition and solution processing techniques. Vacuum-deposited devices were fabricated employing 20 wt% doping concentration of **5tCzMeB** (Device 1) and **5tCzBP** (Device 1a) emitters in a DPEPO host (see **Fig. 8 (a)**).

The following device configuration was used: ITO/ NPB (30 nm)/ TCTA (20 nm)/ CzSi (10 nm)/ **emitter** (20 wt%):DPEPO (20 nm)/ DPEPO (10 nm)/ TPBi (30 nm)/ LiF (1 nm)/ Al (100 nm). Non-doped vacuum-processed OLEDs had similar stack configuration with only emissive layer replaced by neat emitter. Proof-of-principle solution-processed devices were fabricated by spin coating three layers and then thermally evaporating HBL and EIL in the stack as follows: ITO/ PEDOT:PSS (30 nm)/ PVK (20 nm)/ **emitter** (20 nm)/ DPEPO (10 nm)/ TPBi (30 nm)/ LiF (1 nm)/ Al (100 nm).

Device 1 based on **5tCzMeB** doped into the DPEPO host at 20 wt% demonstrated relatively low turn-on voltage (4.0 V) with EL peak at 481 nm (see **Fig. 8 (b)**) corresponding to sky-blue emission with CIE coordinates of (0.19, 0.32). Because of brilliant Φ_{PL} (0.99) and efficient TADF, Device 1 exhibited extraordinarily high maximum EQE values reaching 24.6%, whereas the maximum EQE of Device 1a based on **5tCzBP** was only 12.5%,

which is in good agreement with Φ_{PL} measurements (0.53) if light outcoupling efficiency of 20-30% is considered.

Fig. 8 (a) Structure and energy level diagrams of the fabricated devices. Devices 1, 2, 1a and 2a were vacuum deposited using doped or neat emitting layer based on **5tCzMeB** or **5tCzBP**; devices 3 and 3a were fabricated by solution processing using emitters as neat emitting layers. (b) EL spectra of the investigated devices. (c) EQE vs. luminance curves. (d) Current density (solid symbols) and luminance (empty symbols) as a function of applied voltage of investigated OLEDs and photos of working devices.

Weak concentration quenching of PL allowed us to check how these TADF emitters would perform in non-doped OLEDs. Device 2 based on **5tCzMeB** neat film exhibited a maximum EQE of 13.4% and slightly red-shifted EL peak (at 488 nm) as compared to the doped Device 1. Meanwhile Device 2a based on **5tCzBP** neat film demonstrated a maximum EQE of 10.3% with green EL peaking at 508 nm. Results were found to be consistent with the photophysical measurements (see Φ_{PL} of the neat films in **Table 1**) implying that the main efficiency losses in non-doped devices occur due to the concentration quenching of PL in the neat films. Nevertheless, in the low luminescence region (<200 cd/m^2), OLEDs based on **5tCzMeB** and prepared by vacuum evaporation delivered excellent performance in terms of EQE, thus confirming effective suppression of non-radiative triplet quenching and ensuring efficient TADF.

Main characteristics in numbers of the investigated doped TADF OLEDs based on **5tCzBP** and **5tCzMeB** are summarized in the **Table 2**. In this table the turn-on voltage is estimated at the luminance of 1 cd/m^2. EQE, current efficiency (CE), and luminous efficacy (LE) are grouped by maximum values and by the values at the luminance of 100 cd/m^2.

Table 2 Main characteristics of the investigated doped TADF-OLEDs based on **5tCzMeB** and **5tCzBP** emitters.

| Device | Emitter | Turn-on (V) | Maximum values | | | |
			EQE (%)	CE (cd/A)	L (cd/m^2)	LE (lm/W)
1	**5tCzMeB**	4.0	24.6	59.4	378	46.7
1a	**5tCzBP**	4.1	12.5	34.9	568	27.3

| Device | Emitter | Values at L = 100 cd/m^2 | | | | |
		EQE (%)	CE (cd/A)	LE (lm/W)	CIE (x, y)	λ_{max} (nm)
1	**5tCzMeB**	16.5	33	18.2	0.19, 0.32	481
1a	**5tCzBP**	7.5	18.0	9.5	0.23, 0.41	497

Full table with characteristics of all investigated OLEDs can be found in paper **A1**.

1.2. Summary of the results

Accelerated non-radiative triplet decay in benzophenone-derived TADF compounds frequently employed in blue OLEDs has been tackled. The enhanced triplet deactivation explicitly related to the loose phenyl moiety in the benzophenone acceptor was found to compete with the rISC process, thereby decreasing TADF efficiency even in compounds with high k_{rISC} ($>10^6$ s^{-1}). To address this problem and reduce the triplet quenching equivalent by rate to rISC ($k_{\text{nr}}^{\text{T}} \approx k_{\text{rISC}}$) in compound **5tCzBP** possessing benzophenone, the loose phenyl moiety in the acceptor was replaced by a methoxy group so as to result in methyl benzoate (compound **5tCzMeB**). The modification enabled to suppress the non-radiative triplet quenching by one order of magnitude thereby enhancing the $k_{\text{rISC}}/k_{\text{nr}}^{\text{T}}$ ratio yet maintaining an unchanged k_{rISC}. This benefited in complete harvesting of the triplets via the rISC resulting in almost unity PL QY in the doped DPEPO films and $\Phi_{\text{PL}} = 0.58$ in the neat films, which in the latter case was limited only by concentration quenching. The fabricated sky-blue TADF OLEDs based on **5tCzMeB** delivered outstanding maximum EQE values of 24.6% and 13.4% in the doped and non-doped devices, whereas at 100 cd/m^2 the devices exhibited 16.5% and 7.7% EQEs, respectively. Hence, from the perspective of material design, the methyl benzoate acceptor seems to be much more appealing than the popular benzophenone as it can boost the TADF performance of a device while preserving its blue emission wavelength.

2. NAPHTHYRIDINE AND CARBAZOLE BASED TADF OLEDs

In this chapter, the results of papers **A2** and **A5** are presented. Research **A2** comparing two, very similar naphthyridine-derived TADF emitters and their performance in TADF OLEDs demonstrates the suitability of naphthyridine-based emitter to be used in both vacuum- and solution-processed blue OLEDs. Later, paper **A5** investigates a series of naphthyridine-based TADF emitters with different D and A configurations and shows the advantages of asymmetric D-A-D* architecture.

Motivation

Narrow-band deep-blue (emission peak less than 460 nm) TADF emitters are in demand for commercial OLED display applications, yet the development of efficient emitters with low efficiency roll-off is very challenging. This issue was addressed in this dissertation by studying blue-emitting TADF compounds composing of naphthyridine acceptor and carbazole-derived donor groups, which were designed by using the H-bonding, sterically controlled charge-transfer (CT) interactions between D and A units and asymmetrical donor groups.
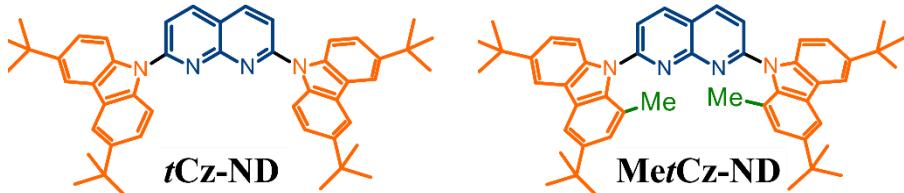
Nitrogen heteroatom-containing naphthyridine acceptor was recently successfully utilized in the construction of TADF emitters [84]–[87]. The combination of naphthyridine with a variety of donors, like those based on acridane, carbazole, phenoxazine and phenothiazine regularly employed for designing efficient TADF compounds, produced yellow/green/blue emitters with peak wavelength way above 460 nm, but the use of those emitters in high efficiency OLEDs resulted in surprisingly low EQE roll-off [86], [87].

High k_{rISC} promoting efficient delayed fluorescence is among the key features required for the realization of efficient TADF-based OLEDs. A common strategy to achieve high k_{rISC} is to minimize the energy gap between the lowest excited singlet and triplet states. Low ΔE_{ST} values can be achieved in the compounds with a strong CT character [88], typically, in D-A or D-A-D type compounds with large dihedral angles between the D and A fragments resulting in highly separated HOMO and LUMO [37]. This strategy effectively reduces ΔE_{ST}, but it also decreases k_r and causes both the lowest triplet and singlet excited states to have a strong CT character. This reduces spin-orbit coupling, since spin conversion between pure CT states is forbidden [89] and such material may not guarantee fast rISC, so, additional locally excited (LE) triplet state laying near CT states is required [89]–[92].

2.1. Sterically controlled naphthyridines for vacuum- and solution-processed TADF OLEDs

To achieve narrow blue TADF a rigid and sterically hindered or donor-interlocked molecular structure with separated HOMO-LUMO and weak CT character is required [57], [93], [94]. Additionally, H-bonding interactions between nitrogen heteroatoms in the A and neighboring C-H bonds in the D unit can also deliver narrow blue TADF emission [64]. The combination of both H-bonding and CT interactions in a controlled manner could be an attractive strategy to achieve high-performance blue OLEDs, and more importantly, to gain understanding of the TADF mechanism of D–A systems containing nitrogen heteroatoms in their building blocks.

To reveal the potential of naphthyridine acceptors for the formation of deep-blue TADF emitters, a couple of 1,8-naphthyridine (ND) based compounds with tert-butyl-carbazole (*t*Cz) moieties as donors were designed. Shown in **Fig. 9** are the two investigated compounds with ***t*Cz-ND** being the original compound and **Me*t*Cz-ND** containing additional methyl (Me) moieties at the first position of the tCz donors. Me substitution was employed to alter steric hindrance and induce the dihedral angle between the D and A units. The modification permitted assessing the impact of intramolecular D-A interaction and CT strength on TADF properties of the studied compounds and on their performance in both solution- and vacuum-processed OLEDs.
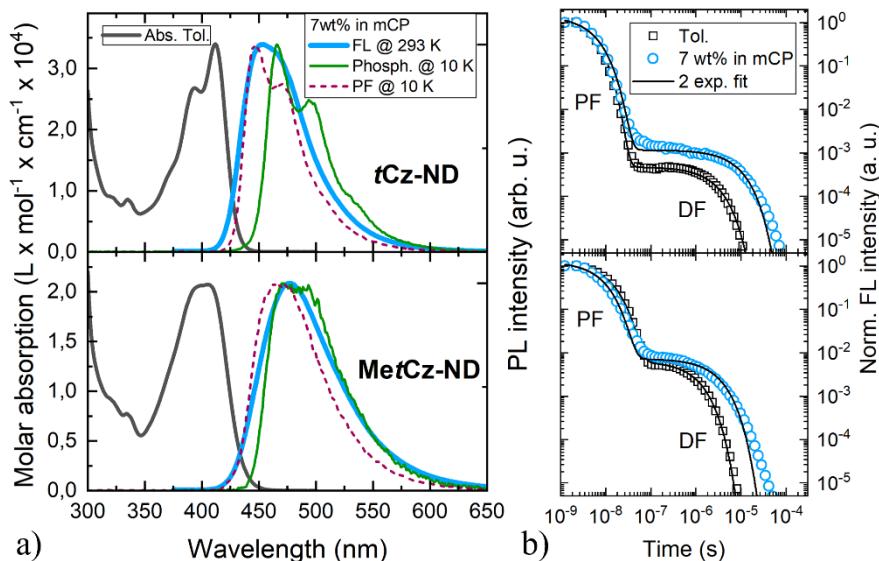
Fig. 9 Molecular structures of investigated naphthyridine compounds.

To gain insight into the photophysical properties of the investigated compounds, their excitation energies, oscillator strengths, dihedral angles between D and A units and HOMO and LUMO distributions were calculated by using DFT at the B3LYP/6-31G(d) level (see Fig.2 and Table S2 in ESI of paper **A2**). Unsubstituted **t*Cz-ND** demonstrated rather weak CT character due to the small dihedral angle (31°) between *t*Cz donor and ND acceptor. Methyl substituents in **Me*t*Cz-ND** imposed larger steric hindrance, increasing dihedral angle up to 55°, boosting CT strength, reducing oscillator strength and lowering ΔE_{ST}. Analysis of molecular structures in optimized ground state

geometries revealed proximity between the N atoms of the ND acceptor and the nearest H atoms of neighboring D groups in both compounds suggesting an involvement of intramolecular H-bonding interactions expected to increase the rigidity of the investigated compounds and thus impact their photophysical properties.

Absorption spectra of the investigated ND derivatives in toluene solutions were measured (see **Fig. 10** (a)). Compound *t*Cz-ND expressed intense absorption with well-resolved vibronic structure, indicating weak CT character and a less-twisted molecular geometry, whereas **Me*t*Cz-ND** exhibited a less structured spectrum with 1.5-fold reduced oscillator strength likely due to enhanced CT and electron-vibronic coupling.

Fig. 10 (a) Absorption (in toluene), fluorescence and phosphorescence spectra (in mCP, oxygen-free environment) of *t*Cz-ND and **Me*t*Cz-ND** at room temperature and 10 K, respectively, and prompt FL spectra at 10 K. (b) FL decay transients of compounds in toluene (squares) and in mCP host at 7 wt% doping concentration (circles) in an oxygen-free environment. Solid lines represent double exponential fits. PF and DF components are indicated.

The change of the solvent polarity from nonpolar (cyclohexane) to highly polar (acetonitrile) resulted in a strong red shift and broadening of the FL spectra, which were obviously more pronounced for **Me*t*Cz-ND** than for *t*Cz-ND indicating stronger CT character of the former (see Fig. S4, ESI of the paper **A2**).

Both compounds demonstrated oxygen-sensitive FL in solutions with distinct prompt (PF) and delayed (DF) FL components, signifying the presence of TADF see **Fig. 10** (b)). Decent Φ_{PL} values of 0.53 and 0.64 were obtained in toluene solutions for **tCz-ND** and **MetCz-ND**, respectively. PL QY was enhanced up to 0.76 and 0.86 when the emitters were dispersed in rigid mCP host at 7 wt% concentration. The improved Φ_{PL} values were accompanied by notably enhanced contributions of the DF components, implying reduced non-radiative decay from the triplet states most likely due to suppressed vibronic coupling to the ground state. DF and PF lifetimes in different media were obtained by fitting the transients with double exponential decay profiles. Slight deviation of the experimental DF points from the fits in the mCP host at the latest times could arise due to the small conformational disorder of the molecular geometry in the solid film [95]. The determined lifetimes along with Φ_{PL} and DF/PF ratios were further used to calculate the rISC rate according to the previously described procedures assuming that non-radiative decay occurs mainly from the triplet states (as discussed in § 1).
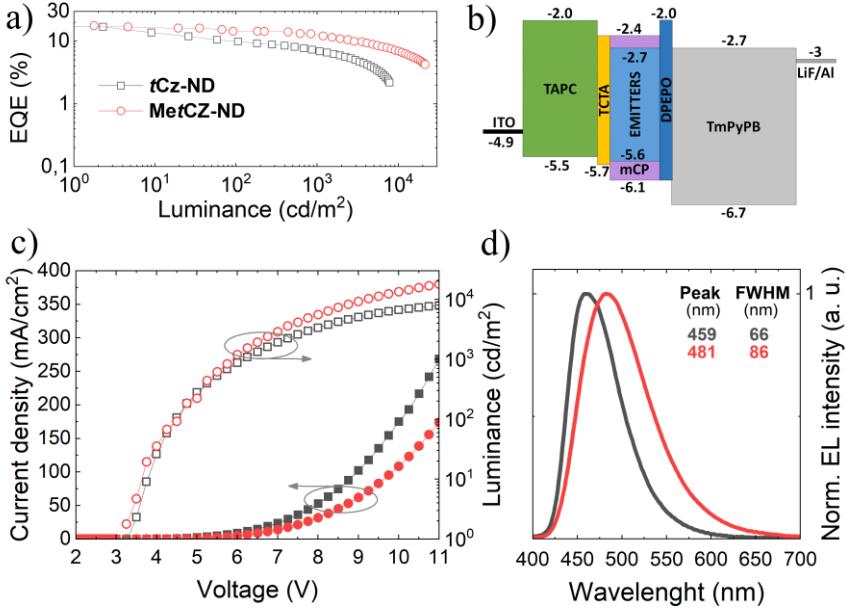
While the main photophysical properties are shown in **Table 3**, it is important to stress that k_{rISC} was found to be more than 3 times larger for **MetCz-ND** (1.06×10^6 s^{-1} in mCP) as compared to that of the unmodified **tCz-ND** (0.34×10^6 s^{-1}), which could be a result of the enhanced coupling between S_1 and T_1 due to the small ΔE_{ST} (0.09 eV) and stronger vibronic coupling because of the more labile molecular structure. On the contrary, less structurally twisted **tCz-ND** showed higher radiative decay rate (4.4×10^7 s^{-1}), together with deep blue (λ_{max} = 452 nm) and narrow (FWHM = 66 nm) emission, this emitter may be a good candidate for pure blue TADF OLEDs.

Table 3 Main photophysical properties of investigated naphthyridine-doped mCP films. Rates $\times 10^6$ s^{-1}.

Compound	λ_{max} (nm)	Φ_{PL}	Φ_{DF}/Φ_{PF}	τ_{PF} (ns)	τ_{DF} (μs)	$k_r/k_{rISC}/k_{ISC}$
tCz-ND	452	0.76	0.53/ 0.23	5.2	8.8	44/ 0.34/ 148
MetCz-ND	478	0.86	0.61/ 0.25	8.3	3.1	30/ 1.06/ 90

To further investigate the naphthyridines electroluminescence properties, blue emitting TADF OLEDs were fabricated, and their working characteristics analyzed. For better comparison of ND emitters, OLEDs were made using the same device architecture, employing TADF compounds as dopants in mCP matrix at the same doping concentration (7 wt%) as for PL measurements. This allowed to link all the obtained device characteristics directly to molecular properties of the investigated compounds.

Vacuum-processed devices were fabricated using the following layer configuration: ITO/ TAPC (30 nm)/ TCTA (5 nm)/ emitter (7 wt%):mCP (20 nm)/ DPEPO (5 nm)/ TmPyPB (50 nm)/ LiF (0.8 nm)/ Al(100 nm), where the emitter was either **tCz-ND** or **MetCz-ND**. While the main characteristics of the vacuum-processed OLEDs are provided in **Fig. 11**, the key parameters of the produced devices are summarized in **Table 4**.

Fig. 11 Characteristics of vacuum-processed OLEDs based on the naphthyridine TADF emitters (7 wt% in mCP): (a) EQE vs. luminance, (b) energy level diagram, (c) current density and luminance vs. applied voltage, and (d) normalized electroluminescence spectra.

OLED stack energy level configuration of is shown in **Fig. 11 (b)**. TAPC and TCTA acted as hole injection and transport layers, whereas LiF and TmPyPB were employed for electron injection and transport, respectively. A thin 5 nm layer of DPEPO possessing a large HOMO–LUMO gap and a high triplet energy (3.0 eV) was used to confine excitons within the emissive layer.

OLEDs based on **tCz-ND** demonstrated a low turn-on voltage of 3.25 V, EL peak at 459 nm and FWHM of 66 nm rendering deep-blue narrow-band emission with CIE coordinates of (0.14, 0.16). The maximum EQE of **tCz-ND**-based devices was 17% and at the practically useful brightness of 100 cd/m^2, EQE decreased down to 9.9% with a further roll-off to 7% at 1000 cd/m^2. Maximum brightness achieved in this device was 8424 cd/m^2. A further increase of applied bias caused degradation of the device performance, most

probably because of the exciton annihilation processes and loss of the current balance.

Me*t*Cz-ND-based vacuum-processed OLEDs showed the same turn-on characteristics with turn-on voltage of 3.25 V. EL of the devices was considerably redshifted with the EL peak at 481 nm matching the PL emission of the compound doped in mCP matrix. Stronger CT character of **Me*t*Cz-ND** also implied broader EL emission of the device (FWHM = 86 nm), which was typical to conventional TADF emitters. The CIE coordinates of this device (0.18, 0.32) corresponded to sky-blue emission. **Me*t*Cz-ND** based devices exhibited a bit higher maximum EQE of 17.6% at low brightness. However, in contrast to **tCz-ND**, **Me*t*Cz-ND** based OLEDs demonstrated reduced efficiency roll-off. Explicitly, EQE was reduced only down to 14.4% and 12.5% at the brightness of 100 cd/m^2 and 1000 cd/m^2, respectively. The device brightness maxed out at 21 459 cd/m^2 still maintaining EQE above 4%.
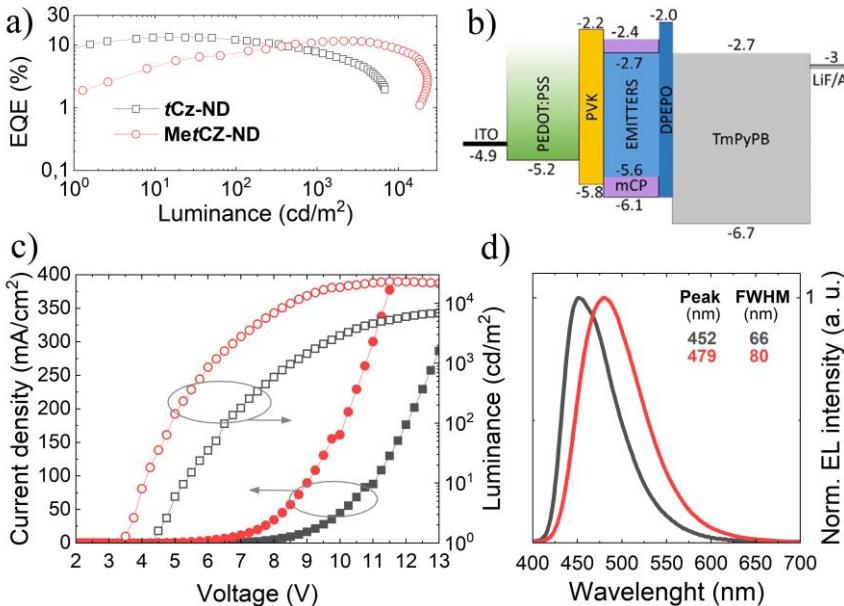
Fast efficiency roll-off of the **tCz-ND**-based devices can be linked to almost 3 times longer τ_{DF} than that measured for **Me*t*Cz-ND**. Long living triplets are increasing the probability of many detrimental annihilation processes like TTA and STA. Furthermore, the fast rISC and short τ_{DF} (3.1 μs) of **Me*t*Cz-ND** notably lowered the triplet population by rapid up-conversion to the singlet manifold resulting in less than 30% loss of device efficiency at the brightness of 1000 cd/m^2. At the time of publication of paper **A2**, these ND-based TADF OLEDs were among the best performing blue – deep-blue conventional D-A type TADF OLEDs in terms of the EQE and efficiency roll-off properties (see Table S5 in the ESI of the paper **A2**).

Table 4 Main parameters of vacuum- and solution-processed OLEDs based on the ND(7 wt%):mCP emissive layer. Turn-on voltage measured at 1 cd/m^2, EQE displayed as maximum EQE/ EQE at 100 cd/m^2/ EQE at 1000 cd/m^2.

Tech.	Emitter	V_{on} (V)	EQE (%)	L_{max} (cd/m^2)	λ_{max} (nm)	FWHM (nm)
Vac.	**tCz-ND**	3.25	17.0/ 9.9/ 7.0	8424	459	66
	Me*t*Cz-ND	3.25	17.6/ 14.4/ 12.5	21459	481	88
Sol.	**tCz-ND**	4.30	13.5/ 12.1/ 7.8	6840	452	66
	Me*t*Cz-ND	3.40	11.7/ 7.5/ 11.0	23028	479	80

Additionally, ND compounds were employed to fabricate solution-processed OLEDs. Devices were fabricated with the following layer configuration: ITO/ PEDOT:PSS (50 nm)/ PVK (15 nm)/ emitter (7 wt%):

mCP (25 nm)/ DPEPO (5 nm)/ TmPyPB (50 nm)/ LiF (0.8 nm)/ Al(100 nm). Here, PEDOT:PSS, PVK and emissive layers were deposited using spin-coating technique, and DPEPO and TmPyPB layers together with metallization were produced by vacuum deposition. As can be seen in **Fig. 12**, at high current densities the performance of solution-processed OLEDs was very similar to vacuum-processed devices. Even so, there are some device performance imperfections in terms of increased turn-on voltage and reduced EQE. These problems were attributed to the reduced homogeneity of the solution-processed layers and rather poor hole injection through PVK causing unbalanced electron and hole currents. Increasing the current density raises the EQE of the solution-processed OLEDs close the efficiency of the vacuum-processed devices indicating that the injection regime, close to optimal, is achieved. Recapitulating the demonstrated performance of all devices, we can confirm the suitability of the investigated naphthyridines to be employed not only in vacuum-processed OLEDs, but also as solution-processable deep-blue TADF emitters.

Fig. 12 Characteristics of solution-processed OLEDs based on the naphthyridine TADF emitters (7 wt% in mCP): (a) EQE vs. luminance, (b) energy level diagram, (c) current density and luminance vs. applied voltage, and (d) normalized electroluminescence spectra.
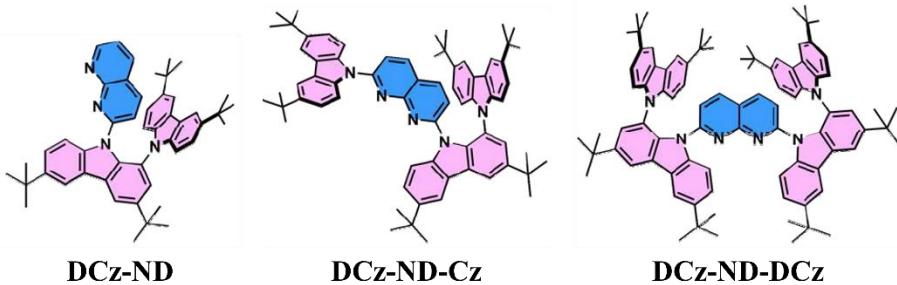
The obtained results imply that sterically controlled CT interactions combined with H-bonding can indeed be promising in attaining narrow deep-blue TADF by employing naphthyridine acceptors.

2.2. Naphthyridine based emitters with asymmetric carbazole-donor motif showing enhanced blue TADF

To dive deeper into naphthyridine-based TADF emitters with carbazole-based donors, we studied a series of ND compounds with variously substituted and positioned donors.

As mentioned above, having both the lowest singlet and triplet excited states to have strong CT character can highly reduce spin conversion, as following the El-Sayed's rule, the spin flip between purely CT states is forbidden [89], and also decrease radiative decay rate. To boost spin-orbit coupling, participation of close laying LE triplet state is needed. One of the methods to achieve such conditions is to design compounds with asymmetric D–A–D* architecture as they facilitate the formation of the mixed CT and LE states, thereby delivering efficient TADF [96], [97].

Here, 1,8-naphthyridine was employed as the electron acceptor in combination with 3,5-di-*tert*-butylcarbazole (D*) and sterically demanding 3,3',6,6'-tetra-*tert*-butyl-9H-1,9'-bicarbazole (D) donating units to create D-A, D-A-D and D-A-D* TADF emitters. Collected results indicate the advantage of the asymmetric molecule geometry, because of enhanced triplet-singlet conversion due to stronger LE character of the lowest triplet state. **Fig. 13** shows designed and synthesized ND-based TADF emitters. **DCz-ND** comprises of a ND A and a bulky D group, **DCz-ND-Cz** consists of a ND A enveloped by a bulky D and a compact D* groups and, finally, **DCz-ND-DCz** employs ND acceptor enclosed by two bulky D groups.

DCz-ND   DCz-ND-Cz   DCz-ND-DCz
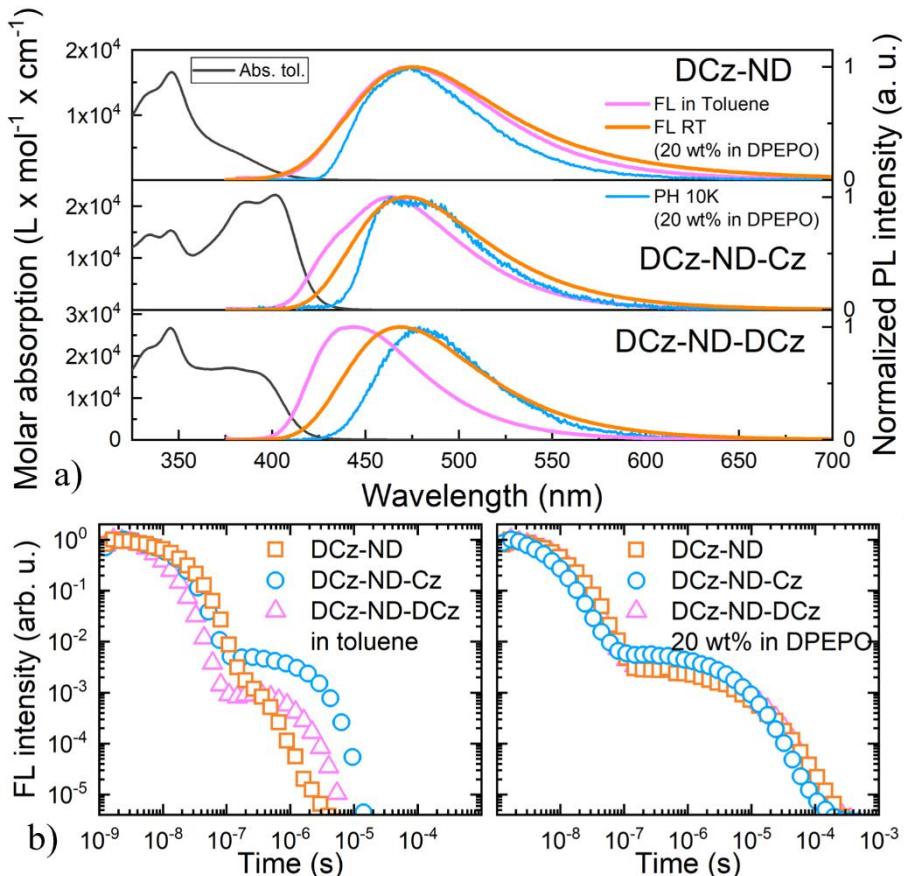
Fig. 13 Molecular structures of investigated naphthyridine compounds.

Time dependent DFT at the 6-31G(d) basis set level was employed to calculate ground to excited state transition energies (E) and oscillator strengths (*f*) and to obtain the HOMO and LUMO levels. For full details on DFT results please refer to the section 3.1 of the paper **A5**. Dihedral angles between carbazole fragments in DCz (67°) was larger than that formed between DCz and ND groups (47-50°). Remarkably smaller dihedral angle (36°) was

determined between Cz and ND fragments in **DCz-ND-Cz** compound. HOMO and LUMO are well separated in all three compounds with HOMO being localized on DCz groups and LUMO – on ND acceptor. Quite weak oscillator strength for transition $S_0 \rightarrow S_1$ was determined for all compounds, but importantly, strong oscillator strength for the $S_0 \rightarrow S_2$ transition was estimated only for **DCz-ND-Cz**, resulting in a more expressed LE character of this transition.

Absorption and fluorescence FL spectra of the investigated ND compounds in dilute toluene solutions are shown in **Fig. 14**. Summarized photophysical properties are displayed in **Table 5**.

**Fig. 14** Main photophysical characteristics of compounds **DCz-ND**, **DCz-ND-Cz** and **DCz-ND-DCz**: (a) absorption and fluorescence (1×10^{-5} mol L^{-1} in toluene), room temperature fluorescence (20 wt% in DPEPO) and phosphorescence (20 wt% in DPEPO at 10 K, delay time 100 ms) spectra and (b) FL transients of the emitters in degassed toluene and DPEPO at 20 wt%.

All ND compounds demonstrated sharp absorption peaks at 346 nm with well-resolved vibronic replicas typical for LE transitions associated with carbazole units. Most important differences in absorption were recorded at longer wavelengths, where **DCz-ND** exhibited broad and structureless CT-like absorption band, meanwhile **DCz-ND-Cz** displayed intense and vibronically-modulated absorption band at 401 nm, typical for LE transition [98], [99]. Most probably this was determined by the smaller dihedral angle between the compact D* group and ND acceptor. Additionally, **DCz-ND-DCz** showed a weaker, yet structured absorption with a peak at 377 nm.

Broad FL spectra of **DCz-ND** toluene solution that peaked at 474 nm confirmed the CT character of the lowest excited state governed by large separation of the HOMO and LUMO localized on a twisted DCz donor against the ND acceptor. Symmetric compound **DCz-ND-DCz** showed narrower and blue-shifted FL with maximum at 443 nm indicating suppressed relaxation of the excited state geometry due to a more rigid molecular structure. Interestingly, FL spectra of asymmetric compound **DCz-ND-Cz** were little bit structured and possessed a shoulder at higher energies and a broad, red-shifted CT-like band at 463 nm. This could be explained by the scenario where FL is visible simultaneously from the LE and CT states.

The FL spectrum of **DCz-ND** dispersed in DPEPO was very similar to that observed in toluene solution. Conversely, **DCz-ND-Cz**, and, particularly, **DCz-ND-DCz** in DPEPO exhibited broad and red-shifted FL (λ_{max} = 471 nm and 468 nm, respectively) indicating more effective stabilization of the CT state due to higher environment polarity as compared to its solution. ΔE_{ST} values were determined to be in the range of 120-130 meV for all three compounds and Φ_{PL} of **DCz-ND**, **DCz-ND-Cz** and **DCz-ND-DCz** in toluene solutions were found to be 0.19, 0.58, 0.33, respectively. PL QY values were highly enhanced in rigid DPEPO host at 20 wt%. The Φ_{PL} of **DCz-ND** reached 0.46, whereas Φ_{PL} values of 0.74 and 0.72 were estimated for **DCz-ND-Cz** and **DCz-ND-DCz**, respectively. Dispersion in DPEPO also increased the lifetimes of triplets, τ_{DF} resulted to be 6.0 and 7.0 μs for **DCz-ND** and **DCz-ND-DCz**, while **DCz-ND-Cz** exhibited shorter τ_{DF} of 4.4 μs, which is quite promising for applications.

Later, using the PL measurement data and formalism described earlier, most important TADF rates were estimated. Regardless of the similar ΔE_{ST} values obtained for the doped DPEPO films, the **DCz-ND-Cz** compound demonstrated a more than two-fold higher rISC rate (k_{rISC} = 1.33×10⁶ s⁻¹) than those observed for **DCz-ND** (k_{rISC} = 4.5×10⁵ s⁻¹) and **DCz-ND-DCz** (k_{rISC} = 4.9×10⁵ s⁻¹). The higher rISC rate of asymmetrically substituted **DCz-ND-Cz** can be justified by the stronger LE character of the T_1 state, which is expected

to facilitate triplet to singlet spin conversion due to the improved spin–orbit coupling with the S_1 state of CT character. Despite, all the studied compounds demonstrated rather short DF lifetimes (<10 μs), asymmetric **DCz-ND-Cz** additionally expressed a combination of fast rISC and relatively high radiative decay rate ($k_r = 1.91 \times 10^7$ s^{-1}), which is advantageous for the application as OLED emitter.
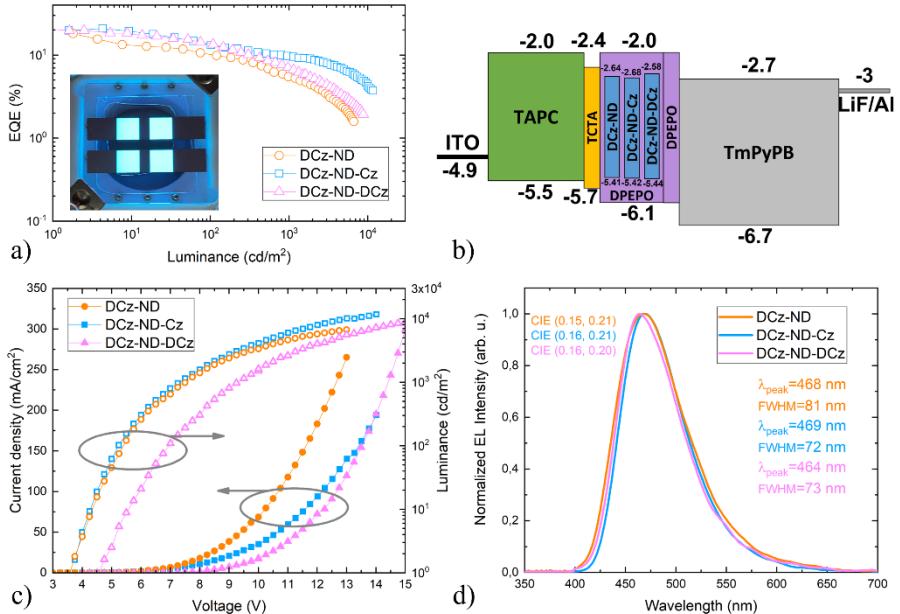
Table 5 Main photophysical properties of investigated naphthyridine toluene solutions and 20 wt% doped DPEPO films. Rates $\times 10^6$ s^{-1}.

Compound	Form	λ_{max} (nm)	Φ_{PL}	Φ_{DF}/Φ_{PF}	τ_{PF} (ns)	τ_{DF} (μs)	$k_r/k_{rISC}/k_{ISC}$
DCz-ND	Film	475	0.46	2.3	11.0	6.0	12.5/ 0.45/ 78
	Sol.	474	0.19	0.03	18.8	0.24	8.6/ 0.91/ 45
DCz-ND-Cz	Film	471	0.74	5.1	6.3	4.4	19.1/ 1.33/ 140
	Sol.	463	0.58	0.69	13.5	2.0	25.5/ 0.52/ 49
DCz-ND-DCz	Film	468	0.72	2.9	9.9	7.0	19.3/ 0. 49/ 82
	Sol.	443	0.33	0.12	8.2	1.5	34.1/ 0.12/ 82

Later, ND compounds were employed in the fabrication of blue TADF OLEDs. To directly link obtain device properties to emitter characteristics, the stacks for three different OLEDs were kept the same, except for the emitter employed. Emissive layers of OLEDs were constructed using 20 wt% doping concentration in DPEPO host, the same as for PL measurements. The main OLED characteristics are presented in **Fig. 15**, while the key parameters are summarized in **Table 6**. Devices were fabricated with the following OLED architecture: ITO/ TAPC (30 nm)/ TCTA (5 nm)/ emitter (20 wt%):DPEPO (20 nm)/ DPEPO (5 nm)/ TmPyPB (50 nm)/ LiF (0.8 nm)/ Al(100 nm).

All the fabricated devices displayed blue electroluminescence peaking at 468, 469 and 464 nm for **DCz-ND**, **DCz-ND-Cz**, **DCz-ND-DCz** devices, respectively, but the turn-on voltage was higher for **DCz-ND-DCz** devices than for other two (4.5 V *vs*. 3.75 V), this can be attributed to bulky DCz groups shielding ND acceptor and resulting in poor electron transport and overall imbalance of electron and hole currents in the device. **DCz-ND** based device demonstrated EL spectra with a FWHM of 81 nm, and the other two devices exhibited narrower emission with FWHM of 72 and 73 nm. CIE 1931 color coordinates of **DCz-ND, DCz-ND-Cz**, and **DCz-ND-DCz** devices were estimated to be (0.15, 0.21), (0.16, 0.21), and (0.16, 0.20), respectively.

OLEDs with **DCz-ND-Cz** and **DCz-ND-DCz** emitters exhibited the same maximum EQE of 20.8%, whereas the **DCz-ND** based device demonstrated a somewhat lower EQE$_{max}$ of 18.1%.

Fig. 15 Main characteristics of naphthyridine-based TADF-OLEDs: (a) EQE vs. luminance with a picture of a working **DCz-ND-Cz** device in the inset; (b) energy level diagram; (c) current density and luminance vs. applied voltage; and (d) EL spectra at 100 cd/m^2.

Since the emitter **DCz-ND-Cz** expresses the shortest τ_{DF} as well as the highest k_{rISC}, this emitter-based device demonstrates a relatively low efficiency roll-off. Besides that, **DCz-ND** emitter-based device suffers from the strongest EQE roll-off due to the longest living triplet species and the slowest rISC rate. EQE losses of **DCz-ND**, **DCz-ND-Cz** and **DCz-ND-DCz** based devices compared to their maximum efficiency are 45, 36 and 35%, respectively, at a luminance of 100 cd/m^2 and 70, 53 and 67%, respectively, at 1000 cd/m^2.

Table 6 Summarized main characteristics of fabricated OLEDs. EQE displayed as maximum EQE/ EQE at 100 cd/m^2/ EQE at 1000 cd/m^2.

Emitter	V_{on} (V)	EQE (%)	L_{max} (cd/m^2)	λ_{max} (nm)	FWHM (nm)	CIE 1931 (x, y)
DCz-ND	3.75	18.1/ 10.0/ 5.4	6666	469	81	(0.15, 0.21)
DCz-ND-Cz	3.75	20.8/ 13.2/ 9.6	11600	468	72	(0.16, 0.21)
DCz-ND-DCz	4.50	20.8/ 13.6/ 6.9	8816	464	73	(0.16, 0.20)

It is worth stressing that asymmetric **DCz-ND-Cz** based OLEDs exhibited the slowest EQE roll-off properties of these three ND emitters-based devices.

2.3. Summary of the results

Relying on H-bonding, sterically controlled CT interactions and asymmetrical donor architecture, blue/deep-blue TADF emitters based on D–A, D-A-D and D-A-D* carbazole–naphthyridine compounds have been developed.

In **§ 2.1** the TADF properties and emission wavelength and band-width of the ND derivatives were mainly governed by the CT strength of the D–A interaction, which could be controlled via methyl substituents introduced at the first linking position of t-butyl-carbazole donors. The less sterically hindered compound *t***Cz-ND** exhibited narrower and shorter wavelength blue TADF as compared to that of the more twisted methyl-substituted compound **Me*t*Cz-ND**, implying a trade-off between the reduced rISC and improved emissive properties. Importantly, the ND compounds were demonstrated to be suitable as TADF emitters for realization of vacuum- and solution-processed TADF OLEDs with low efficiency roll-off in sky-blue and deep-blue spectral ranges. The optimized devices with 7 wt% ND doped in a weakly polar mCP host delivered up to 17.6% and 13.5% EQEs for the vacuum- and solution-processed OLEDs, respectively.

In **§ 2.2** the assessed photophysical properties of the carbazole–naphthyridine derivatives revealed the advantage of the asymmetric donor motif in terms of close-lying CT and LE states with more pronounced LE character, which were also predicted by DFT calculations. The stronger mixing of the different molecular orbital possessing states ensured a 2-fold increased rISC rate (up to 1.33×10^6 s^{-1}) and a shortened delayed fluorescence lifetime (down to 4.4 μs) in the asymmetric donor compound **DCz-ND-Cz** compared to those of symmetric **DCz-ND-DCz** or singly-carbazole-substituted **DCz-ND** compounds. OLEDs employing asymmetric **DCz-ND-Cz** as the TADF emitter demonstrated a high external quantum efficiency of nearly 21% with a reduced efficiency roll-off promoting this asymmetric donor motif for exploitation in TADF-based light emitting devices.

3. OLEDs WITH LOW EFFICIENCY ROLL-OFF

This chapter is based on the research published in papers **A3** and **A4** about approaches to produce blue TADF OLEDs with high efficiency and low efficiency roll-off. Paper **A3** investigates OLEDs based on isophthalonitrile blue TADF emitters, here, simple emitter structure modification empowers substantial TADF OLED performance improvement. Paper **A4** relies on host molecule optimized for blue TADF emitters that allowed to realize low efficiency roll-off blue TADF OLEDs.
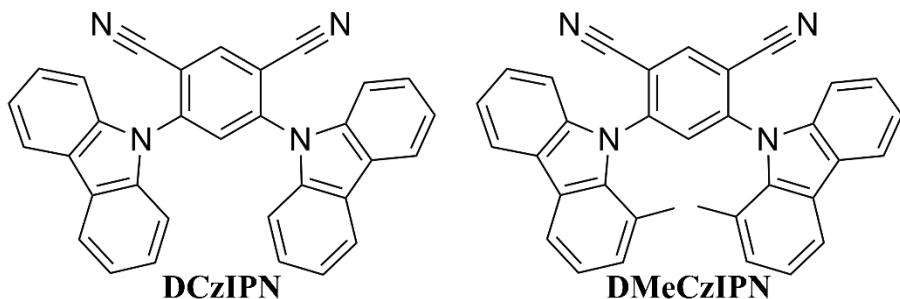
Motivation

Rational material design has enabled TADF-OLED devices with up to 100% internal quantum efficiencies mainly due to an efficient rISC that allows conversion of triplet excitons into emissive singlet states. However, in some organic systems, rISC is a slow process that occurs on a timescale of tens of microseconds [100]–[102]. This is considered as a significant drawback of TADF materials resulting in long-lasting delayed fluorescence, which causes undesirable singlet-triplet (STA) or triplet-triplet (TTA) annihilation in devices, particularly at high current densities. The latter typically results in well-pronounced efficiency roll-offs, thus notably increasing device power consumption at high brightness (>100 cd/m2), which is required for practical applications in OLED displays and lighting [103].

   Aside from emitters, host materials play an essential role in obtaining the desired performance of the OLED. Emitters are frequently doped in a host matrix to decrease detrimental bimolecular effects caused by longer-lived triplet states. The dilution into the host is thus essential to enhance the lifetime, increase the efficiency, and reduce the efficiency roll-off of the device. The hosts, in general, must have high and balanced charge carrier mobility, good thermal and morphological stability, and chemical stability. They also must have high triplet energy to confine the excitons on the emitter, which is particularly challenging for blue-emitting OLEDs [104].

3.1. High efficiency and low roll-off TADF OLEDs based on isophthalonitrile-derived emitters

As mentioned earlier, carbazole donors are preferred in the construction of compounds for OLED applications, since they exhibit good charge transport properties and superior stability. However, regarding its implementation in TADF emitters, carbazole demonstrates weaker electron donating properties and typically forms smaller dihedral angles (~40–50°) with an acceptor. This results in an enlarged ΔE_{ST} and subsequently slow rISC causing strong efficiency roll-off in OLEDs. There are many approaches to force carbazole donor to form larger dihedral angle. Here we are introducing a subtle donor modification (donor methylation) to TADF emitter containing two carbazole donors and isophthalonitrile acceptor. The change increased dihedral angle between sterically demanding D and A units and significantly reduced ΔE_{ST}, resulting in substantial boost of rISC rate and shortening of TADF lifetime. These features ensured superior performance of the modified TADF emitter in an OLED, delivering high efficiency and extremely low efficiency roll-off for the devices fabricated by both solution- and vacuum-process. **Fig. 16** shows the molecular structures of the investigated compounds. **DCzIPN** is used as original compound for comparison and **DMeCzIPN** is methyl-substituted TADF emitter.

DCzIPN   **DMeCzIPN**
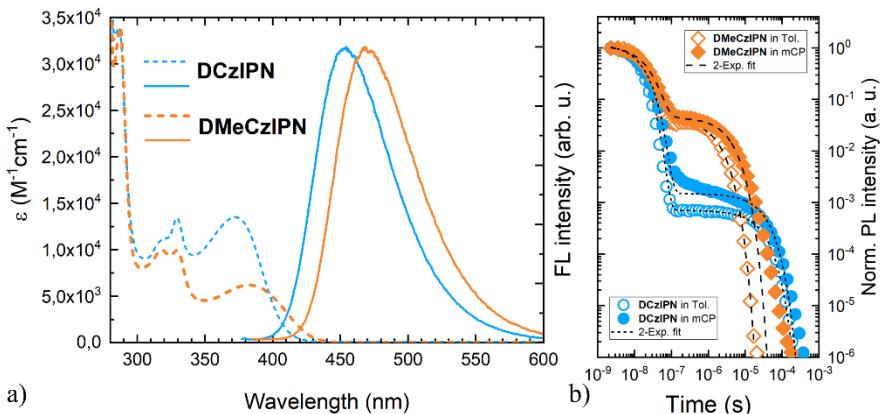
Fig. 16 Molecular structures of investigated isophthalonitrile compounds.

From the DFT calculations (for full details refer to ESI of the paper **A4**) dihedral angles and HOMO – LUMO distributions were obtained. Original compound **DCzIPN** showed obvious CT character with a distinct HOMO and LUMO separation between Cz donors and IPN acceptor. Dihedral angle between D and A groups was determined to be 52° mainly due to the steric hindrance imposed by the nitrile groups of IPN. The strong CT character determined moderately small ΔE_{ST} of 205 meV. Substituted compound **DMeCzIPN** containing sterically demanding methyl groups showed more

twisted molecular geometry with dihedral angles between D and A up to 70°. HOMO and LUMO separation was slightly larger than that for the original compound, significantly reduced ΔE_{ST} (133 meV) indicated substantially enhanced CT character of **DMeCzIPN**.

Absorption and fluorescence (FL) spectra of the investigated IPN derivatives in dilute toluene solutions are shown in **Fig. 17**. The detailed photophysical properties are summarized in **Table 7**. Both compounds exhibited sharp absorption peaks at 330 nm and 290 nm associated with local π-π* transitions of Cz and IPN fragments, respectively, as well as broad and structureless absorption bands at lower energies, 373 and 383 nm, attributed to CT-like $S_0 \rightarrow S_1$ transitions in **DCzIPN** and **DMeCzIPN**, respectively and similarly, broad and structureless FL emission bands peaking in the blue spectral range, at 453 nm and 470 nm, respectively, confirmed CT character of the lowest optical transitions of IPN compounds.

Fig. 17 Main photophysical characteristics of compounds **DCzIPN**, **DMeCzIPN** (a) Absorption (dashed line) and FL (solid line) spectra of IPN compounds in toluene (1×10^{-5} M). (b) FL decay transients of IPN compounds in toluene (empty symbols) and mCP host at 7 wt% concentration (solid symbols); double-exponential fits are shown as dashed lines.

FL quantum yields (ΦFL) of 0.40 and 0.44 were obtained for **DCzIPN** and **DMeCzIPN**, respectively, in degassed toluene solutions. Both compounds expressed oxygen-sensitive FL in solutions with well-resolved nanosecond time-domain PF and microsecond time-domain DF components in FL transients clearly indicating TADF behavior. Fitting the transient with double-exponential decay profiles allowed to estimate radiative decay rate and other important TADF related parameters, like k_{rISC} and k_{ISC}, following previously

described formalism with non-radiative decay associated only with triplet states.

Table 7 Main photophysical properties of investigated isophthalonitrile compounds in toluene solutions. Rates $\times 10^6$ s^{-1}.
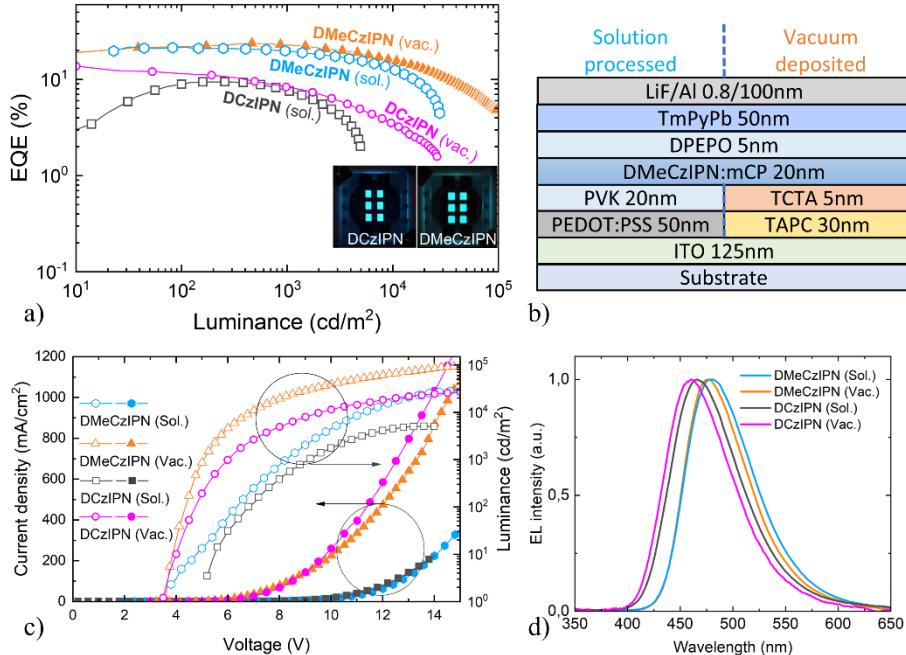
Compound	λ_{max} (nm)	Φ_{PL}	Φ_{DF}/Φ_{PF}	τ_{PF} (ns)	τ_{DF} (μs)	$k_r/k_{rISC}/k_{ISC}$	ΔE_{ST} (eV)
DCzIPN	453	0.40	1.8	12.1	29.4	11.7/ 0.07/ 70.9	0.19
DMeCzIPN	470	0.44	3.8	16.1	1.71	5.65/ 2.47/ 56.5	0.07

Toluene solution of **DCzIPN** exhibited long-lived DF (τ_{DF} = 29.4 µs) and fast PF (τ_{PF} = 12.1 ns) conditioning relatively small ratio of Φ_{DF}/Φ_{PF} (=1.8) because of rather high k_r (1.17×10^7 s^{-1}) and low k_{rISC} (7.0×10^4 s^{-1}). Notably, an introduction of methyl group at first position of carbazolyl in case of **DMeCzIPN** resulted in almost 35-fold boost of k_{rISC} (2.47×10^6 s^{-1}) with k_r (5.65×10^6 s^{-1}) reduced by 2-times only, determining short DF (τ_{DF} = 1.71 µs). The remarkable boost of k_{rISC} can be justified by significantly smaller ΔE_{ST} (70 meV) observed for **DMeCzIPN**, as compared to this value (190 meV) found for **DCzIPN**. S$_1$ and T$_1$ energies for determination of ΔE_{ST} were obtained from the onsets of FL and phosphorescence spectra of the investigated IPN emitters doped in mCP host at optimal 7 wt% concentration (see Fig 3 (b, c) of the paper **A3**).

DCzIPN-doped mCP films showed FL properties similar to those of toluene solutions (see Table S4 in ESI of the paper **A3**), i.e. Φ_{PL} slightly improved up to 0.51, whereas τ_{DF} remained virtually the same (30.8 µs). Conversely, Φ_{PL} of **DMeCzIPN** was notably enhanced up to 0.74 in mCP host followed by an increase of τ_{DF} up to 3.66 µs. Considering that k_{rISC} was insignificantly affected, it implies suppression of nonradiative triplet state deactivation in rigid mCP host as compared to solution.

The studied TADF emitters doped in mCP host at 7 wt% concentration were tested and compared in vacuum- and solution-processed OLEDs as the emissive layers. Solution-processing (e.g., ink-jet printing) offers multiple advantages such as easily scalable manufacturing, possibility to produce large-area devices as well as simple and low-cost fabrication. Solution-processed OLEDs based on **DCzIPN** and **DMeCzIPN** were fabricated by employing the following device architecture: ITO/ PEDOT:PSS (50 nm)/ PVK (20 nm)/ emitter (7 wt%):mCP 20 nm/DPEPO (5 nm)/ TmPyPB (50 nm)/LiF (0.8 nm)/Al (100 nm). The main characteristics of OLEDs are provided in **Fig. 18** and parameters are summarized in **Table 8**.

DCzIPN-based OLED turned on at 5.1 V showing blue EL peaking at 466 nm with full width at half maximum of 75 nm. The maximum EQE was determined to be 9.5% at 257 cd/m2, which fits well the Φ_{PL} of **DCzIPN** in mCP host. The fabricated device exhibited moderate efficiency roll-off resulting in EQE drop down to 7.6% at 1000 cd/m^2 and further decrease down to 2% at a maximum luminance of 4962 cd/m^2.

Fig. 18 Main characteristics of isophthalonitrile-based TADF-OLEDs: (a) EQE vs. luminance with a pictures of a working solution-processed devices in the inset; (b) Schematic representation of OLED structures fabricated by vacuum- and solution-processing; (c) current density and luminance vs. applied voltage; and (d) EL spectra at 1000 cd/m^2.

Solution-processed OLED based on **DMeCzIPN** exhibited lower turn-on voltage (3.8 V) and demonstrated sky-blue EL peaking at 478 nm with CIE color coordinates of (0.16, 0.30). The device reached significantly higher EQE$_{max}$ (21.6%) owing to increased Φ_{PL} of TADF emitter. Importantly, extremely low efficiency roll-off was attained for **DMeCzIPN**-based OLED, i.e., EQE was reduced only to 19.6% at 1000 cd/m^2 and maintained rather high value (12.7%) even at 10,000 cd/m^2. Moreover, the device was able to attain extremely high brightness ($L_{max} = 28007$ cd/m^2) while still demonstrating EQE of 4.5%. The superior performance, particularly the efficiency roll-off of

DMeCzIPN-based device *vs* that based on **DCzIPN**, can be justified by the enhanced k_{rISC} and shortened τ_{DF}. Large k_{rISC} facilitates shortening of τ_{DF}, and thus, reduction of triplet exciton concentration in the EML thereby limiting detrimental TTA and STA processes responsible for efficiency roll-off in TADF-OLEDs.

The investigated TADF emitters were also tested in fully vacuum-deposited OLEDs by using the following device structure: ITO/ TAPC (30 nm)/ TCTA (5 nm)/ emitter (7 wt%):mCP 20 nm / DPEPO (5 nm)/ TmPyPB (50 nm)/LiF (0.8 nm)/Al (100 nm). Here, PEDOT:PSS and PVK were replaced by vacuum-processable TAPC and TCTA for hole injection and electron blocking, respectively.

Table 8 Summarized main parameters of solution- and vacuum-processed OLEDs based on **DCzIPN** and **DMeCzIPN** in mCP host (7 wt%). Turn-on voltage measured at 1 cd/m2, EQE displayed as maximum EQE/EQE at 1000 cd/m2/EQE at 10000 cd/m2.
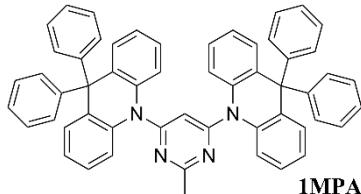
Device	V_{on} (V)	EQE (%)	L_{max} (cd/m^2)	λ_{max} (nm)	FWHM (nm)	CIE 1931 (x, y)
DCzIPN (sol.)	5.1	9.5/ 7.6/ -	4962	466	75	(0.16, 0.20)
DCzIPN (vac.)	3.5	13.3/ 8.3/ 3.4	26280	461	72	(0.15, 0.16)
DMeCzIPN (sol.)	3.8	21.6/ 19.6/ 12.7	28007	478	76	(0.16, 0.30)
DMeCzIPN (vac.)	3.5	23.8/ 22.6/ 16.9	95743	476	70	(0.16, 0.28)

The device based on **DCzIPN** demonstrated EQE$_{max}$ of 13.8%, higher as compared to the solution-processed analogue, and yet it still suffered from a severe efficiency roll-off. The EQE was reduced to 8.3% at 1000 cd/m^2 and down to 3.4% at 10,000 cd/m^2. The vacuum-processed device based on **DMeCzIPN** also performed slightly better as compared to the solution-processed device. The impressive EQE$_{max}$ of 23.8% was achieved with efficiency roll-off of only 5% and 29% at 1000 cd/m^2 and 10000 cd/m^2, respectively. The device was able to operate at extremely high brightness of 95743 cd/m^2 while still demonstrating EQE of 4.8%. Enhanced performance of vacuum-deposited OLEDs in respect to solution-processed counterparts can be explained mainly by improved charge carrier balance, which is indicated by lowered turn-on voltage (3.5 V) and obtained steeper I-V-L characteristic.

Outstanding performance of **DMeCzIPN**-based vacuum- and solution processed devices implies that TADF-OLEDs can be promising candidates even for applications that require extreme brightness (>1000 cd/m2), e.g., lighting.

3.2. Low efficiency roll-off OLEDs employing novel blue TADF optimized host material
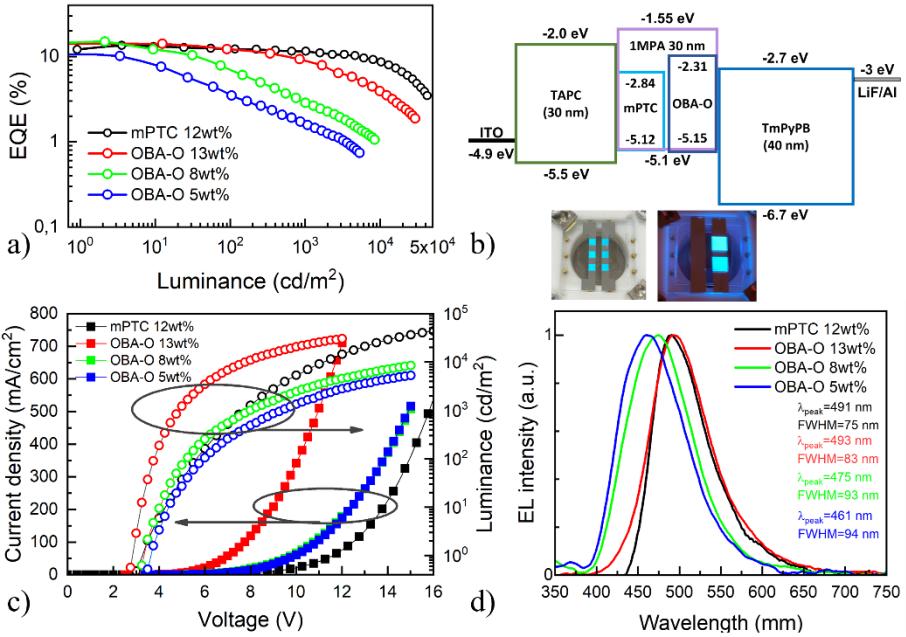
The development of efficient blue emitter–host combinations is one of the biggest challenges in (OLED) research. Host materials play a crucial role when it comes to enhancing the efficiency, improving the lifetime and reducing the efficiency roll-off of the device. The need for new hosts is of prime importance, especially TADF emitters, due to their high exciton energies. As a part of this dissertation, a novel host material with high triplet level of 3.07 eV, designed by carefully selecting donor and acceptor moieties and their linking patterns, is employed to fabricate blue TADF OLEDs with two previously reported emitters, namely, **mPTC** [105] and **OBA-O** [106]. **Fig. 19** shows the molecular structure of **1MPA** host material, that consists of methyl-substituted pyrimidine as an acceptor enclosed by acridine-derived donor moieties.


Fig. 19 Molecular structure of the investigated blue TADF optimized host.

HOMO and LUMO levels of **1MPA** host were obtained from the cyclic voltammetry and optical bandgap measurements (refer to the paper **A4** for details). Quite unusual values of those energy levels were determined with HOMO lying at -5.1 eV and LUMO – at -1.55 eV. For typical OLED materials HOMO level is -5.5 eV and below. Because of the shallow HOMO level, we had to look for blue TADF emitter with as well shallow HOMO. Two blue TADF emitters with aligning HOMO levels were picked with **mPTC** having HOMO level of -5.12 eV and **OBA-O** – of -5.15 eV.

When designing OLEDs, doping concentration of **mPTC** in **1MPA** was kept at 12 wt% based on photoluminescence quantum yield measurements (see Table S1 of the ESI of the paper **A4**). For the emitter **OBA-O** several doping concentrations (5, 8, and 13 wt%) were employed to examine the emission wavelength tunability of the device. OLEDs were fabricated using the following simple device architecture: ITO/ TAPC (30 nm)/ emitter (**mPTC** or **OBA-O**) (**x** wt%):**1MPA** (30 nm)/ TmPyPB (40 nm)/ LiF (0.8nm)/ Al (100 nm). The main device characteristics are provided in **Fig. 20** and working parameters are summarized in **Table 9**.

Fig. 20 Main properties of the TADF OLED based on the **1MPA** host doped with **mPTC** or **OBA-O** emitters. (a) EQE vs. luminance; (b) Energy level diagram with picture of working device shown below(left – mPTC and right – OBA-O); (c) Current density and luminance vs. applied voltage; (d) Electroluminescence spectrum.

The OLED with **mPTC** demonstrated a low turn-on voltage of 3.25 V, greenish-blue electroluminescence at 491 nm with FWHM of 75 nm resulting CIE coordinates of (0.2, 0.4). EQE_{max} was determined to be 13.6%, which is in good agreement with PLQY of **mPTC** in **1MPA**. The fabricated device exhibited low efficiency roll-off at practically useful brightness, at 100 cd/m^2 EQE dropped down to 12.3% and to 11.6% at 1000 cd/m^2. Notably, EQE remained above 10% up to the very high brightness of 5000 cd/m^2. This behavior could be explained by the optimal device architecture and well-balanced electron and hole currents. The maximum luminance achieved by the device was nearly 44 000 cd/m^2.

The **OBA-O** device with a similar doping concentration (13 wt%) as the one based on **mPTC** expressed comparable emission properties. Explicitly, peak emission wavelength, bandwidth, CIE color coordinates, and maximum EQE were found to be alike. On the other hand, much steeper I-V and L-V curves of the **OBA-O** device indicate a significantly improved charge carrier mobility in the EML. Reducing **OBA-O** concentration down to 5 wt% in the

EML shifted emission wavelength from greenish-blue (493 nm) to deep-blue (461 nm), demonstrating the potential of **1MPA** to host deep-blue TADF emitters. Picture of the deep-blue emitting OLED is shown in the **Fig. 20 (b)**. The reduced emitter concentration concomitantly caused a broadening of emission bandwidth (up to 94 nm) and an accelerated EQE roll-off. In OLEDs, EQE roll-off typically arises from exciton–polaron quenching and from exciton–exciton annihilation. The increased roll-off with lower emitter concentrations can arise from either effect. Since there is a barrier of about 1.15 eV for electron injection onto the host yet not for injection onto the emitter, the likely scenario is that electron transport proceeds by hopping between emitter molecules while hole transport occurs via the host, where hole injection is barrier-free This results in a charge carrier imbalance that favors exciton–hole quenching. However, at low emitter concentrations percolative transport across emitting sites is no longer possible, so that the recombination zone narrows towards the electron injecting side. This decrease in recombination zone implies an increase of both exciton and charge carrier density, so that in addition to exciton–hole quenching there can also be a contribution from triplet–triplet annihilation. It is worth noting that the dominant lifetime of delayed fluorescence in **mPTC** (2 μs) is shorter than that in **OBA-O** (9 μs), consistent with its lower susceptibility to exciton quenching processes.

Table 9 Summarized main parameters of **1MPA** host-based OLEDs with **mPTC** and **OBA-O** emitters. Turn-on voltage measured at 1 cd/m2, EQE displayed as maximum EQE/EQE at 100 cd/m2/EQE at 1000 cd/m2.

Device	V_{on} (V)	EQE (%)	L_{max} (cd/m^2)	λ_{max} (nm)	FWHM (nm)	CIE 1931 (x, y)
mPTC (12 wt%)	3.25	13.6/ 12.3/ 11.5	43911	491	75	(0.2, 0.4)
OBA-O (13 wt%)	2.75	14.2/ 11.9/ 8.9	30247	493	83	(0.2, 0.38)
OBA-O (8 wt%)	3.25	14.9/ 6.8/ 2.9	8449	475	93	(0.16, 0.21)
OBA-O (5 wt%)	3.5	10.6/ 3.5/ 1.6	5283	461	94	(0.16, 0.18)

The obtained results show that high-triplet-energy host **1MPA** is suitable for the fabrication of efficient blue TADF OLEDs, delivering low efficiency roll-off even beyond the practical brightness of 1000 cd/m^2.

3.3. Summary of the results

Aiming for enhanced TADF performance, the structure of earlier reported isophthalonitrile-based TADF emitter **DCzIPN** was modified by introducing methyl substituents at 1-position of carbazole donors to cause increased D-A twisting. The modified blue-emitting compound **DMeCzIPN** expressed significantly reduced ΔE_{ST} (down to 70 meV) and impressive 35-fold boost of k_{rISC} (up to 2.47×10^6 s^{-1}). Fast rISC and high PL QY ($\Phi_{PL} = 0.74$) of **DMeCzIPN** in mCP host accompanied by good compound solubility enabled the realization of highly efficient (EQE$_{max}$ = 21.6%) solution-processed blue OLED. Furthermore, the fabricated device delivered exceptionally low efficiency roll-off preserving high EQE of 19.6% and 12.7% at 1000 cd/m^2 and an extreme brightness of 10,000 cd/m^2. Such low efficiency roll-off of the device was mainly attributed to the short DF lifetime ($\tau_{DF} = 3.66$ μs) of **DMeCzIPN**, which allowed to suppress detrimental exciton annihilation processes in the emissive layer. Importantly, the performance of the device was found to be comparable to its vacuum-deposited analogue and was among the best solution-processed TADF-OLEDs (in terms of EQE and efficiency roll-off properties) reported in literature. The obtained results demonstrate the potential of isophthalonitrile-based TADF emitters for high-brightness OLED applications such as displays and lighting.

As host materials with high triplet energy and good thermal stability properties are still under development, here, we proposed host material, named **1MPA**, constructed by using D-A-D architecture with methyl-substituted pyrimidine as an acceptor enclosed by acridine-derived donor moieties. **1MPA** was employed as the host material to fabricate blue TADF OLEDs. Using the emitter **mPTC** sky-blue OLED with electroluminescence at 491 nm and a maximum EQE of 13.6%, combined with a low roll-off, was fabricated. The host **1MPA** is also shown to be suitable for deep-blue emitters like **OBA-O**, delivering blue OLEDs with color coordinates of (0.16, 0.18).

CONCLUSIONS

1. Method to suppress the triplet quenching in TADF compound possessing benzophenone acceptor with loose phenyl moiety was suggested. The method relies on replacing the loose moiety with methoxy group and enables to suppress the non-radiative triplet quenching by one order of magnitude thereby enhancing the k_{rISC}/k_{nr}^{T} ratio yet maintaining an unchanged k_{rISC}. This benefits in complete harvesting of the triplets via the rISC resulting in almost unity PL QY and outstanding maximal EQE values (up to 24.6%) of OLEDs.

2. To reduce the ΔE_{ST} of the TADF emitter designed by employing *tert*-butyl-carbazole donors and naphthyridine acceptor (*t*Cz-ND), H-bonding and sterically controlled CT interactions methods were employed. Modification by methylation of D units of *t*Cz-ND at the first linking positions allowed to boost rISC rate more than three times by lowering singlet – triplet gap without altering radiative decay rate. Investigated **ND** compounds were also shown to be suitable as TADF emitters not only in vacuum-, but also in solution-processed blue OLEDs.

3. Asymmetric carbazole-donor configuration versus symmetric one is advantageous for blue-emitting naphthyridine-acceptor based TADF compounds as it facilitates spin-flip process due to the pronounced LE character of the lowest triplet state. The stronger mixing of CT and LE states ensures 2-fold increased rISC rate and shortened delayed fluorescence lifetime, thereby suppressing EQE roll-off in the OLEDs.

4. The methylation of carbazole donors in isophthalonitrile-carbazole (D-A-D type) TADF emitter increases the dihedral angle between the D and A groups, hence reducing ΔE_{ST} and increasing the rISC rate by 35 times. TADF devices based on modified isophthalonitrile compound, **DMeCzIPN**, fabricated by vacuum- and solution-processing exhibited EQE$_{max}$ of 23.8% and 21.6%, respectively, with extremely low efficiency roll-off.

5. New acridine-pyrimidine derived host material (**1MPA**) optimized for blue TADF emitters, was designed by careful D and A fragment selection and direct D-A linking. High-triplet-energy possessing **1MPA** was employed to host two blue TADF emitters with shallow HOMO levels and was shown to enable high efficiency and low roll-off properties in the OLED devices.

SANTRAUKA LIETUVIŲ KALBA

Šiuolaikinėje visuomenėje kasdienybė ir bendravimas neįsivaizduojami be ekranų ir informacijos pateikimo juose. Daugelis žmonių vakarus leidžia prie televizorių, planšetiniu kompiuteriu skaito „laikraščius" ir naudodamiesi vaizdo skambučių paslaugomis kalbasi vieni su kitais per šimtų ar tūkstančių kilometrų atstumą. Nė vienas iš šių dalykų nebūtų įmanomas be ekranų.

Viena iš patraukliausių ekrano technologijų tipų yra organiniai šviesos diodai (OLED). Štai keletas OLED ekranų pranašumų, palyginti su LCD ekranais: 1. pagerinta vaizdo kokybė dėl geresnio kontrasto, didesnio ryškumo, platesnio spalvų diapazono ir daug didesnio atnaujinimo dažnio; 2. Mažesnis energijos suvartojimas; 3. Paprastesnis dizainas, leidžiantis sukurti labai plonus, lankščius ir net skaidrius ekranus [1]–[4]. Todėl gamintojai OLED ekranus savo įrenginiuose bando įdiegti jau daugiau nei 20 metų. Pirmasis plataus vartojimo produktas su komercializuotais OLED buvo Pioneer prekės ženklo automobilių radijo pultas, turėjęs pasyvios matricos OLED ekraną [4]. Vėliau, 2003 m., garsi fotokamerų kompanija Kodak išleido skaitmeninį fotoaparatą, kuris buvo pirmasis gaminys su aktyvios matricos AMOLED ekranu [5]. Po kelerių metų, 2008 m., „Nokia" paskelbė apie pirmąjį masinės gamybos mobilųjį telefoną su AMOLED ekranu (N85), o 2010 m. „Samsung" pradeda ilgiausiai veikiančią (jau daugiau nei trylika metų) „Galaxy" seriją su išmaniojo telefono modeliu S, ši serija buvo gaminama išskirtinai. su OLED ekranais nuo pat pradžių [6]. Šiandien, „Samsung" tiesiog dominuoja išmaniųjų telefonų OLED ekranų rinkoje su maždaug puse visos rinkos mažų ir vidutinio dydžio OLED ekranų su Samsung pavadinimu, „LG displays" savo ruožtu didžiausias pasaulyje OLED technologijos televizorių gamintojas su daugiau nei 60% rinkos. [7], [8].

Buitinės elektronikos verslas yra didžiulis, nes yra labai daug vartotojų, kurie kas antrus metus nori naujų prietaisų. Dėl šios priežasties OLED ekranų rinka sparčiai auga ir padvigubėja kas ketverius metus [9]. „Display Supply Chain Consultants" apskaičiavo, kad 2022 m. bus pagaminta daugiau nei 1 milijardas vienetų OLED ekranų, o bendros OLED rinkos pajamos sieks beveik 50 milijardų JAV dolerių [10]. Dar 50 milijardų JAV dolerių šiuo metu yra užrakinta televizijos rinkoje, nes tik 7 procentus visos TV rinkos sudaro OLED, prognozuojama, kad po dešimties metų OLED televizoriai sudarys mažiausiai 15 procentų TV rinkos ir pridės dar 10 milijardų JAV dolerių prie OLED rinkos pajamų. Apibendrinant galima pasakyti, kad kiekvienas žmogus iš išsivysčiusių šalių naudoja mažiausiai 4 skirtingus įrenginius, o daugelis jų paremti OLED technologijos ekranais. Didžiulei rinkai reikia ne tik didžiulių

pramonės pajėgumų, bet ir didelio mokslo bendruomenės indėlio, siūlant naujas medžiagas, pažangias technologijas ir ateities perspektyvas.

Nepaisant to, kad OLED technologija dominuoja išmaniųjų telefonų rinkoje ir siekia užvaldyti kitus sektorius, OLED bendruomenė vis dar susiduria su daugybe iššūkių. Kai kurie iš jų yra grynai inžinerinės problemos, pavyzdžiui, kaip ekraną padidinti ar kaip padaryti geresnę skiriamąją gebą? Tačiau dauguma problemų, su kuriomis susiduriama, yra susijusios su fizika, ar tai būtų skleidžiamos spalvos grynumas, šviestukų efektyvumas, stabilumas ir panašiai [11].

Svarbiausias OLED komponentas yra šviesą emituojanti medžiaga. Įprastai vadinama emiteriu. Nuo OLED atsiradimo yra išskiriamos trys pagrindinės emiterių kartos [12]. Pirmoji karta, vadinama fluorescenciniais emiteriais, gali sėkmingai panaudoti iki 25 % elektrinių sužadinimų. Antrosios kartos, fosforescentiniai, emiteriai gali išnaudoti 100% sužadinimų, tačiau dėl sudėtingos sintezės ir tauriųjų metalų, tokių kaip platina, paladis ar iridis, poreikio, 2 kartos emiteriai yra labai brangūs [13], [14]. Prieš dešimtmetį buvo pristatyti naujos kartos emiteriai [15]. Procesas slypintis už 3-osios kartos emiterių, buvo pavadintas Šiluma Aktyvuota Uždelsta Fluorescencija (angl. - TADF). Dėl išmanios molekulinės sintezės TADF emiteriai gali išnaudoti 100 % sužadinimų, nereikalaujant jokių brangių elementų, tad tokius emiterius pagaminti yra pigu ir jie gali būti labai efektyvūs.

Pažvelkime šiek tiek giliau į OLED emiterius. Elektrinio sužadinimo metu tik 25% visų eksitonų susidaro kaip „šviesūs" singletai, ir net 75% – kaip „tamsieji" tripletai [16]. 1-osios kartos emiteriai gali panaudoti tik singletinius sužadinimus, tačiau tripletai visam laikui prarandami nelygioje kovoje su kvantine mechanika. Jei sulygiuotume 1-osios kartos emiterio singleto ir tripleto energijos lygmenis taip, kad du tripletai būtų labai arti vieno singleto energijos, galėtume pasiekti naudingas tripleto-tripleto anihiliacijos (TTA) sąlygas, kai du tripletiniai eksitonai yra paverčiami vienu singletiniu eksitonu [17]. Šis procesas gali pridėti dar 37,5%, o vidinis emiterio efektyvumas pasiekia 62,5% [18], [19]. Kaip minėta aukščiau, 2-osios kartos emiteriai gali panaudoti 100% eksitonų, dėl sustiprintos interkombinacinės konversijos, kurią palengvina sunkaus metalo atomo efektas, singletai paverčiami tripletais ir iš čia efektyviai rekombinuoja spinduliniu būdu [20]. Išmanioji molekulinė inžinerija leido suvienodinti singletų ir tripletų energijos lygmenis ir padedant terminei energijai, efektyviai versti tripletinius sužadinimus į singletinę būseną, kur singletai efektyviai panaudojami šviesos gaminimui. Manoma, kad tokio tipo spinduliuotės yra OLED technologijų ateitis, tačiau vis dar reikia atlikti tikrus tyrimus, kad būtų galima rasti būdą, kaip gaminti efektyvius mėlynus 3 kartos OLED.

Šios disertacijos tikslas

Norėdami gaminti efektyvius OLED, turime ištirti būdus, kaip valdyti ir panaudoti „tamsiąsias" tripletines būsenas. Kadangi žalias ir raudonas TADF OLED yra pasirengę patekti į rinką, mokslo bendruomenė turi rasti efektyvius ir stabilius mėlynus TADF spinduolius ir panaudoti juos optimizuotose OLED konfigūracijose.

Pagrindinis šio darbo tikslas buvo sukurti naujus ir efektyvius mėlynus emiterius, pasižyminčius šiluma aktyvuojama uždelstąja fluorescencija, ir pritaikyti juos didelio našumo OLED gamybai naudojant vakuuminio garinimo ir liejimo iš tirpalo technologijas. Norint pasiekti tikslą, buvo iškeltos kelios užduotys:

1. Sukurti naujus TADF spinduolius su mėlyna emisija ir įvertinti tripletų įtaką bendrai emisijai.

2. Įvertinti svarbiausius naujai susintetintų emiterių TADF parametrus ir nustatyti kiekvienam iš emiterių tinkamiausias funkcines medžiagas OLED.

3. Suprojektuoti OLED struktūras su atitinkamais funkciniais sluoksniais, pagaminti TADF šviestukus ir charakterizuoti veikiančius įrenginius.

4. Išanalizuoti surinktus rezultatus ir, jei reikia, optimizuoti OLED struktūrą, kad pagerintumėte įrenginio veikimą.

Naujumas ir svarba

Siekiant padidinti mėlynųjų TADF šviestukų, pagrįstų benzofenono akceptoriumi, našumą, buvo pasiūlytas naujas tripletų gesinimo mažinimo metodas. Laisvos fenilo dalies pakeitimas metoksi grupe leido nuslopinti tripletinių būsenų gesinimą ir pasiekti beveik šimtaprocentinį kvantinį našumą.

Pasiektas aukštas izoftalonitrilo pagrindu pagaminto OLED našumas, atsižvelgiant į EQE ir efektyvumo mažėjimą buvo vienas geriausių iš tirpalo pagamintų TADF šviestukų, spinduliuojančių mėlynos spalvos spektro diapazone, ir buvo panašus į geriausius žalius prietaisus. Tai ypač aktualu šioje srityje, nes parodo pasiektą pažangą ir ekonomiškos gamybos iš tirpalo technologijos potencialą.

Pramonė reikalauja sodriai mėlynos spalvos ($\lambda_{max} < 460$ nm) ir siauros juostos TADF spinduolių, kad būtų galima pagaminti pilnai TADF ekranus, tačiau efektyvių emiterių su mažu našumo nuokryčiu kūrimas yra labai sudėtingas. Naftiridino pagrindu pagaminti TADF emiteriai su karbazolo

pagrindo donorais leido pagaminti didelio našumo siauros juostos giliai mėlynus OLED ir buvo vieni iš geriausiai veikiančių įprastinių D-A tipo mėlynos/giliai mėlynos spalvos TADF emiterių pagal našumo ir našumo nuokryčio savybes šviestukuose.

Ginamieji teiginiai

1. Nespindulinis tripletinių eksitonų gesinimas nulemtas laisvo fenilo fragmento benzofenono pagrindo TADF emiteriuose yra efektyviai nuslopinamas pakeičiant laisvąjį fenilo žiedą į metoksi grupę ir taip pasiekiant beveik 100% fluorescencijos našumą.

2. Karbazolo donoro *metilinimas* pirmoje padėtyje paskatina intramolekulinį sukimąsi taip sumažindamas iš karbazolo-naftiridino ir karbazolo-izoftalonitrilo gautų TADF junginių singleto-tripleto energijų tarpą, todėl padidėja TADF indėlis ir pagerėja emisijos kvantinė išeiga (iki 86 %).

3. Asimetriškas karbazolo donoro motyvas, palyginti su simetriniu, palengvina krūvio pernašos (CT) ir lokaliai sužadintos (LE) tripletinės būsenos maišymąsi naftiridino akceptoriaus pagrindu sukurtuose TADF emiteriuose; tai padvigubina RISC spartą (iki $1,3 \times 10^6$ s^{-1}) ir sutrumpina uždelstos fluorescencijos gyvavimo laiką (iki 4,4 µs), todėl gaunami didelio efektyvumo OLED (išorinis kvantinis efektyvumas 21 %) su sumažintu našumo nuokryčiu.

4. Naujoviška akridino(D)-pirimidino(A) pagrindo matrica *betiltelinėje* D-A konfigūracijoje su aukštu tripletiniu lygmeniu(>3eV) yra tinkama ypač mažo našumo nuokryčio mėlynų TADF šviestukų gamybai.

Disertacijos išdėstymas

Ši disertacija parašyta kaip straipsnių rinkinys, kurio 1–3 skyriuose pateikiami pagrindiniai publikacijų akcentai. Publikacijos yra žymimos **A1** – **A5** chronologine paskelbimo tvarka.

Pirmajame skyriuje, remiantis straipsniu **A1**, aptariamas plačiai naudojamo benzofenono akceptoriaus, kaip tripletinių sužadinimų gesiklio, vaidmuo, siūlomas sprendimas, kaip šį gesinimą slopinti, ir parodoma gili įžvalga apie emiterio eksitoninius procesus. Antrasis skyrius yra pagrįstas moksliniais darbais **A2** ir **A5**. Šiame skyriuje analizuojame skirtingai pakeistų naftiridino akceptorių ir karbazolo donorų mėlynųjų TADF spinduolių OLED.

Diskutuojama apie TADF parametrų ir OLED veikimo parametrų priklausomybę nuo emiterio architektūros. Galiausiai, trečiajame skyriuje, paremtame moksliniais tyrimais **A3** ir **A4**, aptariami galimi būdai, kaip įgyvendinti OLED prietaisu su mažu efektyvumo nuokryčiu. Kai eksitonų tankis didelis, gali vykti kai kurie anihiliacijos procesai, pvz., tripleto-tripleto anihiliacija, singleto-tripleto anihiliacija. Anihiliacijos procesai sumažina eksitonų skaičių ir dėl to sumažėja OLED efektyvumas esant dideliam srovės tankiui. Vienas iš sprendimų, kaip išlaikyti aukštą efektyvumą esant dideliam srovės tankiui, yra sudaryti sąlygas labai greitai atbulinei interkombinacinei konversijai arba pašalinti tripletinių eksitonų slopinamo matricos molekulėse sąlygas.

Autoriaus indėlis

Autorius pagamino visus ir kiekvieną šioje disertacijoje pateikiamą OLED. Atlikti medžiagų nusodinimo kalibravimo eksperimentai, sukurtos atskirų OLED prietaisų konfigūracijos, ištirti OLED prietaisų veikimo parametrai naudojant modernią matavimo techniką, išanalizuoti rezultatai ir pasiūlyti struktūros konfigūracijos pakeitimai, siekiant pagerinti prietaisų veikimo parametrus, ir vėl pagaminti prietaisai bei ištirtos jų charakteristikos. Viename moksliniame darbe su optimizuotais OLED prietaisais buvo pagaminta apie 20 OLED partijų, šiek tiek pakeičiant sluoksnių konfigūraciją. Kiekvieną partiją sudaro mažiausiai 6 padėklai su 6 šviečiančiais taškeliais, susumuojant, pagaminta daugiau nei 3600 atskirų pikselių ir didelis jų kiekis ištirtas.

Autorius taip pat pagamino bandinius foto-fizikiniams tyrimams ir atliko kai kuriuos foto-fizikinius matavimus.

Šioje disertacijoje pateiktų molekulių sintezė buvo atlikta trijose skirtingose organinės chemijos grupėse, kurioms vadovauja prof. Edvinas Orentas (Vilniaus universitetas), prof. Juozas V. Gražulevičius (Kauno technologijos universitetas) ir prof. Peter Strohriegl (Bayreuth universitetas). DFT modeliavimą atliko dr. Gediminas Kreiza (Vilniaus universitetas) ir Stavros Athanasopoulos (Madrido Karlo III universitetas), foto-fizikinį naujų junginių charakterizavimą atliko dr. Gediminas Kreiza (Vilniaus universitetas), Justina Jovaišaitė (Vilniaus universitetas), Karolina Maleckaitė (Vilniaus universitetas) ir Francesco Rodella (Bayreuth universitetas). Kristalografinę analizę atliko dr. Gediminas Kreiza (Vilniaus universitetas).

Autorius dėkoja visiems kolegoms už jų nuoširdų indėlį.

Tripletų nespindulinio gesinimo slopinimas

Efektyvi TADF priklauso nuo našios atbulinės interkombinacinės konversijos (angl. – rISC) tripletinius sužadinimus verčiančios singletiniais. rISC proceso sparta turi būti didesnė nei nespindulinės tripletų relaksacijos sparta. Jei nespindulinis tripletinių sužadinimų gesinimas nevyksta arba vysta lėtai – net ir su maža rISC proceso sparta galima pasiketi efektyvų TADF. Kai santykis tarp atbulinės interkombinacinės konversijos ir nespindulinės tripletų relaksacijos ($k_\text{rISC}/k_\text{nr}^\text{T}$) yra didelis, dauguma tripletinių eksitonų galima panaudoti efektyviai TADF emisijai.

Benzofenono grupė plačiai naudojama mėlynuosiuose TADF emiteriuose kaip akceptorius [74]–[77]. Buvo įrodyta, kad benzofenono fragmentas yra kaltas dėl nespindulinio tripletinių eksitonų gesinimo [75], [77], [78], kai benzofenonas yra jungiamas su kitais TADF molekulės fragmentais taip, kad vienas fenilo žiedas yra paliekamas laisvas. Tripletų nespindulinė relaksacija vyksta per intramolekulinius pasisukimus ir virpesius [79] ir negali būti užslopinti net ir kietoje būsenoje, todėl TADF spinduoliai nesiekia 100% vidinio našumo [75], [80]. Tikimasi, kad išsprendus nespindulinio tripletų gesinimo problemą, pagerės TADF parametrai ir atitinkamai benzofenono pagrindo šviestukų našumas.

Norėdami įvertinti, kaip benzofenono sukeltas tripletinių eksitonų gesinimas gali būti slopinamas, publikacijoje **A1**, pasiūlėme nespindulinio gesinimo slopinimo variantą ir ištyrėme, kaip skiriasi molekulių su laisvu fenilo žiedu benzofenono fragmente ir patobulintos molekulės savybės, įskaitant TADF. Vienas junginys, pavadinimu **5tCzBP**, buvo sukurtas su benzofenono akceptoriumi ir šiame tyrime buvo laikomas tripletus gesinančiu etalonu, o antrasis junginys, pavadintas **5tCzMeB**, turėjo modifikuotą iš fenono išvestą metilbenzoato akceptorių. Spinduolių molekulinės struktūros yra pateiktos **Fig. 5** paveikslėlyje.

Buvo atlikti išsamūs sugerties spektroskopijos, stacionarios bei laikinės fotoliuminescencijos spektroskopijos tyrimai įvairiuose terpėse (mažos koncentracijos tolueno tirpalai, kieta DPEPO medžiagos matrica, grynas emiterio sluoksnis). Apdorojus PL matavimų rezultatus ir pasitelkiant literatūroje aprašytą formalizmą [50] buvo suskaičiuoti įvairių vyksmų našumai ir spartos (pradinės ir uždelstosios fluorescencijų našumai, interkombinacinių konversijų našumai, singletų spindulinės relaksacijos sparta, interkombinacinių konversijų spartos, tripletų nespindulinės relaksacijos sparta).

Paaiškėjo, kad modifikuotas spinduolis **5tCzMeB** demonstruoja tris kartus didesnę singletų spindulinės relaksacijos spartą nei originalus spinduolis

5tCzBP. Ir nors rISC proceso sparta ženkliai nepasikeitė, 10 kartų sumažėjo tripletų nespindulinės relaksacijos sparta (**5tCzBP** emiteriui $k_{nr}^T = 3.3 \times 10^6$ s^{-1} ir **5tCzMeB** spinduoliui $k_{nr}^T = 0.33 \times 10^6$ s^{-1}). Lėta tripletų gesinimo sparta leidžia konvertuoti daugiau tripletinių eksitonų į singletinę būseną ir panaudoti juos šviesos generavimui. Žvelgiant detaliau, tolueno tirpale pavienės **5tCzBP** molekulės demonstravo 4% uždelstosios fluorescencijos našumą, pakeitus laisvąjį fenilo žiedą metoksi grupe, molekulė **5tCzMeB** tolueno tirpale turėjo beveik aštuonis kartus didesnį TADF našumą. O patalpinus šias spinduolių molekules į kietą DPEPO matricą ir dar labiau apribojus virpesinį gesinimą buvo pasiektas beveik 100% našumas modifikuotoje molekulėje ir kiek daugiau nei 50% našumas **5tCzBP**.

Dėl labai aukšto modifikuotos molekulės našumo tiek DPEPO medžiagos matricoje, tiek ir gryname sluoksnyje buvo patikrintas šių medžiagų veikimas organiniuose šviestukuose. Naudojant technologiškai pažangiausią terminio garinimo vakuume metodiką buvo pagaminti gryno emisinio sluoksnio šviestukai ir šviestukai su legiruotu emisinio sluoksniu. Tokia OLED sluoksnių konfigūracija buvo pritaikyta šviestukų formavimui: ITO/ NPB (30 nm)/ TCTA (20 nm)/ CzSi (10 nm)/ **EML** (20 nm)/ DPEPO (10 nm)/ TPBi (30 nm)/ LiF (1 nm)/ Al (100 nm). Čia EML yra grynas arba 20% legiruotas DPEPO matricoje sluoksnis. Dėl prie donorų grupių prijungtų *tert*-butil fragmentų spinduolių tirpumas buvo tenkinantis ir šviestukų liejimo iš tirpalo technologijos reikalavimus, tad greta vakuume formuotų šviestukų pagal toliau pateiktą struktūrą buvo liejimo būdu pagaminti šviestukai: ITO/ PEDOT:PSS (30 nm)/ PVK (20 nm)/ **EML** (20 nm)/ DPEPO (10 nm)/ TPBi (30 nm)/ LiF (1 nm)/ Al (100 nm). Liejimo iš tirpalo būdu buvo formuojami tik gryno emisinio sluoksnio šviestukai.

Pagaminti dangaus mėlynumo TADF OLED, pagrįsti **5tCzMeB** spinduoliu, demonstravo išskirtines 24,6% ir 13,4% išorinio našumo vertes legiruotuose ir nelegiruotuose įrenginiuose, o esant 100 cd/m2, prietaisai atitinkamai buvo 16,5% ir 7,7% išorinio našumo. Šios išmatuotos išorinio našumo vertės yra beveik 2 kartus didesnės nei našumo vertės, kurias demonstravo šviestukai pagaminti su originaliu **5tCzBP** spinduoliu. Taigi, žvelgiant iš medžiagos dizaino perspektyvos, metilbenzoato akceptorius atrodo daug patrauklesnis nei populiarusis benzofenonas, nes jis gali pagerinti įrenginio TADF našumą, išsaugant jo mėlynos spinduliuotės bangos ilgį.

Apibendrinant, galime teigti, kad šioje disertacijoje siūlomas benzofenono pagrindo emiterių patiriamas tripletinių eksitonų nespindulinis gesinimas gali būti efektyviai nuslopintas pakeičiant laisvą fenilo fragmentą metoksi grupe, o iš emiterių sintezės požiūrio – benzofenono grupę pakeičiant metilbenzoatu.

Šviestukai su naujais naftiridino – karbazolo pagrindo TADF spinduoliais

Siauros juostos giliai mėlynos spalvos (emisijos spektro maksimumas mažiau nei 460 nm) TADF spinduoliai yra paklausūs komerciniams OLED ekranų taikymams, tačiau sukurti efektyvius emiterius su mažu našumo nuokryčiu yra labai sudėtinga. Šis klausimas buvo nagrinėjamas disertacijoje tiriant mėlyną spinduliuotę skleidžiančius TADF junginius, sudarytus iš naftiridino akceptoriaus ir karbazolo pagrindo donorų grupių, kurios buvo sukurtos naudojant erdviškai kontroliuojamą vandenilio ryšių ir krūvio pernašos (CT) sąveiką tarp D ir A fragmentų ir asimetrinę donorų architektūrą.

Azoto hetero-atomą turintis naftiridino akceptorius neseniai buvo sėkmingai panaudotas kuriant TADF emiterius [84]–[87]. Naftiridino derinys su įvairiais donorais, tokiais kaip akridanais, karbazolais, fenoksazinais ir fenotiazinais, reguliariai naudojamais kuriant efektyvius TADF junginius. Pagaminti geltoni, žali, mėlyni spinduoliai, kurių spektro smailės bangos ilgis viršijo 460 nm, tačiau naudojant tuos emiterius didelio efektyvumo šviestukai demonstravo stebėtinai mažą našumo nuokrytį [86], [87].

Aukšta atbulinės interkombinacinės konversijos sparta, skatinanti veiksmingą uždelstą fluorescenciją, yra viena iš pagrindinių savybių, reikalingų norint sukurti efektyvius TADF pagrindu veikiančius OLED. Įprasta strategija norint pasiekti aukštą k_{rISC} yra sumažinti energijos skirtumą tarp žemiausio sužadinimo singleto ir tripleto būsenų. Mažas ΔE_{ST} reikšmes galima pasiekti junginiuose, turinčiuose stiprų CT pobūdį [88], paprastai D-A arba D-A-D tipo junginiuose su dideliais erdviniais kampais tarp D ir A fragmentų, todėl HOMO ir LUMO yra labai atskirti [37]. Ši strategija veiksmingai sumažina ΔE_{ST}, bet taip pat sumažina k_r ir lemia, kad tiek žemiausios tripletinės, tiek singletinės sužadintosios būsenos turi stiprų CT pobūdį. Tai sumažina sukinio-orbitos sąveiką, nes sukinio konvertavimas tarp grynų CT būsenų yra draudžiamas [89] ir tokia medžiaga gali negarantuoti greito rISC, todėl reikalingas papildomas lokaliai sužadintos (LE) tripleto būsenos buvimas šalia CT būsenų [89]–[92].

Tam, kad geriau suprastume TADF mechanizmus skirtingose naftiridino pagrindo D-A-D sistemose, publikacijoje **A2** tyrėme naftiridino – karbazolo pagrindo spinduolius, kurie vienas nuo kito skyrėsi tik trikdžiu, o publikacijoje **A5** gilinomės į skirtingų architektūrų D-A, D-A-D* ir D-A-D naftiridino akceptoriaus ir karbazolo pagrindo donorų TADF spinduolių mechanizmus.

Norint pasiekti siaurą mėlyną TADF, reikalinga standi ir erdviškai išsukta arba donorais surakinta molekulinė struktūra su atskirtomis HOMO ir LUMO orbitalėmis ir silpnu CT pobūdžiu [57], [93], [94]. Be to, vandenilinė sąveika

tarp azoto hetero-atomų akceptoriuje ir gretimų C-H jungčių donoro fragmente taip pat gali sukelti siaurą mėlyną TADF emisiją [64]. Vandenilinės ir CT sąveikos derinys kontroliuojamu būdu galėtų būti patraukli strategija norint pasiekti didelio našumo mėlynus OLED.

Paveikslėlyje **Fig. 9** vaizduojamos TADF spinduolių su naftiridino akceptoriumi ir *tert*-butil-karbazolo donorais molekulinės struktūros. Junginys *t***Cz-ND** šiame darbe buvo naudojamas palyginimui su metilo grupe pakeisto spinduolio **Me*t*Cz-ND** savybėmis. Metilo grupės įvedimas buvo naudojamas erdvinės kliūties sukūrimui ir kampo tarp donoro ir akceptoriaus fragmentų padidinimui. Modifikacija leido įvertinti intramolekulinės D-A sąveikos ir CT stiprumo įtaką tiriamų junginių TADF savybėms ir jų veikimui tiek vakuume, tiek iš tirpalo formuotuose OLED prietaisuose.

Panašiai, kaip ir publikacijoje **A1**, buvo atlikti išsamūs sugerties bei fotoliuminescencijos spektroskopijos tyrimai įvairiuose terpėse (mažos koncentracijos tolueno tirpaluose bei kietoje mCP medžiagos matricoje). Apdorojus PL matavimų rezultatus buvo suskaičiuoti įvairių vyksmų našumai ir spartos.

Abu junginiai rodė deguoniui jautrią FL tirpaluose su skirtingomis greitosios (PF) ir uždelstosios (DF) FL komponentėmis. *t***Cz-ND** ir **Me*t*Cz-ND** tolueno tirpaluose buvo gautos solidžios Φ_{PL} vertės – 0,53 ir 0,64. PL QY buvo padidintas iki 0,76 ir 0,86, kai emiteriai buvo disperguoti standžioje mCP matricoje, 7% koncentracija. Padidėjusias Φ_{PL} vertes lydėjo žymiai išaugęs DF komponentės indėlis, o tai reiškia, kad sumažėjo nespindulinis relaksavimas iš tripletinių būsenų.

Svarbu pabrėžti, kad **Me*t*Cz-ND** k_{RISC} buvo daugiau nei 3 kartus didesnis (1.06×10^6 s^{-1} mCP matricoje), palyginti su nemodifikuoto *t***Cz-ND** ($0,34 \times 10^6$ s^{-1}). Tai gali būti dėl mažo ΔE_{ST} (0,09 eV) ir stipresnės virpesinės sąveikos.

Siekdami ištirti naftiridino pagrindo junginių elektroliuminescencines savybes, pagaminome mėlynai šviečiančius TADF OLED. Kad galėtume geriau palyginti emiterius, OLED prietaisai buvo pagaminti naudojant tą pačią OLED struktūrą, naudojant TADF junginius kaip legirantus mCP matricoje ir esant tokiai pačiai legiravimo koncentracijai. Tai leido visas gautas prietaisų charakteristikas tiesiogiai susieti su tiriamų junginių molekulinėmis savybėmis.

Vakuume formuoti OLED buvo gaminami pagal tokią struktūrą: ITO/ TAPC (30 nm)/ TCTA (5 nm)/ **TADF** (7 wt%):mCP (20 nm)/ DPEPO (5 nm)/ TmPyPB (50 nm)/ LiF (0.8 nm)/ Al(100 nm), čia TADF žymi *t***Cz-ND** arba **Me*t*Cz-ND**. Savo ruožtu iš tirpalo formuoti prietaisai buvo gaminami pagal

tokią struktūrą: ITO/ PEDOT:PSS (50 nm)/ PVK (15 nm)/ **TADF** (7 wt%): mCP (25 nm)/ DPEPO (5 nm)/ TmPyPB (50 nm)/ LiF (0.8 nm)/ Al(100 nm).

OLED, pagaminti naudojant *t*Cz-ND, pasižymėjo žema įjungimo įtampa – 3,25 V, emisijos smaile ties 459 nm ir 66 nm spektro puspločiu, o tai perteikė giliai mėlyną siaurajuosčią emisiją su CIE koordinatėmis (0,14, 0,16). Maksimalus *t*Cz-ND pagrįstų OLED našumas buvo 17%, o esant praktiškai naudingam 100 cd/m^2 ryškumui, našumas sumažėjo iki 9,9% ir iki 7% prie 1000 cd/m^2. Maksimalus šio įrenginio ryškumas buvo 8424 cd/m^2.

Me*t*Cz-ND pagrindo vakuuminiu būdu pagaminti OLED rodė tas pačias įjungimo charakteristikas, kai įjungimo įtampa buvo 3,25 V. Prietaisų EL buvo pasislinkusi į raudoną pusę, o emisijos smailė buvo ties 481 nm. Stipresnis **Me*t*Cz-ND** CT pobūdis taip pat reiškė platesnę šviestuko spinduliuotę (FWHM = 86 nm), skaičius būdingas įprastiems TADF spinduoliams. Šviestukų maksimalus našumas buvo šiek tiek didesnis nei *t*Cz-ND – 17,6 % esant mažam ryškumui. Tačiau, priešingai nei *t*Cz-ND, **Me*t*Cz-ND** pagrįsti OLED demonstravo mažesnį našumo nuokrytį. Našumas sumažėjo tik iki 14,4% ir 12,5%, esant atitinkamai 100 cd/m^2 ir 1000 cd/m^2 ryškumui. Įrenginio ryškumo maksimumas buvo 21 459 cd/m^2, išlaikant virš 4% našumą.

Greitas *t*Cz-ND pagrįstų šviestukų efektyvumo kritimas gali būti susietas su beveik 3 kartus ilgesne τ_{DF} nei išmatuota **Me*t*Cz-ND**. Ilgai gyvuojantys tripletai padidina daugelio žalingų sunaikinimo procesų, tokių kaip TTA ir STA, tikimybę. Be to, greitas rISC ir trumpas **Me*t*Cz-ND** τ_{DF} (3,1 µs) žymiai sumažino tripletų populiaciją, greitai versdamas juos singletais, todėl prietaiso efektyvumas liko aukštas net kai ryškumas buvo 1000 cd/m^2.

Iš tirpalo pagaminti OLED prietaisai demonstravo labai panašias spektrines ir maksimalaus našumo savybes, tačiau dėl neišspręstų krūvininkų injekcijos ir balanso problemų šviestukai yra prastesnių veikimo parametrų nei vakuume formuoti prietaisai. Nepaisant to, šioje disertacijoje patvirtinome ir naftiridino pagrindo TADF spinduolių pritaikomumą iš tirpalo gaminamų OLED srityje.

Kitas šios disertacijos tyrimas, išspausdintas publikacijoje **A5**, yra apie siekį išsiaiškinti, kaip sudaryti palankesnes atbulinės interkombinacinės konversijos sąlygas D-A-D architektūros TADF medžiagose. Dažnai donor-akceptorinės TADF molekulės pasižymi labai stipriu CT pobūdžiu tiek žemiausio singleto, tiek tripleto lygmenyse, dėl to gali smarkiai sumažėti rISC sparta, nes pagal El-Sajedo taisyklę, sukinio keitimas tarp grynai CT būsenų yra uždraustas [89], kas lemia ir sumažėjusį našumą.

Norint sustiprinti sukinio ir orbitos sąveiką, reikalingas energetiškai artimos LE tripletinės būsenos dalyvavimas. Vienas iš būdų tokioms sąlygoms

pasiekti yra sukurti junginius su asimetrine D-A-D* architektūra, nes jie palengvina mišrių CT ir LE būsenų susidarymą, taip užtikrinant efektyvų TADF [96], [97].

Šioje disertacijoje, 1,8-naftiridinas buvo naudojamas kaip elektronų akceptorius kartu su 3,5-di-*tert*-butilkarbazolo (D*) ir erdviškai sudėtingu 3,3',6,6'-tetra-*tert*-butil-9H-1,9'-bicarbazolo (D) fragmentais, kad sukurtume D-A, D-A-D ir D-A-D* TADF spinduolius. Surinkti rezultatai rodo asimetrinės molekulės geometrijos pranašumą, nes toks dizainas pagerina tripleto-singleto konversiją dėl stipresnio žemiausios tripletinės būsenos LE pobūdžio. Paveikslėlyje **Fig. 13** vaizduojami naftiridino pagrindu sukurti TADF spinduoliai. **DCz-ND** susideda iš naftiridino akceptoriaus ir didelių gabaritų D grupės, **DCz-ND-Cz** susideda iš naftiridino akceptoriaus, gaubiamos didelių gabaritų D ir kompaktiškos D* grupės, o galiausiai **DCz-ND-DCz** turi naftiridino akceptorių, apsuptą dviejų. didelių gabaritų D grupių.

Visi trys junginiai rodė ryškias sugerties smailes esant 346 nm su gerai išskirtomis vibroninėmis kopijomis, būdingomis LE būsenoms, susijusioms su karbazolo grupėmis. Svarbiausi sugerties skirtumai buvo užfiksuoti esant ilgesniems bangų ilgiams, kai **DCz-ND** pasižymėjo plačia ir be struktūros į CT panašia sugerties juosta, tuo tarpu **DCz-ND-Cz** rodė intensyvią ir vibroniškai moduliuotą sugerties juostą ties 401 nm, būdinga LE būsenai [98], [99]. Greičiausiai tai nulėmė mažesnis erdvinis kampas tarp kompaktiškos D* grupės ir naftiridino akceptoriaus. Be to, **DCz-ND-DCz** turėjo silpnesnę, tačiau struktūrizuotą sugertį, kurios smailė buvo ties 377 nm.

Platūs **DCz-ND** tolueno tirpalo PL spektrai, kurių smailės bangos ilgis siekė 474 nm, patvirtino žemiausio sužadintos būsenos CT pobūdį, kurį lemia didelis HOMO ir LUMO orbitalių atskyrimas. Simetrinis junginys **DCz-ND-DCz** parodė siauresnį ir mėlynai pasislinkusį emisijos spektrą, kurio smailė yra ties 443 nm, o tai rodo prislopintą sužadintos būsenos geometrijos atsipalaidavimą dėl standesnės molekulinės struktūros. Įdomu tai, kad asimetrinio junginio **DCz-ND-Cz** emisijos spektrai buvo šiek tiek struktūrizuoti ir turėjo dvi komponentes – didesnės energijos siaurą ir raudonai pasislinkusią plačią, panašią į CT juostą ties 463 nm. Tai galima paaiškinti tuo, kad emisija yra matoma vienu metu iš LE ir CT būsenų. TADF spinduolių našumai tolueno tirpaluose buvo 19%, 58% ir 33%, atitinkamai **DCz-ND**, **DCz-ND-Cz**, **DCz-ND-DCz**. Patalpinus emiterius į kietą DPEPO medžiagos matricą fluorescencijos našumai paaugo iki 46%, 74% ir 72%.

Nepaisant panašių ΔE_{ST} verčių, gautų su legiruotuose DPEPO sluoksniuose, **DCz-ND-Cz** junginys demonstravo daugiau nei du kartus didesnę rISC spartą nei **DCz-ND** ir **DCz-ND-DCz** (asimetrinio junginio

$k_{rISC}=1.33\times10^6$ s^{-1}). Didesnė asimetrinio **DCz-ND-Cz** rISC spartą gali būti paaiškinama stipresniu T_1 būsenos LE pobūdžiu, kuris, kaip tikimasi, palengvina tripleto sukinio konvertavimą į singletą dėl sustiprintos sukinio-orbitos sąveikos. Nepaisant to, visi tirti junginiai parodė gana trumpą uždelstosios fluorescencijos gyvavimo laiką (<10 μs), asimetrinis **DCz-ND-Cz** papildomai demonstravo ir aukštą spinduliavimo spartą ($k_r = 1.91\times10^7$ s^{-1}), šis derinys yra pageidaujama OLED spinduolių savybė.

Naudojant šiuos tris junginius kaip TADF spinduolius buvo pagaminti OLED prietaisai pagal tokią struktūrą: ITO/ TAPC (30 nm)/ TCTA (5 nm)/ **TADF** (20 wt%):DPEPO (20 nm)/ DPEPO (5 nm)/ TmPyPB (50 nm)/ LiF (0.8 nm)/ Al(100 nm), čia TADF žymime spinduolius.

Visi pagaminti OLED rodė mėlyną elektroliuminescencijos piką ties 468, 469 ir 464 nm atitinkamai **DCz-ND**, **DCz-ND-Cz**, **DCz-ND-DCz** prietaisams, tačiau **DCz-ND-DCz** prietaisų įjungimo įtampa buvo didesnė nei kitų (4,5 V ir 3,75 V), tai gali būti siejama su didelėmis **DCz** grupėmis, apgaubiančiomis naftiridino akceptorių ir dėl to prastomis elektronų pernašos savybėmis bei bendru elektronų ir skylių srovių disbalansu įrenginyje. **DCz-ND** OLED emisijos spektras buvo 81 nm, o kitų prietaisų spektrai rodė siauresnę emisiją ir buvo 72 ir 73 nm puspločio. CIE spalvų koordinatės **DCz-ND**, **DCz-ND-Cz** ir **DCz-ND-DCz** prietaisams yra (0,15, 0,21), (0,16, 0,21) ir (0,16, 0,20), atitinkamai. OLED su **DCz-ND-Cz** ir **DCz-ND-DCz** emiteriais rodė vienodą maksimalų 20,8 % našumą, o **DCz-ND** pagrįstas šviestukas turėjo šiek tiek mažesnį maksimalų našumą – 18,1 %.

Kadangi emiteris **DCz-ND-Cz** išreiškia trumpiausią τ_{DF} ir didžiausią k_{rISC}, su šiuo spinduoliu pagamintas šviestukas demonstruoja santykinai mažiausią našumo kritimą. Be to, **DCz-ND** šviestukas kenčia nuo stipriausio našumo nuokryčio dėl ilgiausiai gyvuojančių tripletų ir lėčiausios rISC spartos. **DCz-ND**, **DCz-ND-Cz** ir **DCz-ND-DCz** pagrindo OLED našumo nuostoliai, palyginti su jų maksimaliu našumo, yra atitinkamai 45%, 36% ir 35%, kai šviesumas yra 100 cd/m^2 ir 70%, 53% ir 67%, atitinkamai prie 1000 cd/m^2.

Apibendrinant, vandenilinių ryšių ir erdvinio trikdymo metodai buvo sėkmingai panaudoti mėlynų naftiridino pagrindo TADF emiterių su aukštu našumu kūrimui. Įvestos metilo grupės prie karbazolo pagrindo donoro ženkliai padidina molekulės erdvinius kampus tarp skirtingų fragmentų, sumažina energinį skirtumą tarp singleto ir tripleto lygmenų ir kelis kartus paspartina tripletų konversijos į singletus spartą. Jei naftiridino akceptorius yra naudojamas asimetrinės D-A-D* molekulės konfigūracijoje, dėl papildomo LE pobūdžio tripletinio lygmens šalia CT lygmenų sustiprinama sukinio-orbitos sąveika ir padidinama rISC sparta. Visa tai leidžia naftiridino pagrindo TADF spinduolius naudoti aukšto našumo mėlynuose šviestukuose.

TADF šviestukai su itin mažu našumo nuokryčiu

Apgalvotas molekulių dizainas leido TADF šviestukams pasiekti iki 100% vidinį kvantinį našumą daugiausia dėl efektyvaus rISC, leidžiančio paversti tripletus eksitonus į efektyviai spinduliuojančias singletines būsenas. Tačiau kai kuriose organinėse sistemose rISC yra lėtas procesas, vykstantis per keliasdešimt mikrosekundžių [100]–[102], tai laikoma reikšmingu TADF medžiagų trūkumu, dėl kurio atsiranda ilgai trunkanti uždelstoji fluorescencija ir šviestukuose, o ypač kai pasiekiamas didelis srovės tankis, gali vykti nepageidaujami singleto-tripleto (STA) ar tripleto-tripleto (TTA) anihiliacija. Dėl pastarosios paprastai stebimas ryškus efektyvumo sumažėjimas, todėl stipriai padidėja įrenginio energijos suvartojimas esant dideliam ryškumui (>100 cd/m^2), kurio reikia naudojant OLED ekranus ir apšvietimą [103].

Neskaitant spinduolių, emisinio sluoksnio matricos medžiagos taip pat vaidina itin svarbų vaidmenį norint pasiekti maksimalų OLED našumą. Emiteriai yra legiruojami į matricos sluoksnį tam, kad būtų apriboti žalingą anihiliacijos procesai, kuriuos sukelia ilgiau gyvuojančios tripletinės būsenos. Todėl spinduolio molekulių „praskiedimas" į matricos sluoksnyje yra būtinas norint pailginti įrenginių tarnavimo laiką, padidinti efektyvumą ir sumažinti našumo nuokrytį. Matricos medžiagos turi turėti didelį ir, pageidautina, subalansuotą krūvininkų judrį, tenkinantį terminį ir morfologinį stabilumą bei cheminį stabilumą. Matricos taip pat turi turėti didelę tripleto energiją, kad apribotų eksitonus emiterio molekulėje, o tai yra ypač sudėtinga mėlynos spalvos OLED [104].

Karbazolo donorai yra pageidaujami kuriant TADF junginius, skirtus OLED taikymams, nes jie pasižymi geromis krūvio pernešimo savybėmis ir puikiu stabilumu. Tačiau karbazolas pasižymi silpnesnėmis elektronų donoro savybėmis ir paprastai sudaro mažesnius erdvinius kampus (~40–50°) su akceptoriumi. Tai lemia prastai atskirtas molekulines orbitales, kas lemia padidėjusį ΔE_{ST}, kas lemia mažą atbulinės interkombinacinės konversijos spartą, kas lemia žymų našumo nuokrytį TADF šviestukuose. Šioje disertacijoje ir publikacijoje **A3** mes įvedame smulkią donoro grupės modifikaciją, tam, kad padidintume izoftalonitrilo akceptoriaus pagrindo TADF spinduolio su karbazolo donorais erdvinius kampus tarp fragmentų, sumažintume ΔE_{ST}, padidintume rISC spartą ir sutrumpintume tripletų gyvavimo trukmę.

Šie pakeitimai užtikrino puikų modifikuoto TADF emiterio našumą, o OLED prietaisuose, pagamintuose tiek iš tirpalo, tiek vakuuminio garinimo būdu, lėmė aukštą efektyvumą ir ypač mažą našumo nuokrytį. Paveikslėlyje

Fig. 16 vaizduojama originalaus **DCzIPN** ir metilo grupe modifikuoto spinduolio **DMeCzIPN** molekulinės struktūros.

Fotoliuminescencijos kvantinė išeiga šiuose izoftalonitrilo pagrindo TADF spinduoliuose buvo 0,40 ir 0,44, atitinkamai **DCzIPN** ir **DMeCzIPN** tolueno tirpaluose be deguonies. Na o emisijos spektrai buvo platūs ir bestruktūriai, kas patvirtina molekulių singletinių lygmenų CT pobūdį, su emisijos maksimumu mėlyname diapazone, atitinkamai 453 nm ir 470 nm.

DCzIPN tolueno tirpalas pasižymėjo ilgalaike uždelstąja fluorescencija (τ_{DF} = 29,4 μs) ir greita pradine fluorescencija (τ_{PF} = 12,1 ns) lemiančia gana mažą Φ_{DF}/Φ_{PF} (tik 1,8) santykį, naudojantis įprastu formalizmu buvo apskaičiuotas gana aukštas k_r (1,17×10^7 s^{-1}) ir mažas k_{rISC} (7,0×10^4 s^{-1}). Pažymėtina, kad metilo grupės įvedimas pirmoje karbazolo padėtyje **DMeCzIPN** atveju beveik 35 kartus padidino k_{rISC} (iki 2,47×10^6 s^{-1}), o k_r sumažėjo tik 2 kartus (iki 5,65×10^6 s^{-1}), kas lemia trumpą uždelstąją fluorescenciją (τ_{DF} = 1,71 μs). Įspūdingą k_{rISC} padidėjimą galima paaiškinti žymiai mažesniu ΔE_{ST} (70 meV) lyginant su šia verte 190 meV, nustatyta originaliam spinduoliui.

DCzIPN legiruotų mCP sluoksnių savybės buvo panašios į tolueno tirpalų savybes – Φ_{PL} šiek tiek padidėjo iki 0,51, o τ_{DF} išliko beveik toks pat (30,8 μs). Kitokia situacija su **DMeCzIPN** spinduoliu – Φ_{PL} mCP matricoje buvo ženkliai padidinta iki 0,74, o τ_{DF} padidėjo iki 3,66 μs. Atsižvelgiant į tai, kad k_{rISC} buvo pakeistas nežymiai, tai reiškia, kad standžioje mCP matricoje, palyginti su tirpalu, yra slopinamas nespindulinis tripletinės būsenos gesinimas.

Siekiant patikrinti izoftalonitrilo pagrindo TADF spinduolių pritaikomumą mėlynuose šviestukuose, buvo gaminami OLED prietaisai. Dėl patenkinamų emiterių tirpumo savybių ir ypatingai svarbių liejimo būdu gamintų šviestukų pranašumų, tokių kaip lengvas gamybos masto didinimas, galimybė apdoroti didelius plotus vienu metu, gamybos pigumas ir paprastumas, izoftalonitrilo – karbazolo spinduolių pagrindo šviestukai buvo pagaminti tiek liejimo iš tirpalo, tiek ir terminio garinimo vakuume būdu. Liejimo iš tirpalo būdu formuoti šviestukai gaminti pagal tokią architektūrą: ITO/ PEDOT:PSS (50 nm)/ PVK (20 nm)/ **IPN** (7 wt%):mCP 20 nm/DPEPO (5 nm)/ TmPyPB (50 nm)/LiF (0.8 nm)/Al (100 nm), čia IPN yra žymimi TADF spinduoliai.

DCzIPN pagrindu gamintas OLED demonstravo 5,1 V įsijungimo įtampą, mėlyną emisiją su smaile ties 466 nm, o emisijos pusplotis buvo 75 nm. Nustatyta, kad maksimalus našumas buvo 9,5 % esant 257 cd/m^2. Prietaisas pasižymėjo prastu efektyvumo nuokryčiu, dėl kurio efektyvumas sumažėjo iki 7,6 % esant 1000 cd/m^2 ir iki 2 % prie didžiausio 4962 cd/m^2 šviesumas.

OLED su **DMeCzIPN** spinduoliu turėjo mažesnę įsijungimo įtampą (3,8 V) ir demonstravo mėlyną emisiją su smaile ties 478 nm. Prietaisas pasiekė žymiai didesnį maksimalų našumą (21,6 %). Svarbu tai, kad **DMeCzIPN** pagrindu sukurtame OLED buvo pasiektas itin mažas efektyvumas kritimas, t.y. našumas sumažėjo tik iki 19,6 % esant 1000 cd/m^2 ir išlaikė gana aukštą vertę (12,7 %) net esant 10000 cd/m^2. Be to, šviestukas sugebėjo pasiekti itin didelį ryškumą (28007 cd/m^2), o našumas buvo daugiau nei 4 %. Puikūs veikimo parametrai, o ypač lėtas **DMeCzIPN** spinduoliu pagrįsto šviestuko našumo nuokrytis, palyginti su **DCzIPN** pagrindo šviestuku, gali būti aiškinamas smarkiai išaugusiu k_{rISC} ir sumažintu τ_{DF}. Didelis k_{rISC} sumažina tripletinių eksitonų koncentraciją emisiniame sluoksnyje ir taip apriboja žalingus TTA ir STA procesus, atsakingus už našumo nuokrytį TADF-OLED.

Šie TADF emiteriai taip pat buvo išbandyti vakuuminiu būdu gamintuose OLED naudojant tokią įrenginio struktūrą: ITO/ TAPC (30 nm)/ TCTA (5 nm)/ IPN (7 wt%):mCP 20 nm / DPEPO (5 nm)/ TmPyPB (50 nm)/LiF (0.8 nm)/Al (100 nm). Šviestukas su **DCzIPN**, rodė 13,8 % maksimalų našumą, didesnį nei iš tirpalo formuotas šviestukas, tačiau vis tiek patyrė didelį efektyvumo kritimą. Našumas sumažėjo iki 8,3 % esant 1000 cd/m^2 ir iki 3,4 % esant 10000 cd/m^2. Vakuuminiu būdu gamintas šviestukas su **DMeCzIPN** spinduoliu, taip pat turėjo šiek tiek geresnes veikimo savybes, nei iš tirpalo gamintas prietaisas. Įspūdingas 23,8 % maksimalus našumas ir tik 5 % ir 29 % efektyvumo nuokrytis esant atitinkamai 1000 cd/m^2 ir 10000 cd/m^2 ryškumui. OLED demonstravo itin didelį 95743 cd/m^2 maksimalų ryškumą ir vis tiek buvo 4,8 % našumo. Geresnis vakuume formuoto OLED veikimas gali būti paaiškintas pagerėjusiu krūvininkų balansu, kurį rodo sumažėjusi įjungimo įtampa (3,5 V) ir gauta statesnė I-V-L charakteristika.

Išskirtinis **DMeCzIPN** emiteriu pagrįstų vakuuminiu ir liejimo iš tirpalo būdu pagamintų šviestukų našumas reiškia, kad TADF-OLED gali būti perspektyvūs kandidatai net ir ypatingo ryškumo (>1000 cd/m2) reikalaujantiems taikymams, pvz., apšvietime.

Dar vienas šios disertacijos tyrimas, publikuotas **A4**, yra apie naujo akridino – pirimidino pagrindu sukurto aukštos tripleto energijos (>3eV), todėl mėlyniems šviestukams tinkančios matricos medžiagos pritaikymą mažą našumo nuokrytį turinčiuose TADF šviestukuose. Šviestukams parinkti literatūroje žinomi mėlyni TADF spinduoliai **mPTC** [105] ir **OBA-O** [106]. Paveikslėlis **Fig. 19** vaizduoja naujos akridino – pirimidino pagrindo matricos medžiagos molekulinę struktūrą.

Gana neįprastos HOMO ir LUMO energijos lygmenų reikšmės buvo nustatytos **1MPA** medžiagai. HOMO lygmuo 5,1 eV, o LUMO – 1,55 eV. Įprastai OLED medžiagų HOMO lygmuo yra 5,5 eV ir daugiau. Dėl negilios HOMO padėties turėjome ieškoti mėlyno TADF emiterio su panašiai sekliu HOMO. Parinkti du mėlyni TADF emiteriai su panašiu HOMO lygmeniu, **mPTC** HOMO yra 5,12 eV, o **OBA-O** – 5,15 eV.

Kuriant šviestukus, **mPTC** legiravimo koncentracija **1MPA** matricoje buvo palaikoma 12%, remiantis fotoliuminescencijos kvantinės išeigos matavimais. Emiteriui **OBA-O** buvo naudojamos kelios legiravimo matricoje koncentracijos (5%, 8% ir 13%), siekiant ištirti įrenginio emisijos bangos ilgio derinamumą. OLED buvo pagaminti naudojant tokią prietaiso architektūrą: ITO/ TAPC (30 nm)/ **TADF** (**x** wt%):**1MPA** (30 nm)/ TmPyPB (40 nm)/ LiF (0.8nm)/ Al (100 nm), čia TADF žymimi spinduoliai, o **x** – legiravimo koncentracija.

OLED su **mPTC** rodė žemą 3,25 V įsijungimo įtampą, elektro-liuminescenciją ties 491 nm, ir 75 nm spektro pusplotį. Maksimalus našumas buvo 13,6%. Pagamintas prietaisas pasižymėjo mažu efektyvumo kritimu, ir kai ryškumas buvo 100 cd/m^2, našumas sumažėjo iki 12,3% ir iki 11,6%, esant 1000 cd/m^2 ryškumui. Pažymėtina, kad našumas išliko virš 10% iki labai didelio 5000 cd/m^2 ryškumo. Tokias veikimo savybes galima paaiškinti optimalia įrenginio architektūra ir gerai subalansuotomis elektronų ir skylių srovėmis. Maksimalus prietaiso ryškumas buvo beveik 44 000 cd/m^2.

OBA-O šviestukas, kurio legiravimo koncentracija panaši (13 %), kaip ir **mPTC** šviestukas, išreiškė panašias emisijos savybes. Nustatyta, kad didžiausias emisijos bangos ilgis, juostos plotis, CIE spalvų koordinatės ir maksimalus našumas yra labai panašūs. Kita vertus, daug statesnės **OBA-O** šviestuko srovės ir ryškumo kreivės nuo įtampos rodo ženkliai pagerėjusį krūvininkų judrį emisiniame sluoksnyje. Sumažinus **OBA-O** koncentraciją iki 5 %, emisijos buvo sodriai mėlyną (smailė ties 461 nm), o tai rodo **1MPA** potencialą pritaikymui giliai mėlynuose TADF šviestukuose. Sumažėjusi emiterio koncentracija kartu padidino emisijos juostos plotį (iki 94 nm) ir pagreitino našumo kritimą. Šviestukų našumo nuokrytis paprastai atsiranda dėl eksitono-polarono gesinimo arba eksitono-eksitono anihiliacijos. Didesnis nuokrytis esant mažesnei emiterio koncentracijai gali atsirasti dėl bet kurio iš šių efektų. Dėl aukšto (apie 1,15 eV) barjero elektronų injekcijai į matricą, bet ne į emiterį, tikėtina, kad elektronų pernaša vyksta šokinėjant tarp emiterio molekulių, o skylių pernaša vyksta per matricą, kur skylės injekcijai barjerų nėra. Dėl to atsiranda krūvininkų disbalansas, kuris skatina eksitono-skylės gesinimą. Tačiau esant žemai emiterio koncentracijai perkoliavimas per emiterio molekules nebėra įmanomas, todėl rekombinacijos zona susiaurėja

link elektronų injekcijos pusės. Šis rekombinacijos zonos sumažėjimas reiškia tiek eksitonų, tiek krūvininkų tankio padidėjimą, todėl prie eksitono-skylės gesinimo gali prisidėti ir tripleto-tripleto anihiliacija. Verta paminėti, kad dominuojanti uždelstosios fluorescencijos trukmė **mPTC** (2 μs) yra trumpesnė nei **OBA-O** (9 μs), o tai atitinka mažesnį jautrumą eksitonų gesinimo procesams.

Gauti rezultatai rodo, kad didelės tripleto energijos matricos medžiaga **1MPA** yra tinkama efektyvių mėlynų TADF OLED gamybai ir užtikrina mažą efektyvumo kritimą net ir didelio ryškumo sąlygomis.

Išvados

1. Pasiūlytas metodas, kaip atsikratyti tripletinių eksitonų gesinimo benzofenono akceptorių su laisva fenilo grupe turinčiuose TADF junginiuose. Pakeitus laisvą fenilo žiedą benzofenono akceptoriuje metoksi grupe, nespindulinis tripleto gesinimas buvo sumažintas 10 kartų, išlaikant aukštą rISC spartą ir tokiu būdu padidinant k_{rISC}/k_{nr}^{T} santykį. Tai leidžia užtikrinti 100 % vidinį našumą ir pasiekti labai aukštą maksimalų OLED našumą (iki 24,6%).

2. Siekiant sumažinti TADF emiterio, sukurto naudojant *tert*-butil-karbazolo donorus ir naftiridino akceptorių, ΔE_{ST}, buvo taikomi vandenilinio ryšio ir erdviškai kontroliuojamos krūvio pernašos sąveikų metodai. Modifikacija *metilinant* tCz fragmentus pirmoje padėtyje leido padidinti rISC spartą daugiau nei tris kartus ir sumažinti singleto ir tripleto lygmenų skirtumą, nekeičiant spinduliavimo spartos k_r. Taip pat įrodyta, kad tirti naftiridino junginiai yra tinkami kaip TADF spinduoliai ne tik vakuume formuotiems, bet ir iš tirpalų gamintiems OLED.

3. Asimetrinė karbazolo donoro konfigūracija, palyginti su simetriška, yra naudinga mėlyną spinduliuotę skleidžiantiems naftiridino-akceptorių TADF junginiams, nes palengvina sukinio keitimo procesą dėl stipraus žemiausios tripletinės būsenos LE pobūdžio. Stipresnis CT ir LE būsenų maišymas užtikrina 2 kartus didesnę rISC spartą ir sutrumpina uždelstos fluorescencijos trukmę, taip slopindamas šviestuko našumo nuokrytį.

4. Karbazolo donorų pakeitimas *metilinant* izoftalonitrilo-karbazolo D-A-D architektūros TADF emiteryje leido padidinti erdvinį kampą tarp D ir A grupių, sumažinti ΔE_{ST} ir 35 kartus padidinti rISC spartą. Modifikuoto junginio, **DMeCzIPN**, pagrindu vakuuminio garinimo ir liejimo iš tirpalo būdais pagaminti TADF šviestukai demonstravo atitinkamai 23,8% ir 21,6% našumą, o našumo kritimas buvo ypač mažas.

5. Nauja akridino-pirimidino pagrindo medžiaga (**1MPA**), optimizuota mėlyniesiems TADF spinduoliams, buvo sukurta kruopščiai atrinkus D ir A fragmentus ir tiesiogiai juos sujungiant. Didelę tripleto energiją, turinti **1MPA**, buvo naudojama su dviem mėlynais TADF emiteriais, pasižyminčiais sekliu HOMO lygmeniu, buvo įrodyta, kad OLED įrenginiuose užtikrinamas didelis efektyvumas ir mažas našumo nuokrytis.

BIBLIOGRAPHY

[1] J. Bauri, R. B. Choudhary, and G. Mandal, 'Recent advances in efficient emissive materials-based OLED applications: a review', *J. Mater. Sci.*, vol. 56, no. 34, pp. 18837–18866, Dec. 2021, doi: 10.1007/s10853-021-06503-y.

[2] N. Sun, C. Jiang, Q. Li, D. Tan, S. Bi, and J. Song, 'Performance of OLED under mechanical strain: a review', *J. Mater. Sci. Mater. Electron.*, vol. 31, no. 23, pp. 20688–20729, Dec. 2020, doi: 10.1007/s10854-020-04652-5.

[3] E. Hsiang, Z. Yang, Q. Yang, Y. Lan, and S. Wu, 'Prospects and challenges of mini-LED, OLED, and micro-LED displays', *J. Soc. Inf. Disp.*, vol. 29, no. 6, pp. 446–465, Jun. 2021, doi: 10.1002/jsid.1058.

[4] R. Mertens, *The OLED Handbook: a Guide to OLED Technology, Industry & Market*, 2016 edition. Milton Keynes UK: Lightning Source UK Ltd., 2016.

[5] G. Parthasarathy, J. Liu, and A. R. Duggal, 'Organic Light Emitting Devices: From Displays to Lighting', *Electrochem. Soc. Interface*, vol. 12, no. 2, pp. 42–47, Jun. 2003, doi: 10.1149/2.F10032IF.

[6] J. Donelan, '2011 SID Display of the Year Award Winners', *Inf. Disp.*, vol. 27, no. 5–6, pp. 10–15, May 2011, doi: 10.1002/j.2637-496X.2011.tb00389.x.

[7] 'Strategy Analytics: OLED Drives the Smartphone Display Panel Market in 2021', Mar. 24, 2022. https://www.businesswire.com/news/home/20220324005004/en/Strategy-Analytics-OLED-Drives-the-Smartphone-Display-Panel-Market-in-2021 (accessed May 19, 2022).

[8] K. E. D. Global, 'Samsung, LG dominate global TV market with premium models', *KED Global*. https://www.kedglobal.com/electronics/newsView/ked202202200002 (accessed May 19, 2022).

[9] R. Mertens, *The OLED Handbook: a Guide to OLED Technology, Industry & Market*, 2019 edition. Milton Keynes UK: Lightning Source UK Ltd., 2019.

[10] 'DSCC: the OLED market will grow 19% in 2019 to reach $31 billion in revenues | OLED-Info'. https://www.oled-info.com/dscc-oled-market-will-grow-19-2019-reach-31-billion-revenues (accessed Feb. 17, 2022).

[11] 'Challenges in OLED Research and Development: Emitters', *Energy.gov*. https://www.energy.gov/eere/ssl/text-alternative-version-challenges-oled-research-and-development-emitters (accessed Feb. 17, 2022).

[12] H. Yersin, Ed., *Highly Efficient OLEDs: Materials Based on Thermally Activated Delayed Fluorescence*. Weinheim, Germany: Wiley-VCH Verlag GmbH & Co. KGaA, 2018. doi: 10.1002/9783527691722.

[13] H. Yersin, A. F. Rausch, R. Czerwieniec, T. Hofbeck, and T. Fischer, 'The triplet state of organo-transition metal compounds. Triplet

harvesting and singlet harvesting for efficient OLEDs', *Coord. Chem. Rev.*, vol. 255, no. 21, pp. 2622–2652, Nov. 2011, doi: 10.1016/j.ccr.2011.01.042.

[14] D. Volz *et al.*, 'From iridium and platinum to copper and carbon: new avenues for more sustainability in organic light-emitting diodes', *Green Chem.*, vol. 17, no. 4, pp. 1988–2011, Apr. 2015, doi: 10.1039/C4GC02195A.

[15] H. Uoyama, K. Goushi, K. Shizu, H. Nomura, and C. Adachi, 'Highly efficient organic light-emitting diodes from delayed fluorescence', *Nature*, vol. 492, no. 7428, pp. 234–238, Dec. 2012, doi: 10.1038/nature11687.

[16] M. A. Baldo, D. F. O'Brien, M. E. Thompson, and S. R. Forrest, 'Excitonic singlet-triplet ratio in a semiconducting organic thin film', *Phys. Rev. B*, vol. 60, no. 20, pp. 14422–14428, Nov. 1999, doi: 10.1103/PhysRevB.60.14422.

[17] A. P. Monkman, C. Rothe, and S. M. King, 'Singlet Generation Yields in Organic Light-Emitting Diodes', *Proc. IEEE*, vol. 97, no. 9, pp. 1597–1605, Sep. 2009, doi: 10.1109/JPROC.2009.2021868.

[18] D. Y. Kondakov, T. D. Pawlik, T. K. Hatwar, and J. P. Spindler, 'Triplet annihilation exceeding spin statistical limit in highly efficient fluorescent organic light-emitting diodes', *J. Appl. Phys.*, vol. 106, no. 12, p. 124510, Dec. 2009, doi: 10.1063/1.3273407.

[19] S. M. King *et al.*, 'The contribution of triplet–triplet annihilation to the lifetime and efficiency of fluorescent polymer organic light emitting diodes', *J. Appl. Phys.*, vol. 109, no. 7, p. 074502, Apr. 2011, doi: 10.1063/1.3561430.

[20] C. Adachi, M. A. Baldo, M. E. Thompson, and S. R. Forrest, 'Nearly 100% internal phosphorescence efficiency in an organic light-emitting device', *J. Appl. Phys.*, vol. 90, no. 10, pp. 5048–5051, Oct. 2001, doi: 10.1063/1.1409582.

[21] W. Helfrich and W. G. Schneider, 'Transients of Volume-Controlled Current and of Recombination Radiation in Anthracene', *J. Chem. Phys.*, vol. 44, no. 8, pp. 2902–2909, Apr. 1966, doi: 10.1063/1.1727152.

[22] H. Yersin, 'Triplet Emitters for OLED Applications. Mechanisms of Exciton Trapping and Control of Emission Properties', in *Transition Metal and Rare Earth Compounds: Excited States, Transitions, Interactions III*, H. Yersin, Ed. Berlin, Heidelberg: Springer, 2004, pp. 1–26. doi: 10.1007/b96858.

[23] A. F. Rausch, H. H. H. Homeier, and H. Yersin, 'Organometallic Pt(II) and Ir(III) Triplet Emitters for OLED Applications and the Role of Spin–Orbit Coupling: A Study Based on High-Resolution Optical Spectroscopy', in *Photophysics of Organometallics*, A. J. Lees, Ed. Berlin, Heidelberg: Springer, 2010, pp. 193–235. doi: 10.1007/3418_2009_6.

[24] A. F. Rausch, H. H. H. Homeier, P. I. Djurovich, M. E. Thompson, and H. Yersin, 'Spin-orbit coupling routes and OLED performance: studies of blue-light emitting Ir(III) and Pt(II) complexes', San Diego, CA, Sep. 2007, p. 66550F. doi: 10.1117/12.731225.

[25] S. Obara et al., 'Highly Phosphorescent Iridium Complexes Containing Both Tridentate Bis(benzimidazolyl)-benzene or -pyridine and Bidentate Phenylpyridine: Synthesis, Photophysical Properties, and Theoretical Study of Ir-Bis(benzimidazolyl)benzene Complex', Inorg. Chem., vol. 45, no. 22, pp. 8907–8921, Oct. 2006, doi: 10.1021/ic060796o.

[26] Z. Abedin-Siddique, T. Ohno, K. Nozaki, and T. Tsubomura, 'Intense Fluorescence of Metal-to-Ligand Charge Transfer in [Pt(0)(binap)2] [binap = 2,2'-Bis(diphenylphosphino)-1,1'-binaphthyl]', Inorg. Chem., vol. 43, no. 2, pp. 663–673, Jan. 2004, doi: 10.1021/ic034527z.

[27] H. Yersin, A. F. Rausch, and R. Czerwieniec, 'Organometallic Emitters for OLEDs: Triplet Harvesting, Singlet Harvesting, Case Structures, and Trends', in Physics of Organic Semiconductors, John Wiley & Sons, Ltd, 2012, pp. 371–424. doi: 10.1002/9783527654949.ch13.

[28] S. Lamansky et al., 'Highly Phosphorescent Bis-Cyclometalated Iridium Complexes: Synthesis, Photophysical Characterization, and Use in Organic Light Emitting Diodes', J. Am. Chem. Soc., vol. 123, no. 18, pp. 4304–4312, May 2001, doi: 10.1021/ja003693s.

[29] M. A. Baldo et al., 'Highly efficient phosphorescent emission from organic electroluminescent devices', Nature, vol. 395, no. 6698, Art. no. 6698, Sep. 1998, doi: 10.1038/25954.

[30] G. J. Hedley, A. Ruseckas, and I. D. W. Samuel, 'Ultrafast luminescence in Ir(ppy)3', Chem. Phys. Lett., vol. 450, no. 4, pp. 292–296, Jan. 2008, doi: 10.1016/j.cplett.2007.11.028.

[31] T. Hofbeck and H. Yersin, 'The Triplet State of fac-Ir(ppy)3', Inorg. Chem., vol. 49, no. 20, pp. 9290–9299, Oct. 2010, doi: 10.1021/ic100872w.

[32] R. E. Daniels et al., 'When two are better than one: bright phosphorescence from non-stereogenic dinuclear iridium(III) complexes', Dalton Trans., vol. 45, no. 16, pp. 6949–6962, Apr. 2016, doi: 10.1039/C6DT00881J.

[33] C.-Y. Lu et al., 'Achieving Above 60% External Quantum Efficiency in Organic Light-Emitting Devices Using ITO-Free Low-Index Transparent Electrode and Emitters with Preferential Horizontal Emitting Dipoles', Adv. Funct. Mater., vol. 26, no. 19, pp. 3250–3258, 2016, doi: 10.1002/adfm.201505312.

[34] R. Czerwieniec, K. Kowalski, and H. Yersin, 'Highly efficient thermally activated fluorescence of a new rigid Cu(I) complex [Cu(dmp)(phanephos)]+', Dalton Trans., vol. 42, no. 27, pp. 9826–9830, Jun. 2013, doi: 10.1039/C3DT51006A.

[35] A. Monkman, 'Why Do We Still Need a Stable Long Lifetime Deep Blue OLED Emitter?', *ACS Appl. Mater. Interfaces*, Jul. 2021, doi: 10.1021/acsami.1c09189.

[36] C. Adachi, 'High Performance TADF for OLEDs', 2014, p. 26.

[37] T. Chen *et al.*, 'Understanding the Control of Singlet-Triplet Splitting for Organic Exciton Manipulating: A Combined Theoretical and Experimental Approach', *Sci. Rep.*, vol. 5, no. 1, Art. no. 1, Jul. 2015, doi: 10.1038/srep10923.

[38] J. U. Kim *et al.*, 'Nanosecond-time-scale delayed fluorescence molecule for deep-blue OLEDs with small efficiency rolloff', *Nat. Commun.*, vol. 11, no. 1, Art. no. 1, Apr. 2020, doi: 10.1038/s41467-020-15558-5.

[39] H. Liu *et al.*, 'Modulating the acceptor structure of dicyanopyridine based TADF emitters: Nearly 30% external quantum efficiency and suppression on efficiency roll-off in OLED', *Chem. Eng. J.*, vol. 401, p. 126107, Dec. 2020, doi: 10.1016/j.cej.2020.126107.

[40] P. L. dos Santos, J. S. Ward, M. R. Bryce, and A. P. Monkman, 'Using Guest–Host Interactions To Optimize the Efficiency of TADF OLEDs', *J. Phys. Chem. Lett.*, vol. 7, no. 17, pp. 3341–3346, Sep. 2016, doi: 10.1021/acs.jpclett.6b01542.

[41] H. Nakanotani, Y. Tsuchiya, and C. Adachi, 'Thermally-activated Delayed Fluorescence for Light-emitting Devices', *Chem. Lett.*, vol. 50, no. 5, pp. 938–948, May 2021, doi: 10.1246/cl.200915.

[42] Z. Yang *et al.*, 'Recent advances in organic thermally activated delayed fluorescence materials', *Chem. Soc. Rev.*, vol. 46, no. 3, pp. 915–1016, Feb. 2017, doi: 10.1039/C6CS00368K.

[43] 'The Electronic Structure of Organic Semiconductors', in *Electronic Processes in Organic Semiconductors*, Weinheim, Germany: Wiley-VCH Verlag GmbH & Co. KGaA, 2015, pp. 1–86. doi: 10.1002/9783527685172.ch1.

[44] M. Pope, H. P. Kallmann, and P. Magnante, 'Electroluminescence in Organic Crystals', *J. Chem. Phys.*, vol. 38, no. 8, pp. 2042–2043, Apr. 1963, doi: 10.1063/1.1733929.

[45] C. W. Tang, S. A. VanSlyke, and C. H. Chen, 'Electroluminescence of doped organic thin films', *J. Appl. Phys.*, vol. 65, no. 9, pp. 3610–3616, May 1989, doi: 10.1063/1.343409.

[46] D. J. Gaspar and E. Polikarpov, Eds., *OLED Fundamentals: Materials, Devices, and Processing of Organic Light-Emitting Diodes*, 1st edition. Boca Raton, FL: CRC Press, 2015.

[47] M. C. Gather and S. Reineke, 'Recent advances in light outcoupling from white organic light-emitting diodes', *J. Photonics Energy*, vol. 5, p. 057607, Jan. 2015, doi: 10.1117/1.JPE.5.057607.

[48] G. Gu, D. Z. Garbuzov, P. E. Burrows, S. Venkatesh, S. R. Forrest, and M. E. Thompson, 'High-external-quantum-efficiency organic light-emitting devices', *Opt. Lett.*, vol. 22, no. 6, pp. 396–398, Mar. 1997, doi: 10.1364/OL.22.000396.

[49] F. B. Dias *et al.*, 'Triplet Harvesting with 100% Efficiency by Way of Thermally Activated Delayed Fluorescence in Charge Transfer OLED Emitters', *Adv. Mater.*, vol. 25, no. 27, pp. 3707–3714, Jul. 2013, doi: 10.1002/adma.201300753.

[50] F. B. Dias, T. J. Penfold, and A. P. Monkman, 'Photophysics of thermally activated delayed fluorescence molecules', *Methods Appl. Fluoresc.*, vol. 5, no. 1, p. 012001, Mar. 2017, doi: 10.1088/2050-6120/aa537e.

[51] M. Y. Wong and E. Zysman-Colman, 'Purely Organic Thermally Activated Delayed Fluorescence Materials for Organic Light-Emitting Diodes', *Adv. Mater.*, vol. 29, no. 22, p. 1605444, 2017, doi: 10.1002/adma.201605444.

[52] H. F. Higginbotham, C.-L. Yi, A. P. Monkman, and K.-T. Wong, 'Effects of Ortho-Phenyl Substitution on the rISC Rate of D–A Type TADF Molecules', *J. Phys. Chem. C*, vol. 122, no. 14, pp. 7627–7634, Apr. 2018, doi: 10.1021/acs.jpcc.8b01579.

[53] H. Noda, H. Nakanotani, and C. Adachi, 'Highly efficient thermally activated delayed fluorescence with slow reverse intersystem crossing', *Chem. Lett.*, vol. 48, no. 2, pp. 126–129, 2019, doi: 10.1246/cl.180813.

[54] K. Matsuo and T. Yasuda, 'Blue thermally activated delayed fluorescence emitters incorporating acridan analogues with heavy group 14 elements for high-efficiency doped and non-doped OLEDs', *Chem. Sci.*, vol. 10, no. 46, pp. 10687–10697, Nov. 2019, doi: 10.1039/C9SC04492B.

[55] Q. Zhang, B. Li, S. Huang, H. Nomura, H. Tanaka, and C. Adachi, 'Efficient blue organic light-emitting diodes employing thermally activated delayed fluorescence', *Nat. Photonics*, vol. 8, no. 4, pp. 326–332, Apr. 2014, doi: 10.1038/nphoton.2014.12.

[56] M. Numata, T. Yasuda, and C. Adachi, 'High efficiency pure blue thermally activated delayed fluorescence molecules having 10H-phenoxaborin and acridan units', *Chem. Commun.*, vol. 51, no. 46, pp. 9443–9446, May 2015, doi: 10.1039/C5CC00307E.

[57] L.-S. Cui, H. Nomura, Y. Geng, J. U. Kim, H. Nakanotani, and C. Adachi, 'Controlling Singlet-Triplet Energy Splitting for Deep-Blue Thermally Activated Delayed Fluorescence Emitters', *Angew. Chem. Int. Ed Engl.*, vol. 56, no. 6, pp. 1571–1575, Feb. 2017, doi: 10.1002/anie.201609459.

[58] I. S. Park, J. Lee, and T. Yasuda, 'High-performance blue organic light-emitting diodes with 20% external electroluminescence quantum efficiency based on pyrimidine-containing thermally activated delayed fluorescence emitters', *J. Mater. Chem. C*, vol. 4, no. 34, pp. 7911–7916, Aug. 2016, doi: 10.1039/C6TC02027E.

[59] T. Serevičius *et al.*, 'Single-exponential solid-state delayed fluorescence decay in TADF compounds with minimized conformational disorder', *J. Mater. Chem. C*, vol. 9, no. 3, pp. 836–841, 2021, doi: 10.1039/D0TC05503D.

[60] T. Serevičius et al., 'Optimization of the carbazole–pyrimidine linking pattern for achieving efficient TADF', *J. Mater. Chem. C*, vol. 8, no. 32, pp. 11192–11200, 2020, doi: 10.1039/D0TC02194F.

[61] T. Serevičius et al., 'Achieving efficient deep-blue TADF in carbazole-pyrimidine compounds', *Org. Electron.*, vol. 82, p. 105723, Jul. 2020, doi: 10.1016/j.orgel.2020.105723.

[62] J. W. Sun et al., 'Thermally Activated Delayed Fluorescence from Azasiline Based Intramolecular Charge-Transfer Emitter (DTPDDA) and a Highly Efficient Blue Light Emitting Diode', *Chem. Mater.*, vol. 27, no. 19, pp. 6675–6681, Oct. 2015, doi: 10.1021/acs.chemmater.5b02515.

[63] Y. Wada, S. Kubo, and H. Kaji, 'Adamantyl Substitution Strategy for Realizing Solution-Processable Thermally Stable Deep-Blue Thermally Activated Delayed Fluorescence Materials', *Adv. Mater.*, vol. 30, no. 8, p. 1705641, 2018, doi: 10.1002/adma.201705641.

[64] P. Rajamalli, N. Senthilkumar, P.-Y. Huang, C.-C. Ren-Wu, H.-W. Lin, and C.-H. Cheng, 'New Molecular Design Concurrently Providing Superior Pure Blue, Thermally Activated Delayed Fluorescence and Optical Out-Coupling Efficiencies', *J. Am. Chem. Soc.*, vol. 139, no. 32, pp. 10948–10951, Aug. 2017, doi: 10.1021/jacs.7b03848.

[65] Y. H. Lee et al., 'High-Efficiency Sky Blue to Ultradeep Blue Thermally Activated Delayed Fluorescent Diodes Based on *Ortho* -Carbazole-Appended Triarylboron Emitters: Above 32% External Quantum Efficiency in Blue Devices', *Adv. Opt. Mater.*, vol. 6, no. 17, p. 1800385, Sep. 2018, doi: 10.1002/adom.201800385.

[66] Y. H. Lee et al., 'Rigidity-Induced Delayed Fluorescence by Ortho Donor-Appended Triarylboron Compounds: Record-High Efficiency in Pure Blue Fluorescent Organic Light-Emitting Diodes', *ACS Appl. Mater. Interfaces*, vol. 9, no. 28, pp. 24035–24042, Jul. 2017, doi: 10.1021/acsami.7b05615.

[67] C. Duan et al., 'Multi-dipolar Chromophores Featuring Phosphine Oxide as Joint Acceptor: A New Strategy toward High-Efficiency Blue Thermally Activated Delayed Fluorescence Dyes', *Chem. Mater.*, vol. 28, no. 16, pp. 5667–5679, Aug. 2016, doi: 10.1021/acs.chemmater.6b01691.

[68] Y. Tsuchiya et al., 'Molecular Design Based on Donor-Weak Donor Scaffold for Blue Thermally-Activated Delayed Fluorescence Designed by Combinatorial DFT Calculations', *Front. Chem.*, vol. 8, 2020, Accessed: Mar. 06, 2022. [Online]. Available: https://www.frontiersin.org/article/10.3389/fchem.2020.00403

[69] M. J. Frisch, G. W. Trucks, H. B. Schlegel, G. E. Scuseria, M. A. Robb, J. R. Cheeseman, G. Scalmani, V. Barone, G. A. Petersson, H. Nakatsuji, X. Li, M. Caricato, A. Marenich, J. Bloino, B. G. Janesko, R. Gomperts, B. Mennucci, H. P. Hratchian, J. V. Ortiz, A. F. Izmaylov, J. L. Sonnenberg, D. Williams-Young, F. Ding, F. Lipparini, F. Egidi, J. Goings, B. Peng, A. Petrone, T. Henderson, D. Ranasinghe, V. G. Zakrzewski, J. Gao, N. Rega, G. Zheng, W. Liang, M. Hada, M. Ehara,

K. Toyota, R. Fukuda, J. Hasegawa, M. Ishida, T. Nakajima, Y. Honda, O. Kitao, H. Nakai, T. Vreven, K. Throssell, J. A. Montgomery, Jr., J. E. Peralta, F. Ogliaro, M. Bearpark, J. J. Heyd, E. Brothers, K. N. Kudin, V. N. Staroverov, T. Keith, R. Kobayashi, J. Normand, K. Raghavachari, A. Rendell, J. C. Burant, S. S. Iyengar, J. Tomasi, M. Cossi, J. M. Millam, M. Klene, C. Adamo, R. Cammi, J. W. Ochterski, R. L. Martin, K. Morokuma, O. Farkas, J. B. Foresman, and D. J. Fox, 'Gaussian 09, Revision C.01'. 2016.

[70] S. Leyre *et al.*, 'Absolute determination of photoluminescence quantum efficiency using an integrating sphere setup', *Rev. Sci. Instrum.*, vol. 85, p. 123115, Dec. 2014, doi: 10.1063/1.4903852.

[71] J. C. de Mello, H. F. Wittmann, and R. H. Friend, 'An improved experimental determination of external photoluminescence quantum efficiency', *Adv. Mater.*, vol. 9, no. 3, pp. 230–232, 1997, doi: 10.1002/adma.19970090308.

[72] L.-O. Pålsson and A. p. Monkman, 'Measurements of Solid-State Photoluminescence Quantum Yields of Films Using a Fluorimeter', *Adv. Mater.*, vol. 14, no. 10, pp. 757–758, 2002, doi: 10.1002/1521-4095(20020517)14:10<757::AID-ADMA757>3.0.CO;2-Y.

[73] L. Porrès, A. Holland, L.-O. Pålsson, A. P. Monkman, C. Kemp, and A. Beeby, 'Absolute Measurements of Photoluminescence Quantum Yields of Solutions Using an Integrating Sphere', *J. Fluoresc.*, vol. 16, no. 2, pp. 267–273, Mar. 2006, doi: 10.1007/s10895-005-0054-8.

[74] N. Aizawa, C.-J. Tsou, I. S. Park, and T. Yasuda, 'Aggregation-induced delayed fluorescence from phenothiazine-containing donor–acceptor molecules for high-efficiency non-doped organic light-emitting diodes', *Polym. J.*, vol. 49, no. 1, Art. no. 1, Jan. 2017, doi: 10.1038/pj.2016.82.

[75] S. Y. Lee, T. Yasuda, Y. S. Yang, Q. Zhang, and C. Adachi, 'Luminous Butterflies: Efficient Exciton Harvesting by Benzophenone Derivatives for Full-Color Delayed Fluorescence OLEDs', *Angew. Chem.*, vol. 126, no. 25, pp. 6520–6524, Jun. 2014, doi: 10.1002/ange.201402992.

[76] Y. Li, G. Xie, S. Gong, K. Wu, and C. Yang, 'Dendronized delayed fluorescence emitters for non-doped, solution-processed organic light-emitting diodes with high efficiency and low efficiency roll-off simultaneously: two parallel emissive channels', *Chem. Sci.*, vol. 7, no. 8, pp. 5441–5447, Jul. 2016, doi: 10.1039/C6SC00943C.

[77] S. Y. Lee, T. Yasuda, I. S. Park, and C. Adachi, 'X-shaped benzoylbenzophenone derivatives with crossed donors and acceptors for highly efficient thermally activated delayed fluorescence', *Dalton Trans.*, vol. 44, no. 18, pp. 8356–8359, Apr. 2015, doi: 10.1039/C4DT03608E.

[78] F. Wang, X. Cao, L. Mei, X. Zhang, J. Hu, and Y. Tao, 'Twisted penta-Carbazole/Benzophenone Hybrid Compound as Multifunctional Organic Host, Dopant or Non-doped Emitter for Highly Efficient Solution-Processed Delayed Fluorescence OLEDs', *Chin. J. Chem.*, vol. 36, no. 3, pp. 241–246, 2018, doi: 10.1002/cjoc.201700703.

[79] W. Z. Yuan *et al.*, 'Crystallization-Induced Phosphorescence of Pure Organic Luminogens at Room Temperature', *J. Phys. Chem. C*, vol. 114, no. 13, pp. 6090–6099, Apr. 2010, doi: 10.1021/jp909388y.

[80] P. Rajamalli, V. Thangaraji, N. Senthilkumar, C.-C. Ren-Wu, H.-W. Lin, and C.-H. Cheng, 'Thermally activated delayed fluorescence emitters with a m,m-di-tert-butyl-carbazolyl benzoylpyridine core achieving extremely high blue electroluminescence efficiencies', *J. Mater. Chem. C*, vol. 5, no. 11, pp. 2919–2926, Mar. 2017, doi: 10.1039/C7TC00457E.

[81] D. Zhang, M. Cai, Y. Zhang, D. Zhang, and L. Duan, 'Sterically shielded blue thermally activated delayed fluorescence emitters with improved efficiency and stability', *Mater. Horiz.*, vol. 3, no. 2, pp. 145–151, 2016, doi: 10.1039/C5MH00258C.

[82] B. Wex and B. R. Kaafarani, 'Perspective on carbazole-based organic compounds as emitters and hosts in TADF applications', *J. Mater. Chem. C*, vol. 5, no. 34, pp. 8622–8653, Aug. 2017, doi: 10.1039/C7TC02156A.

[83] B. Yurash, H. Nakanotani, Y. Olivier, D. Beljonne, C. Adachi, and T.-Q. Nguyen, 'Photoluminescence Quenching Probes Spin Conversion and Exciton Dynamics in Thermally Activated Delayed Fluorescence Materials', *Adv. Mater.*, p. 1804490, 2019, doi: 10.1002/adma.201804490.

[84] X. Zhou, H. Yang, Z. Chen, S. Gong, Z.-H. Lu, and C. Yang, 'Naphthyridine-based emitters simultaneously exhibiting thermally activated delayed fluorescence and aggregation-induced emission for highly efficient non-doped fluorescent OLEDs', *J. Mater. Chem. C*, vol. 7, no. 22, pp. 6607–6615, 2019, doi: 10.1039/C9TC00346K.

[85] Y. Lee, S.-J. Woo, J.-J. Kim, and J.-I. Hong, 'Linear-shaped thermally activated delayed fluorescence emitter using 1,5-naphthyridine as an electron acceptor for efficient light extraction', *Org. Electron.*, vol. 78, p. 105600, Mar. 2020, doi: 10.1016/j.orgel.2019.105600.

[86] C. Chen, H.-Y. Lu, Y.-F. Wang, M. Li, Y.-F. Shen, and C.-F. Chen, 'Naphthyridine-based thermally activated delayed fluorescence emitters for multi-color organic light-emitting diodes with low efficiency roll-off', *J. Mater. Chem. C*, vol. 7, no. 16, pp. 4673–4680, 2019, doi: 10.1039/C9TC00503J.

[87] Y.-F. Shen *et al.*, 'Naphthyridine-based thermally activated delayed fluorescence emitters for highly efficient blue OLEDs', *Dyes Pigments*, vol. 178, p. 108324, Jul. 2020, doi: 10.1016/j.dyepig.2020.108324.

[88] T. J. Penfold, F. B. Dias, and A. P. Monkman, 'The theory of thermally activated delayed fluorescence for organic light emitting diodes', *Chem. Commun.*, vol. 54, no. 32, pp. 3926–3935, 2018, doi: 10.1039/C7CC09612G.

[89] M. K. Etherington, J. Gibson, H. F. Higginbotham, T. J. Penfold, and A. P. Monkman, 'Revealing the spin–vibronic coupling mechanism of thermally activated delayed fluorescence', *Nat. Commun.*, vol. 7, no. 1, Art. no. 1, Nov. 2016, doi: 10.1038/ncomms13680.

[90] C. M. Marian, 'Mechanism of the Triplet-to-Singlet Upconversion in the Assistant Dopant ACRXTN', *J. Phys. Chem. C*, vol. 120, no. 7, pp. 3715–3721, Feb. 2016, doi: 10.1021/acs.jpcc.6b00060.

[91] J. Gibson, A. P. Monkman, and T. J. Penfold, 'The Importance of Vibronic Coupling for Efficient Reverse Intersystem Crossing in Thermally Activated Delayed Fluorescence Molecules', *ChemPhysChem*, vol. 17, no. 19, pp. 2956–2961, 2016, doi: 10.1002/cphc.201600662.

[92] D. Berenis *et al.*, 'Different RISC rates in benzoylpyridine-based TADF compounds and their implications for solution-processed OLEDs', *Dyes Pigments*, vol. 182, p. 108579, Nov. 2020, doi: 10.1016/j.dyepig.2020.108579.

[93] Y. J. Cho, S. K. Jeon, S.-S. Lee, E. Yu, and J. Y. Lee, 'Donor Interlocked Molecular Design for Fluorescence-like Narrow Emission in Deep Blue Thermally Activated Delayed Fluorescent Emitters', *Chem. Mater.*, vol. 28, no. 15, pp. 5400–5405, Aug. 2016, doi: 10.1021/acs.chemmater.6b01484.

[94] P. Pander, A. Swist, R. Motyka, J. Soloducho, F. B. Dias, and P. Data, 'Thermally activated delayed fluorescence with a narrow emission spectrum and organic room temperature phosphorescence by controlling spin–orbit coupling and phosphorescence lifetime of metal-free organic molecules', *J. Mater. Chem. C*, vol. 6, no. 20, pp. 5434–5443, May 2018, doi: 10.1039/C8TC00175H.

[95] T. Serevičius, R. Skaisgiris, J. Dodonova, K. Kazlauskas, S. Juršėnas, and S. Tumkevičius, 'Minimization of solid-state conformational disorder in donor–acceptor TADF compounds', *Phys. Chem. Chem. Phys.*, vol. 22, no. 1, pp. 265–272, Dec. 2019, doi: 10.1039/C9CP05907E.

[96] Z. Yang *et al.*, 'A sterically hindered asymmetric D–A–D′ thermally activated delayed fluorescence emitter for highly efficient non-doped organic light-emitting diodes', *Chem. Sci.*, vol. 10, no. 35, pp. 8129–8134, 2019, doi: 10.1039/C9SC01686D.

[97] W. Wei *et al.*, 'Modulation of π-linkers in asymmetric thermally activated delayed fluorescence molecules enabling high performance OLEDs', *J. Mater. Chem. C*, vol. 8, no. 11, pp. 3663–3668, 2020, doi: 10.1039/C9TC06608J.

[98] X. He *et al.*, 'Highly efficient organic light emitting diodes based on a D–A–D type dibenzothiophene derivative exhibiting thermally activated delayed fluorescence with small Δ E ST', *J. Mater. Chem. C*, vol. 4, no. 43, pp. 10205–10208, 2016, doi: 10.1039/C6TC03382B.

[99] U. Subuddhi, S. Haldar, S. Sankararaman, and A. K. Mishra, 'Photophysical behaviour of 1-(4-N,N-dimethylaminophenylethynyl)pyrene (DMAPEPy) in homogeneous media', *Photochem. Photobiol. Sci.*, vol. 5, no. 5, pp. 459–466, May 2006, doi: 10.1039/B600009F.

[100]   Y. Im, M. Kim, Y. J. Cho, J.-A. Seo, K. S. Yook, and J. Y. Lee, 'Molecular Design Strategy of Organic Thermally Activated Delayed Fluorescence Emitters', *Chem. Mater.*, vol. 29, no. 5, pp. 1946–1963, Mar. 2017, doi: 10.1021/acs.chemmater.6b05324.

[101]   U. Shakeel and J. Singh, 'Study of processes of reverse intersystem crossing (RISC) and thermally activated delayed fluorescence (TADF) in organic light emitting diodes (OLEDs)', *Org. Electron.*, vol. 59, pp. 121–124, Aug. 2018, doi: 10.1016/j.orgel.2018.04.035.

[102]   R. Komatsu, T. Ohsawa, H. Sasabe, K. Nakao, Y. Hayasaka, and J. Kido, 'Manipulating the Electronic Excited State Energies of Pyrimidine-Based Thermally Activated Delayed Fluorescence Emitters To Realize Efficient Deep-Blue Emission', *ACS Appl. Mater. Interfaces*, vol. 9, no. 5, pp. 4742–4749, Feb. 2017, doi: 10.1021/acsami.6b13482.

[103]   K. Masui, H. Nakanotani, and C. Adachi, 'Analysis of exciton annihilation in high-efficiency sky-blue organic light-emitting diodes with thermally activated delayed fluorescence', *Org. Electron.*, vol. 14, no. 11, pp. 2721–2726, Nov. 2013, doi: 10.1016/j.orgel.2013.07.010.

[104]   M. Godumala, S. Choi, M. J. Cho, and D. H. Choi, 'Thermally activated delayed fluorescence blue dopants and hosts: from the design strategy to organic light-emitting diode applications', *J. Mater. Chem. C*, vol. 4, no. 48, pp. 11355–11381, Dec. 2016, doi: 10.1039/C6TC04377A.

[105]   D.-Y. Chen *et al.*, 'Isomeric Thermally Activated Delayed Fluorescence Emitters for Color Purity-Improved Emission in Organic Light-Emitting Devices', *ACS Appl. Mater. Interfaces*, vol. 8, no. 26, pp. 16791–16798, Jul. 2016, doi: 10.1021/acsami.6b03954.

[106]   D. Song *et al.*, 'Asymmetric thermally activated delayed fluorescence (TADF) emitters with 5,9-dioxa-13b-boranaphtho[3,2,1-de]anthracene (OBA) as the acceptor and highly efficient blue-emitting OLEDs', *J. Mater. Chem. C*, vol. 7, no. 38, pp. 11953–11963, Oct. 2019, doi: 10.1039/C9TC04115J.

CURRICULUM VITAE

Name: **Dovydas**
Surname: **Banevičius**
Date of birth: 1994-04-29
Place of birth: Mažeikiai, Lithuania
E-mail: dovydas@fidi.lt

Education:

2004 – 2012	Mažeikiai Gabija Gymnasium
2012 – 2016	Vilnius University, Faculty of Physics
	Bachelor's Degree in Electronics Engineering
2016 – 2018	Vilnius University, Faculty of Physics
	Master's Degree in Materials Technology
2018 – 2022	Vilnius University, Faculty of Physics
	PhD Studies in Physics

Work experience:

2016 03 – 2016 06	Vilnius University, Department of Solid-State Electronics
	Laboratory technician
2018 01 – 2022 06	Vilnius University, Institute of Photonics and Nanotechnology
	Project specialist
2018 09 – 2019 06	Vilnius University, Institute of Photonics and Nanotechnology
	Laboratory engineer
2018 10 – current	Vilnius University, Faculty of Physics, Institute of Photonics and Nanotechnology
	Teaching assistant lecturer
2019 06 – 2020 07	Vilnius University, Institute of Photonics and Nanotechnology
	Senior laboratory technician
2020 07 – current	Vilnius University, Institute of Photonics and Nanotechnology
	Junior research fellow

COPIES OF PUBLICATIONS

A1

Suppression of benzophenone-induced triplet quenching for enhanced TADF performance

Gediminas Kreiza, **Dovydas Banevičius**, Justina Jovaišaitė, Karolina Maleckaitė, Dalius Gudeika, Dmytro Volyniuk, Juozas V. Gražulevičius, Saulius Juršėnas, Karolis Kazlauskas

A2

Realization of deep-blue TADF in sterically controlled naphthyridines for vacuum- and solution-processed OLEDs

Gediminas Kreiza, **Dovydas Banevičius**, Justina Jovaišaitė, Saulius Juršėnas, Tomas Javorskis, Vytenis Vaitkevičius, Edvinas Orentas, Karolis Kazlauskas

A3

High efficiency and extremely low roll-off solution- and vacuum-processed OLEDs based on isophthalonitrile blue TADF emitter

Gediminas Kreiza, Domantas Berenis, **Dovydas Banevičius**, Saulius Juršėnas, Tomas Javorskis, Edvinas Orentas, Karolis Kazlauskas

A4

Low efficiency roll-off blue TADF OLEDs employing a novel acridine–pyrimidine based high triplet energy host

Francesco Rodella, Rishabh Saxena, Sergey Bagnich, **Dovydas Banevičius**, Gediminas Kreiza, Stravos Athanasopoulos, Saulius Juršėnas, Karolis Kazlauskas, Anna Kohler, Peter Strohriegl

A5

Enhanced blue TADF in D-A-D type naphthyridine derivative with asymmetric carbazole-donor motif

Dovydas Banevičius, Gediminas Kreiza, Rokas Klioštoraitis, Saulius Juršėnas, Tomas Javorskis, Vytenis Vaitkevičius, Edvinas Orentas, Karolis Kazlauskas